

SPEED ESTIMATION TECHNIQUES FOR SENSORLESS VECTOR
CONTROLLED INDUCTION MOTOR DRIVE

A THESIS SUBMITTED TO
THE GRADUATE SCHOOL OF NATURAL AND APPLIED SCIENCES
OF
MIDDLE EAST TECHNICAL UNIVERSITY

BY

TALİP MURAT ERTEK

IN PARTIAL FULFILLMENT OF THE REQUIREMENTS
FOR
THE DEGREE OF MASTER OF SCIENCE
IN
ELECTRICAL AND ELECTRONICS ENGINEERING

DECEMBER 2005

Approval of the Graduate School of Natural and Applied Sciences

Prof. Dr. Canan ÖZGEN
Director

I certify that this thesis satisfies all the requirements as a thesis for the degree of Master of Science.

Prof. Dr. İsmet ERKMEN
Head of Department

This is to certify that we have read this thesis and that in our opinion it is fully adequate, in scope and quality, as a thesis for the degree of Master of Science.

Prof. Dr. Aydın ERSKAK
Supervisor

Examining Committee Members

Prof. Dr. Muammer ERMİŞ (METU, EE) _____

Prof. Dr. Aydın ERSKAK (METU, EE) _____

Prof. Dr. Işık ÇADIRCI (Hacettepe Univ., EE) _____

Assist. Prof. Dr. Ahmet M. HAVA (METU, EE) _____

Dr. Erbil NALÇACI (Energy Mar. Reg. Authority) _____

I hereby declare that all information in this document has been obtained and presented in accordance with academic rules and ethical conduct. I also declare that, as required by these rules and conduct, I have fully cited and referenced all material and results that are not original to this work.

Name, Last name : TALİP MURAT ERTEK

Signature :

ABSTRACT

SPEED ESTIMATION TECHNIQUES FOR SENSORLESS VECTOR CONTROLLED INDUCTION MOTOR DRIVE

ERTEK, Talip Murat

M. Sc. Department of Electrical and Electronics Engineering

Supervisor: Prof. Dr. Aydın Ersak

December 2005, 132 pages

This work focuses on speed estimation techniques for sensorless closed-loop speed control of an induction machine based on direct field-oriented control technique. Details of theories behind the algorithms are stated and their performances are verified by the help of simulations and experiments.

The field-oriented control as the vector control technique is mainly implemented in two ways: indirect field oriented control and direct field oriented control. The field to be oriented may be rotor, stator, or airgap flux-linkage. In the indirect field-oriented control no flux estimation exists. The angular slip velocity estimation based on the measured or estimated rotor speed is required, to compute the synchronous speed of the motor. In the direct field oriented control the synchronous speed is computed with the aid of a flux estimator. Field Oriented Control is based on projections which transform a three phase time and speed dependent system into a two co-ordinate time invariant system. These projections lead to a structure similar to that of a DC machine control. The flux observer used has an adaptive structure which makes use of both the voltage model and the current model of the machine.

The rotor speed is estimated via Kalman filter technique which has a recursive state estimation feature. The flux angle estimated by flux observer is processed taking the

angular slip velocity into account for speed estimation. For closed-loop speed control of system, torque, flux and speed producing control loops are tuned by the help of PI regulators. The performance of the closed-loop speed control is investigated by simulations and experiments. TMS320F2812 DSP controller card and the Embedded Target for the TI C2000 DSP tool of Matlab are utilized for the real-time experiments.

Keywords: Speed estimation, sensorless closed-loop direct field oriented control, flux estimation.

ÖZ

HIZ DUYAÇSIZ VEKTÖR DENETİMLİ ENDÜKSİYON MOTOR SÜRÜCÜSÜ İÇİN HIZ KESTİRİM TEKNİKLERİ

ERTEK, Talip Murat

Yüksek Lisans, Elektrik ve Elektronik Mühendisliği Bölümü

Tez Yöneticisi: Prof. Dr. Aydın Ersak

Aralık 2005, 132 sayfa

Bu çalışma, hız duyaçsız vektör denetimli motor sürücüsü için hız kestirim tekniklerine odaklanmıştır. Çalışma sırasında kullanılan kestirme yöntemlerinin kuramsal içeriklerinin detayları ayrıntılı olarak anlatılmış ve başarımları benzetim ve denemelerle incelenmiştir.

Vektör denetim tekniği olarak, alan yönlendirmeli denetim, temel olarak dolaylı yönlendirmeli ve doğrudan yönlendirmeli olmak üzere iki farklı yöntem ile gerçekleştirilmektedir. Yönlendirme, rotor, stator ya da hava boşluğu akısına göre yapılabilmektedir. Dolaylı alan yönlendirmede akı kestirmesi yapılmamaktadır. Senkron hız tahmini için ölçülen veya kestirilen rotor hızı slip tahmininde kullanılır. Alan yönlendirmeli denetim zamana ve hıza bağlı üç eksenli sistemlerin, hızdan bağımsız iki eksenli sistemlere dönüştürülmesi yöntemine dayanır. Bu dönüşümler ile DC motor denetimine benzer bir denetim yapısı elde edilir. Kullanılan akı kestiricisi, motorun gerilim modelini, akım modelini kullanan uyarlamalı bir yapıda olup, rotor akısının yerini yüksek doğrulukla kestirebilmektedir.

Rotor hızı durum kestirmesi yapabilen ve tekrarlamalı olarak çalışan, Kalman filtre yöntemiyle kestirilmiştir. Rotor hızının kestirilmesinde, akı gözlemleyicisinin akı

açısı kestirmesi ve rotor hızının bu akı açısı ile olan kayması dikkate alınmıştır. Kapalı döngü hız kontrolü için PI denetlemler kullanılmış; burma, akı ve hız isteği döngülerinin parametreleri ayarlanmıştır. Kapalı döngü hız kontrolünün performansı yapılan benzetim ve denemeler ile araştırılmıştır. TMS320F2812 kontrol kartı ve Matlab programı “Embedded Target for the TI C2000 DSP” yazılımı kullanılarak gerçek zamanlı denemeler gerçekleştirilmiştir.

Anahtar Kelimeler: Hız kestirme yöntemi, duyaçsız kapalı-döngü alan yönlendirmeli denetim, akı kestirme yöntemi.

ACKNOWLEDGEMENTS

I would like to express my sincere gratitude to my supervisor Prof. Dr. Aydın Ersak for his encouragement and valuable supervision throughout the study.

I would like to thank to ASELSAN Inc. for the facilities provided and my colleagues for support during the course of the thesis.

Thanks a lot to my friends, Eray ÖZÇELİK, Günay ŞİMŞEK, Evrim Onur ARI for their helps during experimental stage of this work.

I appreciate my family due to their great trust, encouragement and continuous emotional support.

TABLE OF CONTENTS

PLAGIARISM.....	III
ABSTRACT	IV
ÖZ.....	VI
ACKNOWLEDGEMENTS.....	VIII
TABLE OF CONTENTS.....	IX
LIST OF TABLES	XI
LIST OF FIGURES	XII
LIST OF SYMBOLS.....	XV
CHAPTER	
1 INTRODUCTION.....	1
1.1. INTRODUCTION TO INDUCTION MACHINE CONTROL LITERATURE	1
1.2. THE FIELD ORIENTED CONTROL OF INDUCTION MACHINES	1
1.3. INDUCTION MACHINE FLUX OBSERVATION	2
1.4. INDUCTION MACHINE SPEED ESTIMATION.....	4
1.5. STRUCTURE OF THE CHAPTERS	6
2 INDUCTION MACHINE MODELING, FIELD ORIENTED CONTROL AND PWM WITH SPACE VECTOR THEORY	8
2.1. SYSTEM EQUATIONS IN THE STATIONARY A,B,C REFERENCE FRAME	8
2.1.1. <i>Determination of Induction Machine Inductances</i>	11
2.1.2. <i>Three-Phase to Two-Phase Transformations</i>	15
2.1.2.1. The Clarke Transformation.....	16
2.1.2.2. The Park Transformation	17
2.1.3. <i>Circuit Equations in Arbitrary dq0 Reference Frame</i>	18
2.1.3.1. qd0 Voltage Equations.....	19
2.1.3.2. qd0 Flux Linkage Relation.....	21
2.1.3.3. qd0 Torque Equations.....	22
2.1.4. <i>qd0 Stationary and Synchronous Reference Frames</i>	23
2.2. FIELD ORIENTED CONTROL (FOC)	25
2.3. SPACE VECTOR PULSE WIDTH MODULATION (SVPWM).....	29
2.3.1. <i>Voltage Fed Inverter (VSI)</i>	29
2.3.2. <i>Voltage Space Vectors</i>	32
2.3.3. <i>SVPWM Application to the Static Power Bridge</i>	35
3 FLUX ESTIMATION FOR SENSORLESS DIRECT FIELD ORIENTED CONTROL OF INDUCTION MACHINE.....	44
3.1. FLUX ESTIMATION	44
3.1.1. <i>Estimation of the Flux Linkage Vector</i>	45
3.1.1.1. Flux Estimation in Continuous Time	45
3.1.1.2. Flux Estimation in Discrete Time	49
3.1.1.3. Flux Estimation in Discrete Time and Per-Unit.....	51
4 SPEED ESTIMATION FOR SENSORLESS DIRECT FIELD ORIENTED CONTROL OF INDUCTION MACHINE.....	56
4.1. REACTIVE POWER MRAS SCHEME.....	56

4.1.1.	<i>Reference Model Continuous Time Representation</i>	61
4.1.2.	<i>Adaptive Model Continuous Time Representation</i>	62
4.1.3.	<i>Discrete Time Representation</i>	64
4.1.3.1.	Reference Model	64
4.1.3.2.	Adaptive Model	65
4.2.	OPEN LOOP SPEED ESTIMATOR	67
4.3.	KALMAN FILTER FOR SPEED ESTIMATION	70
4.3.1.	<i>Discrete Kalman Filter</i>	70
4.3.2.	<i>Computational Origins of the Filter</i>	72
4.3.3.	<i>The Discrete Kalman Filter Algorithm</i>	74
5	SIMULATIONS AND EXPERIMENTAL WORK	77
5.1.	SIMULATIONS	77
5.1.1.	<i>Comparison of MRAS Speed Estimator, Open Loop Speed Estimator and Kalman Filter Speed Estimators</i>	78
5.1.2.	<i>Speed Estimator Performance Verification</i>	81
5.2.	EXPERIMENTAL WORK	84
5.2.1.	<i>Experiments to Compare Speed Estimate with Actual Speed of Motor</i>	86
5.2.2.	<i>Experiments of the Speed Estimator in No-Load</i>	91
5.2.3.	<i>The Speed Estimator Performance under Loading</i>	104
6	CONCLUSION	121
	REFERENCES	123
	APPENDIX	128

LIST OF TABLES

Table 2-1 Power Bridge Output Voltages (V_{an} , V_{bn} , V_{cn}).....	35
Table 2-2 Stator Voltages in ($d^s q^s$) frame and related Voltage Vector	36
Table 2-3 Assigned duty cycles to the PWM outputs	41
Table 5-1 Simulation Parameters	77
Table 5-2 Loading measurements	105

LIST OF FIGURES

Figure 2-1 Magnetic axes of three phase induction machine.....	9
Figure 2-2 Relationship between the α , β and the abc quantities.....	16
Figure 2-3 Relationship between the dq and the abc quantities.....	17
Figure 2-4 Phasor diagram of the field oriented drive system.....	28
Figure 2-5 Field oriented induction motor drive system.....	28
Figure 2-6 Indirect field oriented drive system.....	29
Figure 2-7 Direct field oriented drive system.....	29
Figure 2-8 Circuit diagram of VSI.....	30
Figure 2-9 Eight switching state topologies of a voltage source inverter.....	31
Figure 2-10 First switching state V_1	32
Figure 2-11 Representation of topology V_1 in $(d^s q^s)$ plane.....	33
Figure 2-12 Non-zero voltage vectors in $(d^s q^s)$ plane.....	33
Figure 2-13 Representation of the zero voltage vectors in $(d^s q^s)$ plane.....	34
Figure 2-14 Voltage vectors.....	37
Figure 2-15 Projection of the reference voltage vector.....	38
Figure 3-1 Flux estimation structure.....	49
Figure 4-1 MRAS based speed estimator scheme using space vector.....	57
Figure 4-2 Coordinates in stationary reference frame.....	59
Figure 4-3 System structure of rotor speed observer using the tuning signal ϵ	60
Figure 4-4 Kalman filter cycle.....	75
Figure 4-5 The overall sensorless DFOC scheme.....	76
Figure 5-1 Comparison of performances of speed estimators for 250 rpm.....	78
Figure 5-2 Comparison of performances of speed estimators for 500 rpm.....	79
Figure 5-3 Comparison of performances of speed estimators for 1000 rpm.....	79
Figure 5-4 Comparison of performances of speed estimators for 1500 rpm.....	80
Figure 5-5 5rpm reference, Kalman filter performance verification.....	81
Figure 5-6 50rpm reference, Kalman filter performance verification.....	82
Figure 5-7 500rpm reference, Kalman filter performance verification.....	82
Figure 5-8 1000rpm reference, Kalman filter performance verification.....	83
Figure 5-9 1500rpm reference, Kalman filter performance verification.....	83
Figure 5-10 250rpm speed reference actual and estimated motor speeds.....	86

Figure 5-11 500rpm speed reference actual and estimated motor speeds.....	87
Figure 5-12 1000rpm speed reference actual and estimated motor speeds.....	87
Figure 5-13 1500rpm speed reference actual and estimated motor speeds.....	88
Figure 5-14 250rpm 0.1Hz sinusoidal speed reference actual and estimated motor speeds..	89
Figure 5-15 500rpm 0.1Hz sinusoidal speed reference actual and estimated motor speeds..	89
Figure 5-16 1000rpm 0.1Hz sinusoidal speed reference actual and estimated motor speeds	90
Figure 5-17 1500rpm 0.1Hz sinusoidal speed reference actual and estimated motor speeds	90
Figure 5-18 250rpm speed reference, motor phase currents.....	91
Figure 5-19 250rpm speed reference, motor phase voltages.....	92
Figure 5-20 250rpm speed reference, motor speed estimate.....	92
Figure 5-21 500rpm speed reference, motor phase currents.....	93
Figure 5-22 500rpm speed reference, motor phase voltages.....	93
Figure 5-23 500rpm speed reference, motor speed estimate.....	94
Figure 5-24 1000rpm speed reference, motor phase currents.....	94
Figure 5-25 1000rpm speed reference, motor phase voltages.....	95
Figure 5-26 1000rpm speed reference, motor speed estimate.....	95
Figure 5-27 1500rpm speed reference, motor phase currents.....	96
Figure 5-28 1500rpm speed reference, motor phase voltages.....	96
Figure 5-29 1500rpm speed reference, motor phase speed estimate	97
Figure 5-30 250rpm 0.1 Hz speed reference, motor phase currents	98
Figure 5-31 250rpm 0.1 Hz speed reference, motor phase voltages.....	98
Figure 5-32 250rpm 0.1 Hz speed reference, motor speed estimate.....	99
Figure 5-33 500rpm 0.1 Hz speed reference, motor phase current.....	99
Figure 5-34 500rpm 0.1 Hz speed reference, motor phase voltages.....	100
Figure 5-35 500rpm 0.1 Hz speed reference, motor speed estimate.....	100
Figure 5-36 1000rpm 0.1 Hz speed reference, motor phase current.....	101
Figure 5-37 1000rpm 0.1 Hz speed reference, motor phase voltages.....	101
Figure 5-38 1000rpm 0.1 Hz speed reference, motor speed estimate.....	102
Figure 5-39 1500rpm 0.1 Hz speed reference, motor phase current.....	102
Figure 5-40 1500rpm 0.1 Hz speed reference, motor phase voltages.....	103
Figure 5-41 1500rpm 0.1 Hz speed reference, motor speed estimate.....	103
Figure 5-42 Load system electrical block diagram.....	104
Figure 5-43 Kalman filter response improvement for better dynamic response.....	106
Figure 5-44 250rpm speed reference, motor phase currents constant under loading.....	107
Figure 5-45 250rpm speed reference, motor phase voltages constant under loading	107

Figure 5-46 250rpm speed reference, motor speed estimate constant under loading	108
Figure 5-47 500rpm speed reference, motor phase currents constant under loading	108
Figure 5-48 500rpm speed reference, motor phase voltages constant under loading	109
Figure 5-49 500rpm speed reference, motor speed estimate constant under loading	109
Figure 5-50 1000rpm speed reference, motor phase currents constant under loading	110
Figure 5-51 1000rpm speed reference, motor phase voltages under constant loading	110
Figure 5-52 1000rpm speed reference, motor speed estimate under constant loading	111
Figure 5-53 1500rpm speed reference, motor phase currents under constant loading	111
Figure 5-54 1500rpm speed reference, motor phase voltages under constant loading	112
Figure 5-55 1500rpm speed reference, motor speed estimate under constant loading	112
Figure 5-56 250rpm speed reference, motor phase currents under switched loading	113
Figure 5-57 250rpm speed reference, motor phase voltages under switched loading	114
Figure 5-58 250rpm speed reference, motor speed estimate under switched loading	114
Figure 5-59 500rpm speed reference, motor phase currents under switched loading	115
Figure 5-60 500rpm speed reference, motor phase voltages under switched loading	115
Figure 5-61 500rpm speed reference, motor speed estimate under switched loading	116
Figure 5-62 1000rpm speed reference, motor phase currents under switched loading	116
Figure 5-63 1000rpm speed reference, motor phase voltages under switched loading	117
Figure 5-64 1000rpm speed reference, motor speed estimate under switched loading	117
Figure 5-65 1500rpm speed reference, motor phase currents under switched loading	118
Figure 5-66 1500rpm speed reference, motor phase voltages under switched loading	118
Figure 5-67 1500rpm speed reference, motor speed estimate under switched loading	119
Figure A-1 The Experimental Set Up	130
Figure A-2 The Experimental Set Up Block Diagram	131
Figure A-3 Drive System software Matlab Simulink Block Diagram	132

LIST OF SYMBOLS

SYMBOL

e_{md}	Back emf d-axis component
e_{mq}	Back emf q-axis component
i_{ds}^e	d-axis stator current in synchronous frame
i_{qs}^e	q-axis stator current in synchronous frame
i_{ds}^s	d-axis stator current in stationary frame
i_{qs}^s	q-axis stator current in stationary frame
i_{ar}	Phase-a rotor current
i_{br}	Phase-b rotor current
i_{cr}	Phase-c rotor current
i_{as}	Phase-a stator current
i_{bs}	Phase-b stator current
i_{cs}	Phase-c stator current
L_m	Magnetizing inductance
L_{ls}	Stator leakage inductance
L_{lr}	Rotor leakage inductance
L_s	Stator self inductance
L_r	Rotor self inductance
K_k	Kalman gain
P_k	Kalman filter error covariance matrix
q_{md}	Reactive power d-axis component
q_{mq}	Reactive power q-axis component
R_s	Stator resistance
R_r	Referred rotor resistance
T_{em}	Electromechanical torque
τ_r	Rotor time-constant
V_{as}	Phase-a stator voltage
V_{bs}	Phase-b stator voltage
V_{cs}	Phase-c stator voltage

V_{ar}	Phase-a rotor voltage
V_{br}	Phase-b rotor voltage
V_{cr}	Phase-c rotor voltage
V_{ds}^s	d-axis stator voltage in stationary frame
V_{qs}^s	q-axis stator voltage in stationary frame
V_{ds}^e	d-axis stator voltage in synchronous frame
V_{qs}^e	q-axis stator voltage in synchronous frame
V_{dc}	DC-link voltage
w_e	Angular synchronous speed
w_r	Angular rotor speed
w_{sl}	Angular slip speed
x_k	Kalman filter a priori state estimate
\hat{x}_k	Kalman filter a posteriori state estimate
z_k	Kalman filter measurement
θ_e	Angle between the synchronous frame and the stationary frame
θ_d	Angle between the synchronous frame and the stationary frame when d-axis is leading
θ_q	Angle between the synchronous frame and the stationary frame when q-axis is leading
$\theta_{\psi r}$	Rotor flux angle
ψ_{ds}^s	d-axis stator flux in stationary frame
ψ_{qs}^s	q-axis stator flux in stationary frame
ψ_{ds}^e	d-axis stator flux in synchronous frame
ψ_{qs}^e	q-axis stator flux in synchronous frame
ψ_{as}	Phase-a stator flux
ψ_{bs}	Phase-b stator flux
ψ_{cs}	Phase-c stator flux
ψ_{ar}	Phase-a rotor flux
ψ_{br}	Phase-b rotor flux
ψ_{cr}	Phase-c rotor flux

CHAPTER 1

INTRODUCTION

1.1. Introduction to Induction Machine Control Literature

Induction machines have many advantages over other types of electrical machines. They are relatively rugged and inexpensive. They do not have brushes like DC machines and not require periodic maintenance, and their compact structure is insensitive to environment conditions. Therefore much attention is given to control for induction machines, but, due to their non-linear and complex mathematical model, an induction machine requires more sophisticated control techniques compared to DC motors. For long time, open-loop V/f control which adjusts a constant volts-per-Hertz ratio of the stator voltage is used, however, dynamic performance of this type of control methods was unsatisfactory because of saturation effect and the electrical parameter variation with temperature. Recent improvements with lower loss and fast switching semiconductor power switches on power electronics, fast and powerful digital signal processors on controller technology made advanced control techniques of induction machine drives applicable.

1.2. The Field Oriented Control of Induction Machines

The most common induction motor drive control scheme is the field oriented control (FOC). The field oriented control consists of controlling the stator currents represented by a vector. This control is based on projections which transform a three phase time and speed dependent system into a two co-ordinate (d and q co-ordinates) time invariant system. These projections lead to a structure similar to that of a DC machine control.

Moreover, flux and speed estimation are main issues on the field oriented control in the recent years. The induction machine drives without mechanical speed sensors have the attractions of low cost and high reliability. Estimating the magnitude and spatial orientation of the flux in the stator or rotor is also required for such drives.

Rotor flux field orientation is divided mainly into two. These are the direct field orientation, which relies on direct measurement and estimation of rotor flux magnitude and angle, and the indirect field orientation, which utilizes slip relation. Indirect field orientation is a feedforward approach and is naturally parameter sensitive, especially to the rotor time constant. This has led to numerous parameter adapting strategies. [1]- [7]

Direct field oriented control (DFOC) uses flux angle θ_e which is calculated by sensing the air-gap flux with the flux sensing coils. This adds to the cost and complexity of the drive system. To avoid from using these flux sensors on the induction machine drive systems, many different algorithms are proposed for last three decades, to estimate both the rotor flux vector and/or rotor shaft speed. The recent trend in field-oriented control is towards avoiding the use of speed sensors and using algorithms based on the terminal quantities of the machine for the estimation of the fluxes.

Saliency based with fundamental or high frequency signal injection is one of these above referred flux and speed estimation techniques (algorithms). The advantage of the saliency technique is that the saliency is not sensitive to actual motor parameters, however this method does not have sufficient performance at low and zero speed level. Also, when applied with high frequency signal injection, the method may cause torque ripples, vibration and audible noise [8].

1.3. Induction Machine Flux Observation

The special flux sensors and coils can be avoided by estimating the rotor flux from the terminal quantities (stator voltages and currents) [9]. This technique requires the knowledge of the stator resistance along with the stator-leakage, and rotor-leakage

inductances and the magnetizing inductance. The method is commonly known as the Voltage Model Flux Observer (VMFO).

Voltage Model Flux Observer utilizes the measured stator voltage and current and requires a pure integration without feedback. Thus it is difficult to implement them for low excitation frequencies due to the offset and initial condition problems. Due to the lack of feedback which is necessary for convergence, low pass filter is often used to provide stability in practice. Accuracy of voltage model based observer is completely insensitive to rotor resistance but is most sensitive to stator resistance at low velocities. At high velocities the stator resistance IR drop is less significant relative to the speed voltage. This reduces sensitivity to stator resistance. The study of parameter sensitivity shows that the leakage inductance can significantly affect the system performance regarding to stability, dynamic response and utilization of the machine and the inverter.

To overcome the problems caused by the changes in leakage inductance and stator resistance at low speed the Current Model Flux Observer (CMFO) is introduced as alternative approach. Current model based observers use the measured stator currents and rotor velocity. The velocity dependency of the current model is a drawback since this means that even though using the estimated flux eliminates the flux sensor, position sensor is still required. Furthermore, at zero or low speed operation rotor flux magnitude response is sensitive primarily to the rotor resistance, although the phase angle is insensitive to all parameters. Near rated slip, both of them are sensitive to the rotor resistance and magnetizing inductance. In whole speed range accuracy is unaffected by the rotor leakage inductance.

Moreover, there is an estimator type based on pole/zero cancellation. In these methods approximate differentiation of signals is used to cancel the effects of integration. Due to differentiation, such approaches are insensitive to measurement and quantization noise. A full order open-loop observer on the other hand can be formed using only the measured stator voltage and rotor velocity as inputs where the stator current appears as an estimated quantity. Because of its dependency on the stator current estimation, the full order observer will not exhibit better performance

than the current model. Furthermore, parameter sensitivity and observer gain are the problems to be tuned in a full order observer design [10].

The observer structures above are open-loop schemes, based on the induction machine model and they do not use any feedback. Therefore, they are quite sensitive to parameter variations.

A method which provides a smooth transition between current and voltage models was developed by Takahashi and Noguchi. They combined two stator flux models via a first order lag-summing network [11]. Inputs of the current model are measured stator currents and rotor position. The current model is implemented in rotor flux frame because; implementation in stationary frame requires measured rotor velocity. Transformation to the rotor flux frame permits the use of rotor position instead of velocity. Voltage model utilizes measured stator voltages and currents. The smooth transition between current and voltage models flux estimates is governed by rotor flux regulator. A rotor-flux-regulated and oriented system is sensitive to leakage inductance under high slip operation. Both stator-flux-regulated, oriented systems have reduced parameter sensitivity.

A smooth and deterministic transition between flux estimates produced by current and voltage models is given in closed-loop observer approach proposed in [12] [13] [14] which combines the best accuracy attributes of current and voltage models. In [15] stator-flux-regulated, rotor-flux-oriented closed-loop observer is used for direct torque control (DTC) algorithm. The fluxes obtained by current model are compared with those obtained by the voltage model with reference to the current model, or the current model with reference to the voltage model according to the range in which one of these models is superior to other [22].

1.4. Induction Machine Speed Estimation

The torque control problem is overcome in DTC algorithm but to achieve good speed response, rotor speed also must be known. Verghese have approached speed estimation problem from a parameter identification point of view [16] [17] [18]. The

idea is to consider the speed as an unknown constant parameter, and to find the estimated speed that best fits the measured or calculated data to the dynamic equations of the motor. However, parameter variations have significant impact on performance of the estimator. Possible stator resistance variation due to ohmic heating results in deterioration in performance [19].

The method proposed in [20] [21] estimates the speed without assuming that the speed is slowly varying compared to electrical variables studied on non-linear method. They constructed two estimators; main flux estimator and complementary flux estimator. Main flux estimator could not guarantee convergence for all operating conditions. In these operating conditions such as start up complementary estimator is used. Significant sensitivity to parameter uncertainty is observed with this method.

Speed estimator based on Model Reference Adaptive System (MRAS) is studied in [23] [24]. In MRAS, in general a comparison is made between the outputs of two estimators. The estimator which does not contain the quantity to be estimated can be considered as a reference model of the induction machine. The other one, which contains the estimated quantity, is considered as an adjustable model. The error between these two estimators is used as an input to an adaptation mechanism. For sensorless control algorithms most of the times the quantity which differ the reference model from the adjustable model is the rotor speed. When the estimated rotor speed in the adjustable model is changed in such a way that the difference between two estimators converges to zero asymptotically, the estimated rotor speed will be equal to actual rotor speed. In [25], [26], [27] voltage model is assumed as reference model, current model is assumed as the adjustable model and estimated rotor flux is assumed as the reference parameter to be compared. In [24] similar speed estimators are proposed based on the MRAS and a secondary variable is introduced as the reference quantity by putting the rotor flux through a first-order delay instead of a pure integration to nullify the offset. However their algorithm produces inaccurate estimated speed if the excitation frequency goes below certain level. In addition these algorithms suffer from the machine parameter uncertainties because of the reference model since the parameter variation in the reference model

cannot be corrected. [23] Suggests an alternative MRAS based on the electromotive force rather than rotor flux as reference quantity for speed estimation where the integration problem has been overcome. Further in [23], another new auxiliary variable is introduced which represents the instantaneous reactive power for maintaining the magnetizing current. In this MRAS algorithm stator resistance disappears from the equations making the algorithm robust to that parameter.

This work is mainly focused on estimating rotor flux angle by model reference adaptive system and estimating rotor speed by Kalman filter technique. A combination of well-known open-loop observers, voltage model and current model is used to estimate the rotor flux angle and speed which are employed in direct field orientation. For the speed estimation reactive power MRAS speed estimator, open loop speed estimator and Kalman Filter speed estimator using flux angle estimate of the flux observer compared in simulations utilizing real data of closed-speed loop running system. Moreover, closed-speed performance of induction motor system using Kalman filter as speed estimator and adaptive flux estimator as flux observer is verified for whole speed range with no-load and with loading conditions.

1.5. Structure of the Chapters

Chapter 2 presents the induction machine modeling and dynamical mathematical model of the machine in different reference frames. Space vector pulse width modulation technique is given. Also, field oriented control structure is described.

Chapter 3 is related to the adaptive flux estimator and its implementation. Voltage model and current model are explained in detail.

Chapter 4 devoted to speed estimation techniques for sensorless direct field oriented control of induction machine. MRAS speed estimator, open-loop speed estimator and Kalman filter speed estimator are described.

Chapter 5 demonstrates the performance closed-loop speed control of the induction motor drive system by the simulations and experimental analysis. The comparison of the speed estimators are studied in simulations. Moreover, both no-load and with

load tests are conducted for drive system to observe performance of the vector control and that of estimation.

Chapter 6 summarizes the overall study done in the scope of the thesis and concludes the performance of the closed speed loop vector controlled induction motor.

CHAPTER 2

INDUCTION MACHINE MODELING, FIELD ORIENTED CONTROL and PWM with SPACE VECTOR THEORY

This chapter focuses on the, modeling of the induction machine for different reference frames. The state equations of induction machine, which are necessary to develop observers explained in the next chapters are described. Moreover, field orientation is introduced. Finally, the space vector PWM technique is explained in detail.

2.1. System Equations in the Stationary a,b,c Reference Frame

In particular we will assume the winding configuration shown in the Figure 2-1. In this case the winding placement is only conceptually shown with the center line of equivalent inductors directed along the magnetic axes of the windings. An elementary two pole machine is considered. Balanced 3ph windings are assumed for both stator and rotor. That is all 3 stator windings designated as the a_s , b_s and c_s windings are assumed to have the same number of effective turns, N_s , and the b_s and c_s windings are symmetrically displaced from the a_s winding by $\pm 120^\circ$. The subscript 's' is used to denote that these windings are stator or stationary windings. The rotor windings are similarly arranged but have N_r turns. These windings are designated by a_r , b_r and c_r in which second subscript reminds us that these three windings are rotor or rotating windings.

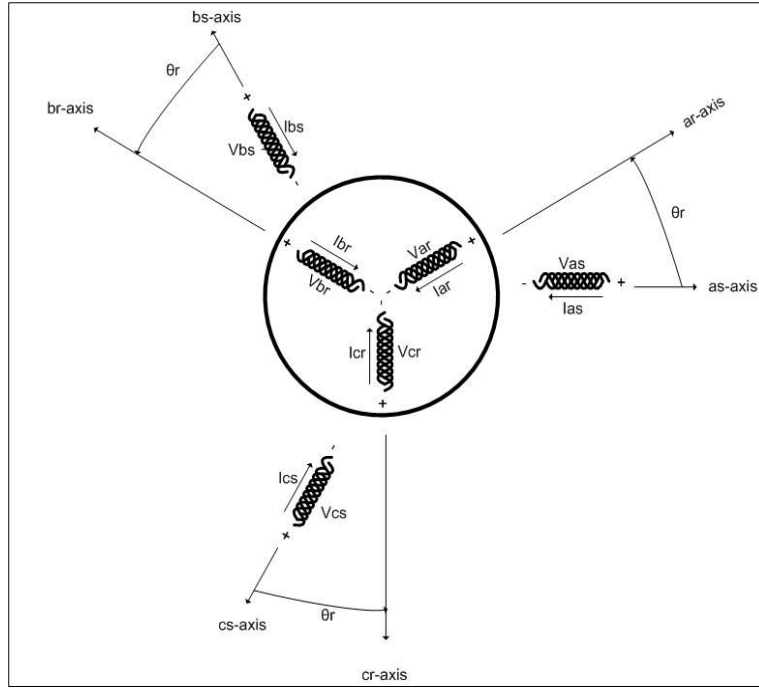


Figure 2-1 Magnetic axes of three phase induction machine

The voltage equations describing the stator and rotor circuits can be written conveniently in the matrix form as

$$\begin{aligned}
 v_{abcs} &= r_s i_{abcs} + \frac{d\psi_{abcs}}{dt} \\
 v_{abcr} &= r_r i_{abcr} + \frac{d\psi_{abcr}}{dt}
 \end{aligned}
 \tag{2-1}$$

v_{abcs} , i_{abcs} and ψ_{abcs} are 3x1 vectors defined by

$$v_{abcs} = \begin{bmatrix} v_{as} \\ v_{bs} \\ v_{cs} \end{bmatrix}; \quad i_{abcs} = \begin{bmatrix} i_{as} \\ i_{bs} \\ i_{cs} \end{bmatrix}; \quad \psi_{abcs} = \begin{bmatrix} \psi_{as} \\ \psi_{bs} \\ \psi_{cs} \end{bmatrix}
 \tag{2-2}$$

Similar definitions apply for the rotor variables v_{abcr} , i_{abcr} and ψ_{abcr} .

In general coupling clearly exists between all of the stator and rotor phases. The flux linkages are therefore related to the machine currents by the following matrix equation.

$$\Psi_{abc} = \Psi_{abc(s)} + \Psi_{abc(r)} \quad (2-3)$$

$$\Psi_{abc} = \Psi_{abc(s)} + \Psi_{abc(r)}$$

where

$$\Psi_{abc(s)} = \begin{bmatrix} L_{as} & L_{abs} & L_{acs} \\ L_{abs} & L_{bs} & L_{bcs} \\ L_{acs} & L_{bcs} & L_{cs} \end{bmatrix} i_{abc} \quad (2-4)$$

$$\Psi_{abc(r)} = \begin{bmatrix} L_{as,ar} & L_{as,br} & L_{as,cr} \\ L_{bs,ar} & L_{bs,br} & L_{bs,cr} \\ L_{cs,ar} & L_{cs,br} & L_{cs,cr} \end{bmatrix} i_{abc} \quad (2-5)$$

$$\Psi_{abc(r)} = \begin{bmatrix} L_{ar} & L_{abr} & L_{acr} \\ L_{abr} & L_{br} & L_{bcr} \\ L_{acr} & L_{bcr} & L_{cr} \end{bmatrix} i_{abc} \quad (2-6)$$

$$\Psi_{abc(s)} = \begin{bmatrix} L_{ar,as} & L_{ar,bs} & L_{ar,cs} \\ L_{br,as} & L_{br,bs} & L_{br,cs} \\ L_{cr,as} & L_{cr,bs} & L_{cr,cs} \end{bmatrix} i_{abc} \quad (2-7)$$

Note that as a result of reciprocity, the inductance matrix in the third flux linkage equation, (2-7), above is simply transpose of the inductance matrix in the second equation, (2-5), because, mutual inductances are equal. (i.e., $L_{as,br} = L_{br,as}$)

2.1.1. Determination of Induction Machine Inductances

While the number of inductances defined is large, task of solving for all of these inductances is straightforward.

The mutual inductance between winding x and winding y is calculated according to equation

$$L_{xy} = \mu_0 N_x N_y \left(\frac{rl}{g} \right) \left(\frac{\pi}{4} \right) \cos \alpha \quad (2-8)$$

Where r is radius, l is length of the motor and g is the length of airgap. N_x is the number of effective turns of the winding x and N_y is the number of effective turns of the winding y . Notice that alpha is the angle between magnetic axes of the phases x and y .

The self inductance of stator phase as is obtained by simply setting $\alpha=0$, and by setting N_x and N_y in (2-8) to N_s . Whereby,

$$L_{am} = \mu_0 N_s^2 \left(\frac{rl}{g} \right) \left(\frac{\pi}{4} \right) \quad (2-9)$$

The subscript m is again used to denote the fact that this inductance is magnetizing inductance. That is, it is associated with flux lines which cross the air gap and link rotor as well as stator windings. In general, it is necessary to add a relatively small, but important, leakage term to (2-9) to account for leakage flux. This term accounts for flux lines which do not cross the gap but instead close with the stator slot itself (slot leakage), in the air gap (belt and harmonic leakage) and at the ends of the machine (end winding leakage). Hence, the total self inductance of phase as can be expressed.

$$L_{as} = L_{ls} + L_{am} \quad (2-10)$$

where L_{ls} represents the leakage term. Since the windings of the bs and the cs phases are identical to phase as , it is clear that the magnetizing inductances of these windings are the same as phase as so that, also

$$L_{bs} = L_{ls} + L_{bm} \quad (2-11)$$

$$L_{cs} = L_{ls} + L_{cm}$$

It is apparent that L_{am} , L_{bm} , L_{cm} are equal making the self inductances also equal. It is therefore useful to define stator magnetizing inductance

$$L_{ms} = \mu_0 N_s^2 \left(\frac{rl}{g} \right) \left(\frac{\pi}{4} \right) \quad (2-12)$$

so that

$$L_{as} = L_{bs} = L_{cs} = L_{ls} + L_{ms} \quad (2-13)$$

The mutual inductance between phases as and bs , bs and cs , and cs and as are derived by simply setting $\alpha=2\pi/3$ and $N_x=N_y=N_s$ in (2-8). The result is

$$L_{abs} = L_{bcs} = L_{cas} = -\mu_0 N_s^2 \left(\frac{rl}{g} \right) \left(\frac{\pi}{8} \right) \quad (2-14)$$

or, in terms of (2-12),

$$L_{abs} = L_{bcs} = L_{cas} = -\frac{L_{ms}}{2} \quad (2-15)$$

The flux linkages of phases as , bs and cs resulting from currents flowing in the stator windings can now be expressed in matrix form as

$$\psi_{abc(s)} = \begin{bmatrix} L_{ls} + L_{ms} & -\frac{L_{ms}}{2} & -\frac{L_{ms}}{2} \\ -\frac{L_{ms}}{2} & L_{ls} + L_{ms} & -\frac{L_{ms}}{2} \\ -\frac{L_{ms}}{2} & -\frac{L_{ms}}{2} & L_{ls} + L_{ms} \end{bmatrix} i_{abc} \quad (2-16)$$

Let us now turn our attention to the mutual coupling between the stator and rotor windings. Referring to Figure 2-1, we can see that the rotor phase ar is displaced by stator phase as by the electrical angle θ_r where θ_r in this case is a variable. Similarly the rotor phases br and cr are displaced from stator phases bs and cs respectively by θ_r . Hence, the corresponding mutual inductances can be obtained by setting $N_x=N_s$, $N_y=N_r$, and $\alpha=\theta_r$ in (2-8).

$$\begin{aligned} L_{as,ar} = L_{bs,br} = L_{cs,cr} &= \mu_0 N_s N_r \left(\frac{rl}{g} \right) \left(\frac{\pi}{4} \right) \cos \theta_r \\ &= \frac{N_r}{N_s} L_{ms} \cos \theta_r \end{aligned} \quad (2-17)$$

The angle between the as and br phases is $\theta_r + 2\pi/3$, so that

$$L_{as,br} = L_{bs,cr} = L_{cs,ar} = \frac{N_r}{N_s} L_{ms} \cos(\theta_r + 2\pi/3) \quad (2-18)$$

Finally, the stator phase as is displaced from the rotor cr phase by angle $\theta_r - 2\pi/3$. Therefore,

$$L_{as,cr} = L_{bs,ar} = L_{cs,br} = \frac{N_r}{N_s} L_{ms} \cos(\theta_r - 2\pi/3) \quad (2-19)$$

The above inductances can now be used to establish the flux linking the stator phases due to currents in the rotor circuits. In matrix form,

$$\Psi_{abcs(r)} = \frac{N_r}{N_s} L_{ms} \begin{bmatrix} \cos \theta_r & \cos(\theta_r + 2\pi/3) & \cos(\theta_r - 2\pi/3) \\ \cos(\theta_r - 2\pi/3) & \cos \theta_r & \cos(\theta_r + 2\pi/3) \\ \cos(\theta_r + 2\pi/3) & \cos(\theta_r - 2\pi/3) & \cos \theta_r \end{bmatrix} i_{abcr} \quad (2-20)$$

The total flux linking the stator windings is clearly the sum of the contributions from the stator and the rotor circuits, (2-16) and (2-20),

$$\Psi_{abcs} = \Psi_{abcs(s)} + \Psi_{abcs(r)} \quad (2-21)$$

It is not difficult to continue the process to determine the rotor flux linkages. In terms of previously defined quantities, the flux linking the rotor circuit due to rotor currents is

$$\Psi_{abcr(r)} = \begin{bmatrix} L_{lr} + \left(\frac{N_r}{N_s}\right)^2 L_{ms} & -\frac{1}{2}\left(\frac{N_r}{N_s}\right)^2 L_{ms} & -\frac{1}{2}\left(\frac{N_r}{N_s}\right)^2 L_{ms} \\ -\frac{1}{2}\left(\frac{N_r}{N_s}\right)^2 L_{ms} & L_{lr} + \left(\frac{N_r}{N_s}\right)^2 L_{ms} & -\frac{1}{2}\left(\frac{N_r}{N_s}\right)^2 L_{ms} \\ -\frac{1}{2}\left(\frac{N_r}{N_s}\right)^2 L_{ms} & -\frac{1}{2}\left(\frac{N_r}{N_s}\right)^2 L_{ms} & L_{lr} + \left(\frac{N_r}{N_s}\right)^2 L_{ms} \end{bmatrix} i_{abcr} \quad (2-22)$$

where L_{lr} is the rotor leakage inductance. The flux linking the rotor windings due to currents in the stator circuit is

$$\Psi_{abcr(s)} = \frac{N_r}{N_s} L_{ms} \begin{bmatrix} \cos \theta_r & \cos(\theta_r - 2\pi/3) & \cos(\theta_r + 2\pi/3) \\ \cos(\theta_r + 2\pi/3) & \cos \theta_r & \cos(\theta_r - 2\pi/3) \\ \cos(\theta_r - 2\pi/3) & \cos(\theta_r + 2\pi/3) & \cos \theta_r \end{bmatrix} i_{abcs} \quad (2-23)$$

Note that the matrix of (2-23) is the transpose of (2-20).

The total flux linkages of the rotor windings are again the sum of the two components defined by (2-22) and (2-23), that is

$$\Psi_{abc} = \Psi_{abc(r)} + \Psi_{abc(s)} \quad (2-24)$$

2.1.2. Three-Phase to Two-Phase Transformations

It is apparent that extensive amount of coupling between the six circuits makes the analysis of this machine a rather formidable task. However we are now in position to determine if there is any simplification that can be expected between these coupled equations.

In the study of generalized machine theory, mathematical transformations are often used to decouple variables, to facilitate the solutions of difficult equations with time varying coefficients, or to refer all variables to a common reference frame. For this purpose, the method of symmetrical components uses a complex transformation to decouple the abc phase variables:

$$[f_{012}] = [T_{012}][f_{abc}] \quad (2-25)$$

The variable, f_{abc} in (2-25) may be the three-phase ac currents, voltages or fluxes. The subscripts a, b and c indicate three distinct phases of three phase systems. The transformation is given by:

$$[T_{012}] = \frac{1}{3} \begin{bmatrix} 1 & 1 & 1 \\ 1 & a & a^2 \\ 1 & a^2 & a \end{bmatrix} \quad (2-26)$$

where $a = e^{j\frac{2\pi}{3}}$. Its inverse is given by:

$$[T_{012}]^{-1} = \frac{1}{3} \begin{bmatrix} 1 & 1 & 1 \\ 1 & a^2 & a \\ 1 & a & a^2 \end{bmatrix} \quad (2-27)$$

The symmetrical component transformation is applicable to steady-state vectors or instantaneous quantities equally. The important subsets of general n -phase to two phase transformation are briefly introduced in the following subsections.

2.1.2.1. The Clarke Transformation

[41] The stationary two-phase variables of the Clarke's transformation are denoted as α, β . α -axis coincides with a -axis and β -axis lags the α -axis by $\frac{\pi}{2}$ as in Figure 2-2.

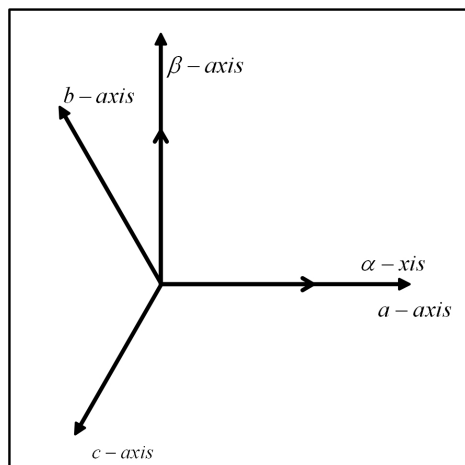


Figure 2-2 Relationship between the α, β and the abc quantities

Then the transform is given as:

$$[f_{\alpha\beta 0}] = [T_{\alpha\beta 0}][f_{abc}] \quad (2-28)$$

where the transformation matrix is given as

$$[T_{\alpha\beta 0}] = \frac{2}{3} \begin{bmatrix} 1 & -\frac{1}{2} & -\frac{1}{2} \\ 0 & \frac{\sqrt{3}}{2} & -\frac{\sqrt{3}}{2} \\ \frac{1}{2} & \frac{1}{2} & \frac{1}{2} \end{bmatrix} \quad (2-29)$$

And its inverse is:

$$[T_{\alpha\beta 0}]^{-1} = \begin{bmatrix} 1 & 0 & 1 \\ -\frac{1}{2} & \frac{\sqrt{3}}{2} & 1 \\ -\frac{1}{2} & -\frac{\sqrt{3}}{2} & 1 \end{bmatrix} \quad (2-30)$$

2.1.2.2. The Park Transformation

The Park's transformation is a well known three-phase to two-phase transformation. The transformation transforms three-phase quantities f_{abc} into two-phase quantities developed on a rotating $dq\theta$ axes system, whose speed is w as shown in the Figure 2-3.

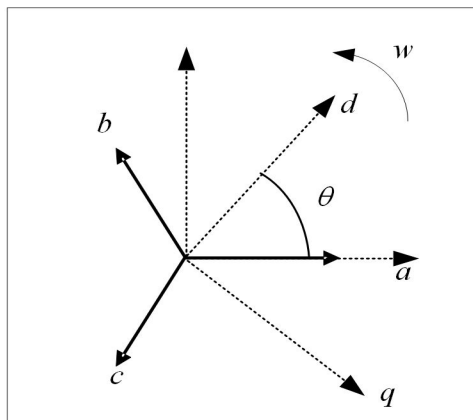


Figure 2-3 Relationship between the *dq* and the *abc* quantities

$$[f_{dq0}] = [T_{dq0}(\theta)][f_{abc}] \quad (2-31)$$

where the $dq0$ transformation matrix is defined as:

$$[T_{dq0}(\theta)] = \frac{2}{3} \begin{bmatrix} \cos \theta & \cos\left(\theta - \frac{2\pi}{3}\right) & \cos\left(\theta + \frac{2\pi}{3}\right) \\ -\sin \theta & -\sin\left(\theta - \frac{2\pi}{3}\right) & -\sin\left(\theta + \frac{2\pi}{3}\right) \\ \frac{1}{2} & \frac{1}{2} & \frac{1}{2} \end{bmatrix} \quad (2-32)$$

and the inverse is given by:

$$[T_{dq0}(\theta)]^{-1} = \begin{bmatrix} \cos \theta & -\sin \theta & 1 \\ \cos\left(\theta - \frac{2\pi}{3}\right) & -\sin\left(\theta - \frac{2\pi}{3}\right) & 1 \\ \cos\left(\theta + \frac{2\pi}{3}\right) & -\sin\left(\theta + \frac{2\pi}{3}\right) & 1 \end{bmatrix} \quad (2-33)$$

where θ is the angle between the phases a and d . Notice that, θ is time integral of ω , which is the rotation speed of the dq reference frame and it is chosen arbitrarily for the sake of generality.

2.1.3. Circuit Equations in Arbitrary dq0 Reference Frame

The $dq0$ reference frames are usually selected on the basis of conveniences or computational reduction. The two common reference frames used in the analysis of induction machine are the stationary frame (i.e. $\omega = 0$), with a frame notation $d^s q^s$, and synchronously rotating frame (i.e. $\omega = \omega_s$, synchronous speed), with a frame notation $d^e q^e$. Each has an advantage for some purpose. In the stationary reference frame, the $d^s q^s$ variables of the machine are in the same frame as those normally used

for the supply network. In the synchronously rotating frame, the $d^e q^e$ variables are dc in steady state. First of all, the equations of the induction machine in the arbitrary reference frame, which is rotating at a speed ω , in the direction of the rotor rotation, will be derived. When the induction machine runs in the stationary frame, these equations of the induction machine, can then be obtained by setting $\omega = 0$. These equations can also be obtained in the synchronously rotating frame by setting $\omega = \omega_e$.

2.1.3.1. qd0 Voltage Equations

In matrix notation, the stator winding abc voltage equations can be expressed as:

$$v_{abc} = r_s i_{abc} + \frac{d\psi_{abc}}{dt} \quad (2-34)$$

Applying the transformations given in (2-32) and (2-33), to the voltage, current and flux linkages, (2-34) becomes

$$v_{dq0s} = [T_{qd0}(\theta)] \frac{d \left([T_{qd0}(\theta)]^{-1} [\psi_{dq0s}] \right)}{dt} + [T_{qd0}(\theta)] r_s \left([T_{qd0}(\theta)]^{-1} [i_{dq0s}] \right) \quad (2-35)$$

applying the chain rule in (2-35)

$$v_{dq0s} = [T_{qd0}(\theta)] \left\{ \left(\frac{d[T_{qd0}(\theta)]^{-1}}{dt} \right) [\psi_{dq0s}] + [T_{qd0}(\theta)]^{-1} \left(\frac{d[\psi_{dq0s}]}{dt} \right) \right\} + r_s [T_{qd0}(\theta)] [T_{qd0}(\theta)]^{-1} [i_{dq0s}] \quad (2-36)$$

which is equal to

$$v_{dq0s} = [T_{qd0}(\theta)] \left(\frac{d[T_{qd0}(\theta)]^{-1}}{dt} \right) [\psi_{dq0s}] + [T_{qd0}(\theta)] [T_{qd0}(\theta)]^{-1} \left(\frac{d[\psi_{dq0s}]}{dt} \right) + r_s [T_{qd0}(\theta)] [T_{qd0}(\theta)]^{-1} [i_{dq0s}] \quad (2-37)$$

Note that

$$[T_{dq0}] \left(\frac{d[T_{dq0}]^{-1}}{dt} \right) = \frac{d\theta}{dt} \begin{bmatrix} 0 & 1 & 0 \\ -1 & 0 & 0 \\ 0 & 0 & 0 \end{bmatrix} \quad (2-38)$$

Then (2-37) becomes:

$$v_{dq0s} = w \begin{bmatrix} 0 & 1 & 0 \\ -1 & 0 & 0 \\ 0 & 0 & 0 \end{bmatrix} \psi_{dq0s} + \frac{d\psi_{dq0s}}{dt} + r_{dq0s} i_{dq0s} \quad (2-39)$$

where

$$w = \frac{d\theta}{dt} \quad \text{and} \quad r_{dq0s} = r_s \begin{bmatrix} 1 & 0 & 0 \\ 0 & 1 & 0 \\ 0 & 0 & 1 \end{bmatrix} \quad (2-40)$$

Likewise, the rotor voltage equation becomes:

$$v_{dq0r} = (w - w_r) \begin{bmatrix} 0 & 1 & 0 \\ -1 & 0 & 0 \\ 0 & 0 & 0 \end{bmatrix} \psi_{dq0r} + \frac{d\psi_{dq0r}}{dt} + r_{dq0r} i_{dq0r} \quad (2-41)$$

2.1.3.2. qd0 Flux Linkage Relation

The stator qd0 flux linkages are obtained by applying $[T_{qd0}(\theta)]$ to the stator abc flux linkages equation.

$$\psi_{dq0s} = [T_{qd0}(\theta)]\psi_{abcs} \quad (2-42)$$

referring (2-21), (2-42) is written as

$$\psi_{dq0s} = [T_{qd0}(\theta)](\psi_{abcs(s)} + \psi_{abcs(r)}) \quad (2-43)$$

putting (2-22) and (2-23) into (2-43);

$$\begin{aligned} \psi_{dq0s} = & [T_{dq0}(\theta)] \begin{bmatrix} L_{ls} + L_{ms} & -\frac{L_{ms}}{2} & -\frac{L_{ms}}{2} \\ -\frac{L_{ms}}{2} & L_{ls} + L_{ms} & -\frac{L_{ms}}{2} \\ -\frac{L_{ms}}{2} & -\frac{L_{ms}}{2} & L_{ls} + L_{ms} \end{bmatrix} i_{abcs} \\ & + [T_{dq0}(\theta)] \frac{N_r}{N_s} L_{ms} \begin{bmatrix} \cos\theta_r & \cos(\theta_r + 2\pi/3) & \cos(\theta_r - 2\pi/3) \\ \cos(\theta_r - 2\pi/3) & \cos\theta_r & \cos(\theta_r + 2\pi/3) \\ \cos(\theta_r + 2\pi/3) & \cos(\theta_r - 2\pi/3) & \cos\theta_r \end{bmatrix} i_{abcr} \end{aligned} \quad (2-44)$$

skipping the transformation steps the stator and the rotor flux linkage relationships can be expressed compactly:

$$\begin{bmatrix} \psi_{qs} \\ \psi_{ds} \\ \psi_{0s} \\ \psi'_{qr} \\ \psi'_{dr} \\ \psi'_{0r} \end{bmatrix} = \begin{bmatrix} L_s & 0 & 0 & L_m & 0 & 0 \\ 0 & L_s & 0 & 0 & L_m & 0 \\ 0 & 0 & L_{ls} & 0 & 0 & 0 \\ L_m & 0 & 0 & L'_r & 0 & 0 \\ 0 & L_m & 0 & 0 & L'_r & 0 \\ 0 & 0 & 0 & 0 & 0 & L'_{lr} \end{bmatrix} \begin{bmatrix} i_{qs} \\ i_{ds} \\ i_{0s} \\ i'_{qr} \\ i'_{dr} \\ i'_{0r} \end{bmatrix} \quad (2-45)$$

Where primed quantities denote referred values to the stator side.

$$L_s = L_{ls} + L_m \quad (2-46)$$

$$L'_r = L'_{lr} + L_m$$

and

$$L_m = \frac{3}{2} L_{ms} = \frac{3}{2} N_s^2 \left(\mu_0 \frac{rl}{g} \right) \frac{\pi}{4}, \quad L'_{lr} = \left(\frac{N_s}{N_r} \right)^2 L_{lr} \quad (2-47)$$

2.1.3.3. qd0 Torque Equations

The sum of the instantaneous input power to all six windings of the stator and rotor is given by:

$$P_{in} = v_{as} i_{as} + v_{bs} i_{bs} + v_{cs} i_{cs} + v'_{ar} i'_{ar} + v'_{br} i'_{br} + v'_{cr} i'_{cr} \quad W \quad (2-48)$$

in terms of dq quantities

$$P_{in} = \frac{3}{2} (v_{qs} i_{qs} + v_{ds} i_{ds} + 2v_{0s} i_{0s} + v'_{qr} i'_{qr} + v'_{dr} i'_{dr} + 2v'_{0r} i'_{0r}) \quad W \quad (2-49)$$

Using stator and rotor voltages to substitute for the voltages on the right hand side of (2-49), we obtain three kinds of terms: $i^2 r$, $i \frac{d\psi}{dt}$, and $w\psi i$. $i^2 r$ terms are the copper losses. The $i \frac{d\psi}{dt}$ terms represent the rate of exchange of magnetic field energy between windings. The electromechanical torque developed by the machine is given by the sum of the $w\psi i$ terms divided by mechanical speed, that is:

$$T_{em} = \frac{3}{2} \frac{p}{2w_r} \left[w(\psi_{ds} i_{qs} - \psi_{qs} i_{ds}) + (w - w_r)(\psi'_{dr} i'_{qr} - \psi'_{qr} i'_{dr}) \right] \quad Nm \quad (2-50)$$

using the flux linkage relationships one can show that:

$$\psi_{ds}i_{qs} - \psi_{qs}i_{ds} = -(\psi'_{dr}i'_{qr} - \psi'_{qr}i'_{dr}) = L_m(i_{dr}i_{qs} - i_{qr}i_{ds}) \quad (2-51)$$

Thus (2-50) can also be expressed as:

$$\begin{aligned} T_{em} &= \frac{3}{2} \frac{p}{2} (\psi'_{qr}i'_{dr} - \psi'_{dr}i'_{qr}) \quad Nm \\ &= \frac{3}{2} \frac{p}{2} (\psi_{ds}i_{qs} - \psi_{qs}i_{ds}) \quad Nm \\ &= \frac{3}{2} \frac{p}{2} L_m (i'_{dr}i_{qs} - i'_{qr}i_{ds}) \quad Nm \end{aligned} \quad (2-52)$$

2.1.4. qd0 Stationary and Synchronous Reference Frames

There is seldom a need to simulate an induction machine in the arbitrary rotating reference frame. But it is useful to convert a unified model to other frames. The most commonly used ones are, two marginal cases of the arbitrary rotating frame, stationary reference frame and synchronously rotating frame. For transient studies of adjustable speed drives, it is usually more convenient to simulate an induction machine and its converter on a stationary reference frame. Moreover, calculations with stationary reference frame are less complex due to zero frame speed (some terms cancelled). For small signal stability analysis about some operating condition, a synchronously rotating frame which yields dc values of steady-state voltages and currents under balanced conditions is used.

Since we have derived the circuit equations of induction machine for the general case that is in the arbitrary rotating reference frame, the circuit equations of the machine in the stationary reference frame (denoted as $d^s q^s$) and synchronously rotating reference frame (denoted as $d^e q^e$) can be obtained by simply setting w to zero and w_e , respectively. To distinguish these two frames from each other, an additional

superscript will be used, s for stationary frame variables and e for synchronously rotating frame variables.

Stator $q^s d^s$ voltage equations:

$$v^s_{qs} = \frac{d\psi^s_{qs}}{dt} + r_s i^s_{qs} \quad (2-53)$$

$$v^s_{ds} = \frac{d\psi^s_{ds}}{dt} + r_s i^s_{ds}$$

Rotor $q^s d^s$ voltage equations:

$$v'^s_{qr} = \frac{d\psi'^s_{qr}}{dt} + (-\omega_r)\psi'^s_{dr} + r'_r i'^s_{qr} \quad (2-54)$$

$$v'^s_{dr} = \frac{d\psi'^s_{dr}}{dt} + (\omega_r)\psi'^s_{qr} + r'_r i'^s_{dr}$$

where

$$\begin{bmatrix} \psi^s_{qs} \\ \psi^s_{ds} \\ \psi'^s_{qr} \\ \psi'^s_{dr} \end{bmatrix} = \begin{bmatrix} L_s & 0 & L_m & 0 \\ 0 & L_s & 0 & L_m \\ L_m & 0 & L'_r & 0 \\ 0 & L_m & 0 & L'_r \end{bmatrix} \begin{bmatrix} i^s_{qs} \\ i^s_{ds} \\ i'^s_{qr} \\ i'^s_{dr} \end{bmatrix} \quad (2-55)$$

Torque Equations:

$$\begin{aligned} T_{em} &= \frac{3}{2} \frac{p}{2} (\psi'^s_{qr} i'^s_{dr} - \psi'^s_{dr} i'^s_{qr}) \quad Nm \\ &= \frac{3}{2} \frac{p}{2} (\psi^s_{ds} i^s_{qs} - \psi^s_{qs} i^s_{ds}) \quad Nm \\ &= \frac{3}{2} \frac{p}{2} L_m (i'^s_{dr} i^s_{qs} - i'^s_{qr} i^s_{ds}) \quad Nm \end{aligned} \quad (2-56)$$

Stator $q^e d^e$ voltage equations:

$$v^e_{qs} = \frac{d\psi^e_{qs}}{dt} + \omega_e \psi^e_{ds} + r_s i^e_{qs} \quad (2-57)$$

$$v^e_{ds} = \frac{d\psi^e_{ds}}{dt} - \omega_e \psi^e_{qs} + r_s i^e_{ds}$$

Rotor $q^e d^e$ voltage equations:

$$v'^e_{qr} = \frac{d\psi'^e_{qr}}{dt} + (\omega_e - \omega_r) \psi'^e_{dr} + r'_r i'^e_{qr} \quad (2-58)$$

$$v'^e_{dr} = \frac{d\psi'^e_{dr}}{dt} - (\omega_e - \omega_r) \psi'^e_{qr} + r'_r i'^e_{dr}$$

where

$$\begin{bmatrix} \psi^e_{qs} \\ \psi^e_{ds} \\ \psi'^e_{qr} \\ \psi'^e_{dr} \end{bmatrix} = \begin{bmatrix} L_s & 0 & L_m & 0 \\ 0 & L_s & 0 & L_m \\ L_m & 0 & L'_r & 0 \\ 0 & L_m & 0 & L'_r \end{bmatrix} \begin{bmatrix} i^e_{qs} \\ i^e_{ds} \\ i'^e_{qr} \\ i'^e_{dr} \end{bmatrix} \quad (2-59)$$

Torque Equations:

$$T_{em} = \frac{3}{2} \frac{p}{2} (\psi'^e_{qr} i'^e_{dr} - \psi'^e_{dr} i'^e_{qr}) \quad Nm \quad (2-60)$$

$$= \frac{3}{2} \frac{p}{2} (\psi^e_{ds} i^e_{qs} - \psi^e_{qs} i^e_{ds}) \quad Nm$$

2.2. Field Oriented Control (FOC)

The concept of field orientation control is used to accomplish a decoupled control of flux and torque, and has three requirements [28]:

- An independently controlled armature current to overcome the effects of armature winding resistance, leakage inductance and induced voltage
- An independently controlled constant value of flux
- An independently controlled orthogonal spatial angle between the flux axis and magneto motive force (MMF) axis to avoid interaction of MMF and flux.

If all of these three requirements are met at every instant of time, the torque will follow the current, allowing an immediate torque control and decoupled flux and torque regulation.

Next, a two phase dq model of an induction machine rotating at the synchronous speed is introduced which will help to carry out this decoupled control concept to the induction machine. This model can be summarized by the following equations:

$$v_{ds}^e = \frac{d\psi_{ds}^e}{dt} - \omega_e \psi_{qs}^e + r_s i_{ds}^e \quad (2-61)$$

$$v_{qs}^e = \frac{d\psi_{qs}^e}{dt} + \omega_e \psi_{ds}^e + r_s i_{qs}^e \quad (2-62)$$

$$0 = \frac{d\psi_{qr}^e}{dt} + (\omega_e - \omega_r) \psi_{dr}^e + r_r i_{qr}^e \quad (2-63)$$

$$0 = \frac{d\psi_{dr}^e}{dt} - (\omega_e - \omega_r) \psi_{qr}^e + r_r i_{dr}^e \quad (2-64)$$

$$\psi_{qs}^e = L_s i_{qs}^e + L_m i'_{qr}^e \quad (2-65)$$

$$\psi_{ds}^e = L_s i_{ds}^e + L_m i'_{dr}^e \quad (2-66)$$

$$\psi'_{qr}^e = L_m i_{qs}^e + L'_r i'_{qr}^e \quad (2-67)$$

$$\psi'_{dr}{}^e = L_m i_{ds}^e + L_r i'_{dr}{}^e \quad (2-68)$$

$$T_{em} = \frac{3p}{2} \frac{L_m}{L_r} (\psi'_{dr}{}^e i_{qs}^e - \psi'_{qr}{}^e i_{ds}^e) \quad (2-69)$$

$$T_{em} = J \frac{dw_r}{dt} + Bw_r + T_L \quad (2-70)$$

This model is quite significant to synthesize the concept of field-oriented control. In this model it can be seen from the torque expression (2-69) that if the rotor flux along the q -axis is zero, then all the flux is aligned along the d -axis and therefore the torque can be instantaneously controlled by controlling the current along q -axis. Then the question will be how it can be guaranteed that all the flux is aligned along the d -axis of the machine. When a three-phase voltage is applied to the machine, it produces a three-phase flux both in the stator and rotor. The three-phase fluxes can be converted into equivalents developed in two-phase stationary ($d^s q^s$) frame. If this two phase fluxes along ($d^s q^s$) axes are converted into an equivalent single vector then all the machine flux will be considered as aligned along that vector. This vector commonly specifies us d^e -axis which makes an angle θ_e with the stationary frame d^s -axis. The q^e -axis is set perpendicular to the d^e -axis. The flux along the q^e -axis in that case will obviously be zero. The phasor diagram Figure 2-4 shows these axes. The angle θ_e keeps changing as the machine input currents change. Knowing the angle θ_e accurately, d -axis of the $d^e q^e$ frame can be locked with the flux vector.

The control input can be specified in terms of two phase synchronous frame i_{ds}^e and i_{qs}^e . i_{ds}^e is aligned along the d^e -axis i.e. the flux vector, so does i_{qs}^e with the q^e -axis. These two-phase synchronous control inputs are converted into two-phase stationary and then to three-phase stationary control inputs. To accomplish this, the flux angle θ_e must be known precisely. The angle θ_e can be found either by Indirect Field

Oriented Control (IFOC) or by Direct Field Oriented Control (DFOC). The controller implemented in this fashion that can achieve a decoupled control of the flux and the torque is known as field oriented controller. The block diagram is as in Figure 2-5.

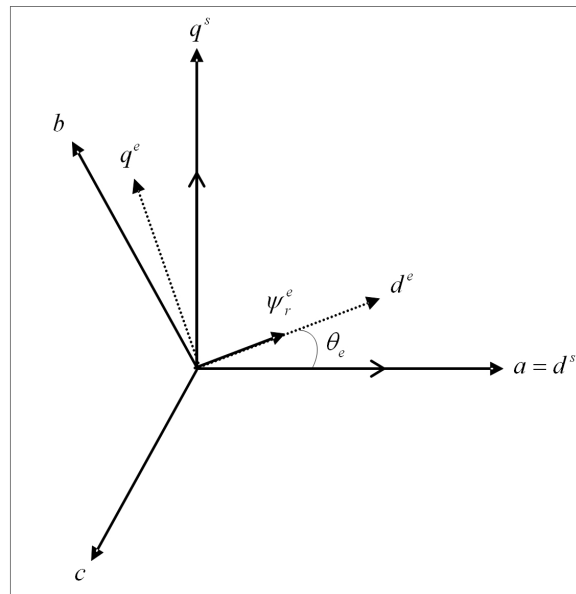


Figure 2-4 Phasor diagram of the field oriented drive system

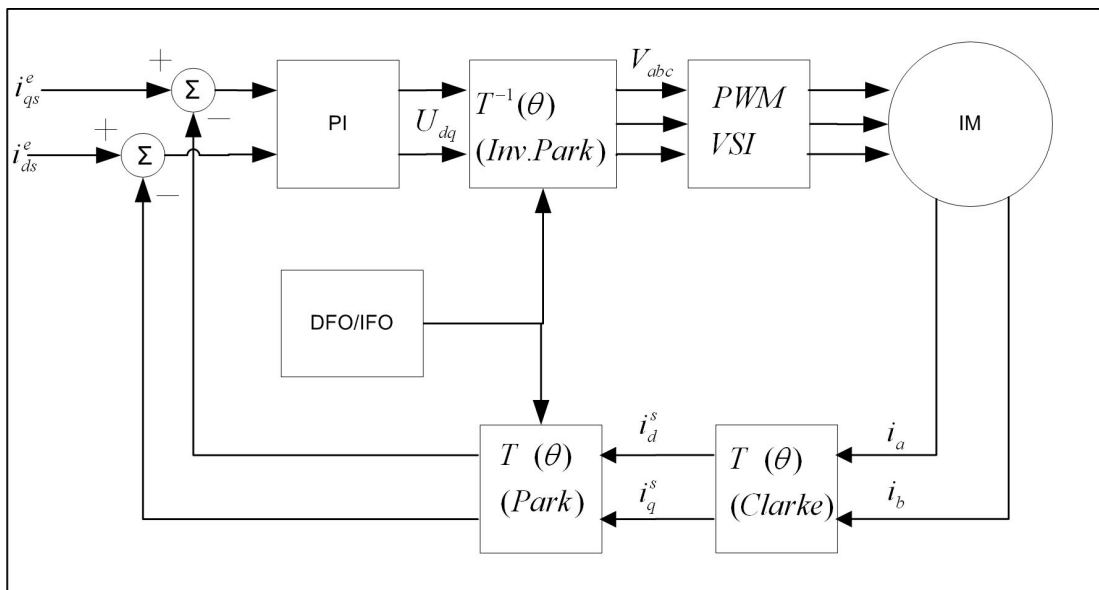


Figure 2-5 Field oriented induction motor drive system

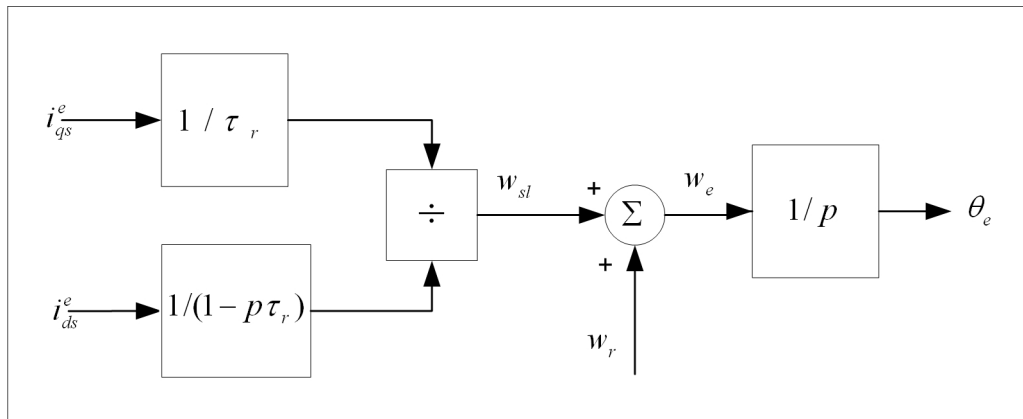


Figure 2-6 Indirect field oriented drive system

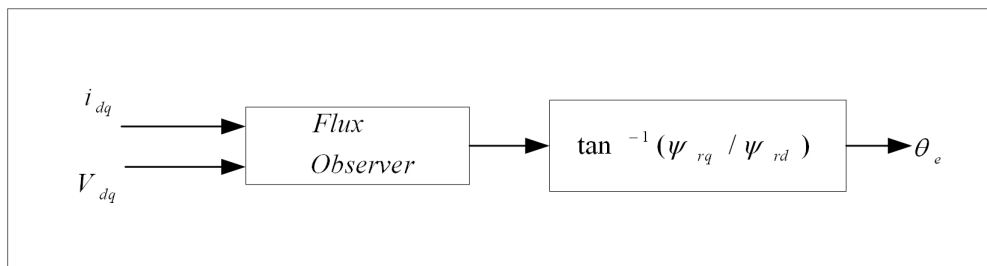


Figure 2-7 Direct field oriented drive system

2.3. Space Vector Pulse Width Modulation (SVPWM)

2.3.1. Voltage Fed Inverter (VSI)

A diagram of the power circuit of a three phase VSI is shown in the Figure 2-8. The circuit has bridge topology with three branches (phases), each consisting of two power switches and two freewheeling diodes. The inverter here is supplied from an uncontrolled, diode-based rectifier, via d.c. link which contains an LC filter in the inverted configuration. It allows the power flow from the supply to the load only. Power flow cannot be reversed, if the load is to feed the power back to the supply due to the diode rectifier structure at the input side of the dc link. Therefore, in drive systems where the VSI-fed motor may not operate as a generator, a more complex

supply system must be used. These involve either a braking resistance connected across the d.c. link or replacement of the uncontrolled rectifier by a dual converter. The inverter may be supported with braking resistance connected across the d.c. link via a free wheeling diode and a transistor. When the power flow is reversed it is dissipated in the braking resistor putting the system into dynamic braking mode of operation.

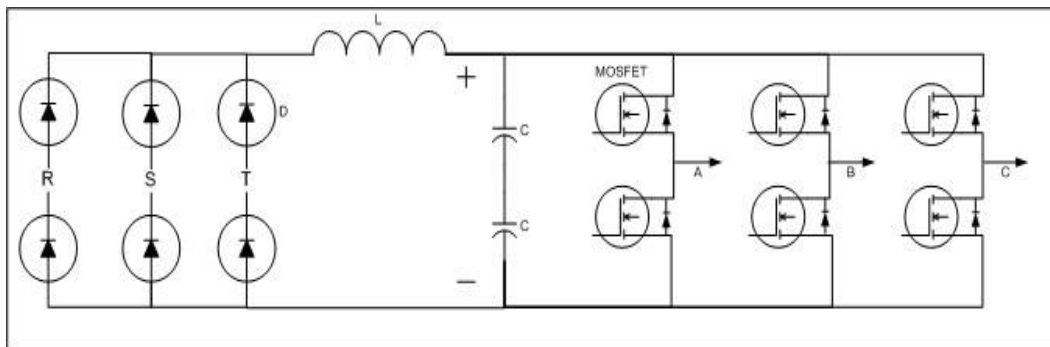


Figure 2-8 Circuit diagram of VSI

Because of the constraint that the input lines must never be shorted and the output current must be continuous a voltage fed inverter can assume in operation only eight distinct topologies. They are shown in Figure 2-9. Six out of these eight topologies produce a non-zero output voltage and are known as non-zero switching states and the remaining two topologies produce zero output and are known as zero switching state.

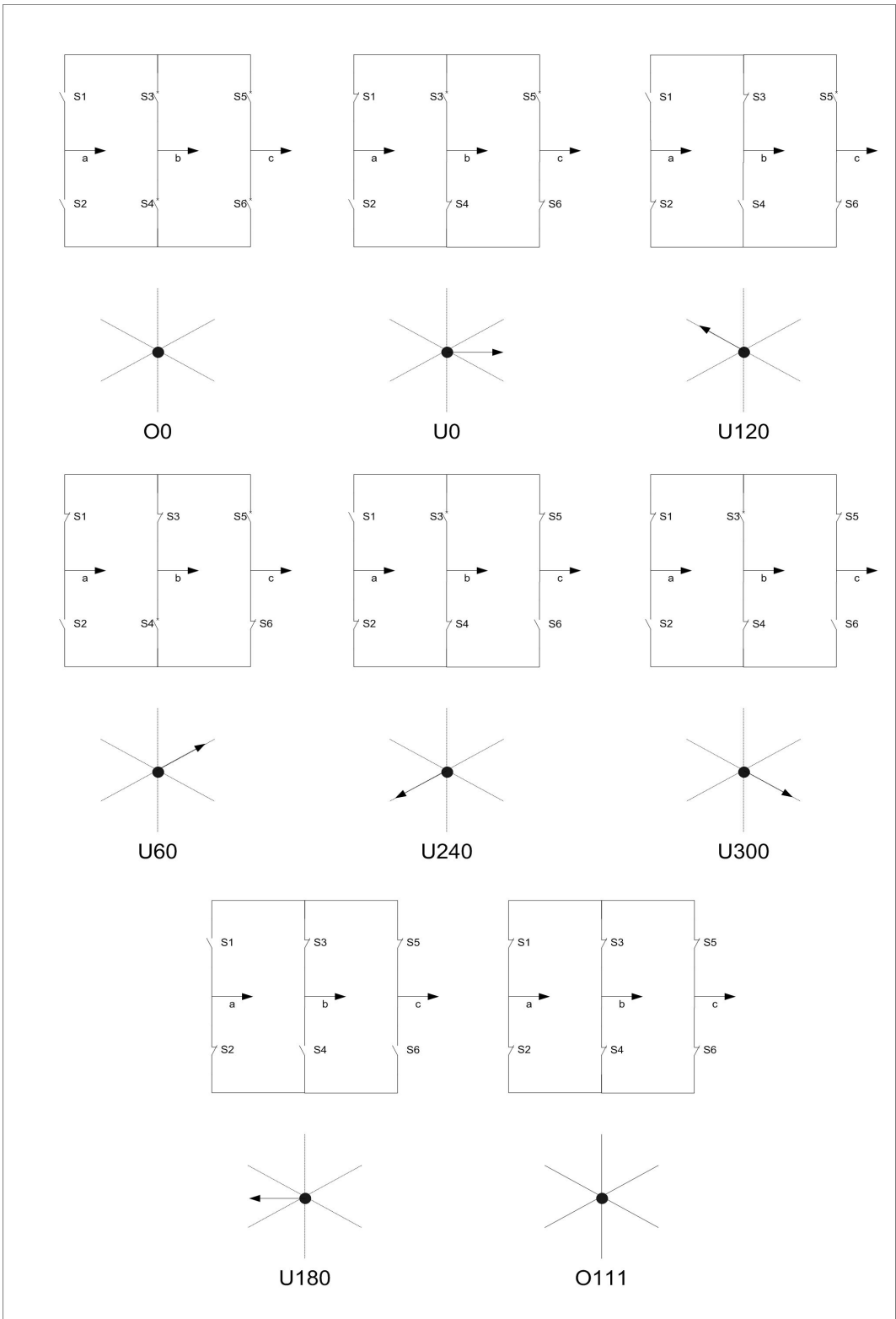


Figure 2-9 Eight switching state topologies of a voltage source inverter

2.3.2. Voltage Space Vectors

Space vector modulation for three leg VSI is based on the representation of the three phase quantities as vectors in two-dimensional ($d^s q^s$) plane. Considering the first switching state in Figure 2-10, line-to-line voltages are given by:

$$V_{ab} = V_s$$

$$V_{bc} = 0$$

$$V_{ca} = -V_s$$

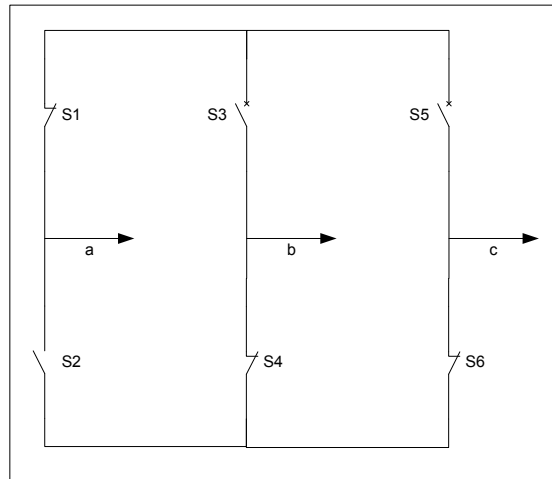


Figure 2-10 First switching state V_1

This can be represented in ($d^s q^s$) plane as shown in Figure 2-11 where V_{ab} , V_{bc} and V_{ca} are the three line voltage vectors displaced 120° in space. The effective voltage vector generated by this topology is represented as V_1 (pnn) in Figure 2-11. Here “ pnn ” refers to the three leg /phases a , b , c being either connected to the positive dc rail “ p ” or to the negative dc rail “ n ”. For the first switching state V_1 , phase a connected to positive dc rail and phases b and c are connected to negative dc

rail. Similar to the V_I , six non-zero voltage vectors can be shown as in Figure 2-12. The tips of these vectors form a regular hexagon. We define the area enclosed by two adjacent vectors, within the hexagon, as a sector.

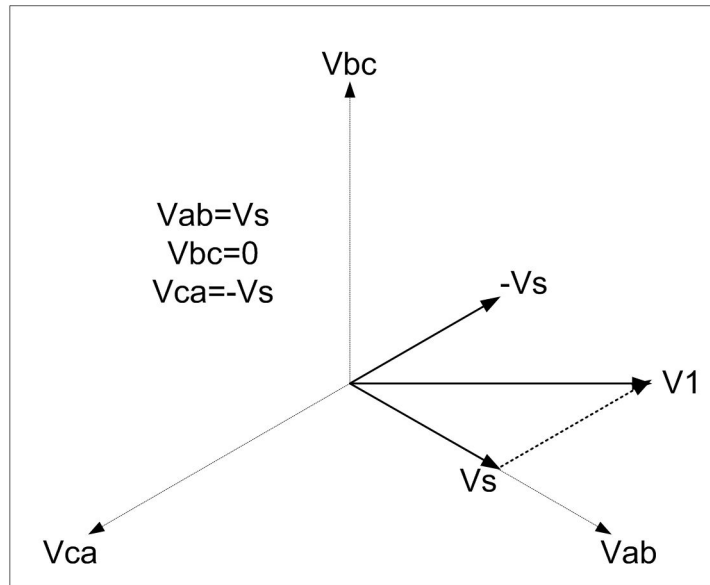


Figure 2-11 Representation of topology $V1$ in $(d^s q^s)$ plane

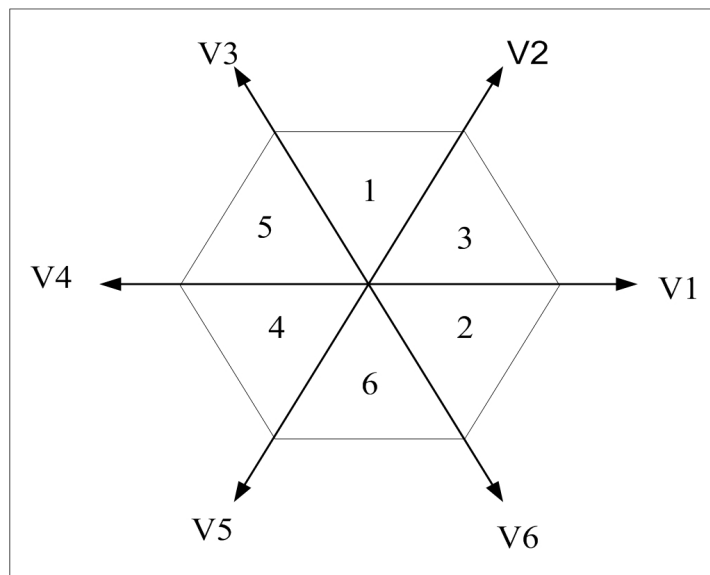


Figure 2-12 Non-zero voltage vectors in $(d^s q^s)$ plane

The first and the last two topologies of Figure 2-9 are zero state vectors. The output line voltages in these topologies are zero.

$$V_{ab} = 0$$

$$V_{bc} = 0$$

$$V_{ca} = 0$$

These are represented as vectors which have zero magnitude and hence are referred as zero switching state vectors. They are represented with dot at the origin instead of vectors as shown in Figure 2-13.

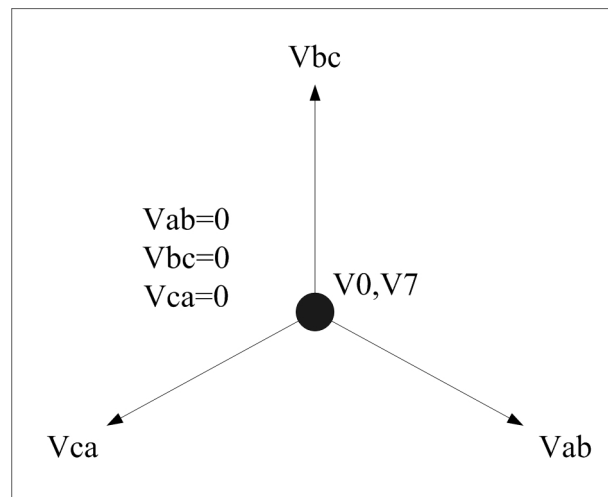


Figure 2-13 Representation of the zero voltage vectors in $(d^s q^s)$ plane

2.3.3. SVPWM Application to the Static Power Bridge

In the case of AC drive applications, sinusoidal voltage sources are not used. Instead, they are replaced by 6 power switches which act as on/off to the rectified DC bus voltage. The aim is to create sinusoidal current in the windings to generate rotating field. Owing to the inductive nature of the phases, a pseudo sinusoidal current is created by modulating the duty-cycle of the power switches. The switches shown in the inverter are activated by signals a , b , c and their complement values. Eight different combinations are available with this three phase VFI including two zero states. It is possible to express each phase to neutral voltages, for each switching combination of switches as listed in Table 2-1.

Table 2-1 Power Bridge Output Voltages (V_{an} , V_{bn} , V_{cn})

Switch Positions			Phase Voltages		
S_1	S_3	S_5	V_{an}	V_{bn}	V_{cn}
0	0	0	0	0	0
0	0	1	$-V_{dc}/3$	$-V_{dc}/3$	$2V_{dc}/3$
0	1	0	$-V_{dc}/3$	$2V_{dc}/3$	$-V_{dc}/3$
0	1	1	$-2V_{dc}/3$	$V_{dc}/3$	$V_{dc}/3$
1	0	0	$2V_{dc}/3$	$-V_{dc}/3$	$-V_{dc}/3$
1	0	1	$V_{dc}/3$	$-2V_{dc}/3$	$V_{dc}/3$
1	1	0	$V_{dc}/3$	$V_{dc}/3$	$-2V_{dc}/3$
1	1	1	0	0	0

In field oriented control algorithm, the control variables are expressed in rotating frame. The current vector $I_{qS_{ref}}$ that directly controls the torque is transformed in a voltage vector after current regulation mechanism and the inverse Park transform. This voltage reference is expressed in the $(d^s q^s)$ frame. Using this transformation

three phase voltages (V_{an} , V_{bn} , V_{cn}) and the reference voltage vector are projected in the ($d^s q^s$) frame. The expression of the three phase voltages in the ($d^s q^s$) frame are given by Clarke transformation:

$$\begin{bmatrix} V_{sd}^s \\ V_{sq}^s \end{bmatrix} = \frac{2}{3} \begin{bmatrix} 1 & -\frac{1}{2} & -\frac{1}{2} \\ 0 & \frac{\sqrt{3}}{2} & -\frac{\sqrt{3}}{2} \end{bmatrix} \begin{bmatrix} V_{AN} \\ V_{BN} \\ V_{CN} \end{bmatrix} \quad (2-71)$$

Since only 8 combinations are possible for the power switches, V_{ds}^s , V_{qs}^s can also take finite number of values in the ($d^s q^s$) frame Table 2-2 according to the command signals a , b , c .

Table 2-2 Stator Voltages in ($d^s q^s$) frame and related Voltage Vector

Switch Positions			($d^s q^s$) frame Voltages		
S_1	S_3	S_5	V_{ds}^s	V_{qs}^s	Vectors
0	0	0	0	0	V0
0	0	1	-Vdc/3	-Vdc/√3	V1
0	1	0	-Vdc/3	Vdc/√3	V2
0	1	1	-2Vdc/3	0	V3
1	0	0	2Vdc/3	0	V4
1	0	1	Vdc/3	-Vdc/√3	V5
1	1	0	Vdc/3	Vdc/√3	V6
1	1	1	0	0	V7

The eight voltage vectors re-defined by the combination of the switches are represented in Figure 2-14.

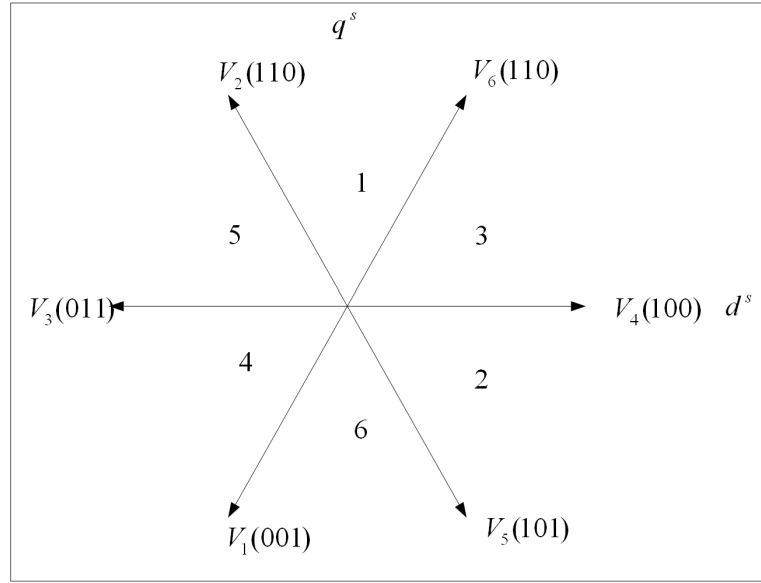


Figure 2-14 Voltage vectors

Given a reference voltage (coming from the inv. Park transform), the following step is used to approximate this reference voltage by the above defined eight vectors. The method used to approximate the desired stator reference voltage with only eight possible states of switches combines adjacent vectors of the reference voltage and modulates the time of application of each adjacent vector. In Figure 2-15, for a reference voltage V_{sref} is in the third sector and the application time of each adjacent vector is given by:

$$T = T_4 + T_6 + T_0 \quad (2-72)$$

$$V_{sref} = \frac{T_4}{T} \vec{V}_4 + \frac{T_6}{T} \vec{V}_6$$

where T_4 and T_6 , T_0 respective duration for vectors V_4 and V_6 an null vector V_0 within period T .

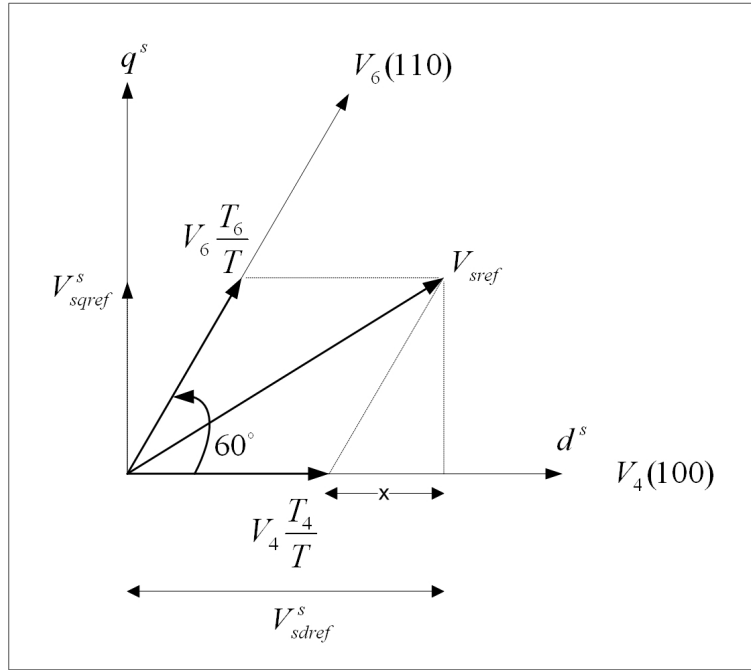


Figure 2-15 Projection of the reference voltage vector

The determination of the amount of times T_4 and T_6 is given by simple projections:

$$V_{sqref}^s = \frac{T_6}{T} \|\vec{V}_6\| \cos(30^\circ)$$

$$V_{sdref}^s = \frac{T_4}{T} \|\vec{V}_4\| + x \quad (2-73)$$

$$x = \frac{V_{sqref}^s}{\text{tg}(60^\circ)}$$

Finally, with the $(d^s q^s)$ component values of the vectors given in Table 2-2, the duration periods of application of each adjacent vector is:

$$T_4 = \frac{T}{2}(\sqrt{3}V_{sd}^s - V_{sq}^s) \quad (2-74)$$

$$T_6 = TV_{sq}^s \quad (2-75)$$

where the vector magnitudes are “ $2V_{dc}/3$ ” and both sides are normalized by maximum phase to neutral voltage $V_{DC}/\sqrt{3}$.

The rest of the period spent in applying the null vector ($T_0=T-T_6-T_4$). For every sector, commutation duration is calculated. The amount of times of vector application can all be related to the following variables:

$$X = V_{sq}^s$$

$$Y = \frac{1}{2}V_{sq}^s + \frac{\sqrt{3}}{2}V_{sd}^s \quad (2-76)$$

$$Z = \frac{1}{2}V_{sq}^s - \frac{\sqrt{3}}{2}V_{sd}^s$$

In the previous example for sector 3, $T_4 = -TZ$ and $T_6 = TX$. Extending this logic, one can easily calculate the sector number belonging to the related reference voltage vector. Then, three phase quantities are calculated by inverse Clarke transform to get sector information. The following basic algorithm helps to determine the sector number systematically.

$$\text{If } V_{ref1} = V_{sq}^s > 0 \text{ then set } A=1 \quad \text{else } A=0$$

$$\text{If } V_{ref2} = \frac{1}{2}(\sqrt{3}V_{sd}^s - V_{sq}^s) > 0 \text{ then set } B=1 \quad \text{else } B=0$$

If $V_{ref3} = \frac{1}{2}(-\sqrt{3}V_{sd}^s - V_{sq}^s) > 0$ then set $C=1$ else $C=0$

Then, Sector = A+2B+4C

The duration of the sector boundary vectors application after normalizing with the period T can be determined as follows:

Sector

1:	$t_1 = Z$	$t_2 = Y$
2:	$t_1 = Y$	$t_2 = -X$
3:	$t_1 = -Z$	$t_2 = X$
4:	$t_1 = -X$	$t_2 = Z$
5:	$t_1 = X$	$t_2 = -Y$
6:	$t_1 = -Y$	$t_2 = -Z$

Saturations

If $(t_1 + t_2) > \text{PWM period}$ then

$$t_{1\text{sat}} = t_1 / (t_1 + t_2) * \text{PWM period}$$

$$t_{2\text{sat}} = t_2 / (t_1 + t_2) * \text{PWM period}$$

The third step is to compute the three necessary duty-cycles. This is shown below:

$$t_{aon} = \frac{PWM \text{ period} - t_1 - t_2}{2}$$

$$t_{bon} = t_{aon} + t_1$$

$$t_{con} = t_{bon} + t_2$$

The last step is to assign the right duty-cycle (t_{xon}) to the right motor phase (in other words, to the Ta , Tb and Tc) according to the sector. Table 2-3 below depicts this determination. (i.e., the on time of the inverter switches)

Table 2-3 Assigned duty cycles to the PWM outputs

	1	2	3	4	5	6
Ta	t _{bon}	t _{aon}	t _{aon}	t _{con}	t _{bon}	t _{con}
Tb	t _{aon}	t _{con}	t _{bon}	t _{bon}	t _{con}	t _{aon}
Tc	t _{con}	t _{bon}	t _{con}	t _{aon}	t _{aon}	t _{bon}

The phase voltage of a general 3-phase motor V_{an} , V_{bn} , V_{cn} can be calculated from the DC-bus voltage (V_{dc}), and three upper switching functions of inverter S_1 , S_3 , and S_5 . The 3-ph windings of motor are connected either Δ or Y without a neutral return path (or 3-ph, 3-wire system).

Each phase of the motor is simply modeled as a series impedance of resistance r and inductance L and back emf e_a , e_b , e_c . Thus, three phase voltages can be computed as:

$$V_{an} = V_a - V_n = i_a r + L \frac{di_a}{dt} + e_a \quad (2-77)$$

$$V_{bn} = V_b - V_n = i_b r + L \frac{di_b}{dt} + e_b \quad (2-78)$$

$$V_{cn} = V_c - V_n = i_c r + L \frac{di_c}{dt} + e_c \quad (2-79)$$

Summing these three phase voltages, yields

$$V_a + V_b + V_c - 3V_n = (i_a + i_b + i_c)r + L \frac{d(i_a + i_b + i_c)}{dt} + e_a + e_b + e_c \quad (2-80)$$

For a 3-phase system with no neutral path and balanced back emfs, $i_a + i_b + i_c = 0$, and $e_a + e_b + e_c = 0$. Therefore, (2-80) becomes, $V_{an} + V_{bn} + V_{cn} = 0$. Furthermore, the neutral voltage can be simply derived from (2-80) as

$$V_n = \frac{1}{3}(V_a + V_b + V_c) \quad (2-81)$$

Now three phase voltages can be calculated as:

$$V_{an} = V_a - \frac{1}{3}(V_a + V_b + V_c) = \frac{2}{3}V_a - \frac{1}{3}V_b - \frac{1}{3}V_c \quad (2-82)$$

$$V_{bn} = V_b - \frac{1}{3}(V_a + V_b + V_c) = \frac{2}{3}V_b - \frac{1}{3}V_a - \frac{1}{3}V_c \quad (2-83)$$

$$V_{cn} = V_c - \frac{1}{3}(V_a + V_b + V_c) = \frac{2}{3}V_c - \frac{1}{3}V_a - \frac{1}{3}V_b \quad (2-84)$$

Three voltages V_a , V_b , V_c are related to the DC-bus voltage V_{dc} and three upper switching functions S_1 , S_3 , and S_5 as:

$$V_a = S_1 V_{dc} \quad (2-85)$$

$$V_b = S_3 V_{dc} \quad (2-86)$$

$$V_c = S_5 V_{dc} \quad (2-87)$$

where S_1 , S_3 , and $S_5 = \text{either } 0 \text{ or } 1$, and $S_2=1-S_1$, $S_4=1-S_3$, and $S_6=1-S_5$.

As a result, three phase voltages in (2-82) to (2-84) can also be expressed in terms of DC-bus voltage and three upper switching functions as:

$$V_{an} = V_{dc} \left(\frac{2}{3} S_1 - \frac{1}{3} S_3 - \frac{1}{3} S_5 \right) \quad (2-88)$$

$$V_{bn} = V_{dc} \left(\frac{2}{3} S_3 - \frac{1}{3} S_1 - \frac{1}{3} S_5 \right) \quad (2-89)$$

$$V_{cn} = V_{dc} \left(\frac{2}{3} S_5 - \frac{1}{3} S_1 - \frac{1}{3} S_3 \right) \quad (2-90)$$

It is emphasized that the S_1 , S_3 , S_5 are defined as the upper switching functions. If the lower switching functions are available instead, then the out-of-phase correction of switching function is required in order to get the upper switching functions as easily computed from equation ($S_2=1-S_1$, $S_4=1-S_3$, and $S_6=1-S_5$). Next the Clarke transformation is used to convert the three phase voltages V_{an} , V_{bn} , and V_{cn} to the stationary dq -axis phase voltages V_{ds}^s and V_{qs}^s . Because of the balanced system ($V_{an} + V_{bn} + V_{cn}=0$) V_{cn} is not used in Clarke transformation.

CHAPTER 3

FLUX ESTIMATION FOR SENSORLESS DIRECT FIELD

ORIENTED CONTROL OF INDUCTION MACHINE

This chapter focuses on adaptive flux observer for direct field-orientation (DFO). The field orientation is implemented in two ways as Direct Field Orientation and Indirect Field Orientation. The basic difference of these methods underlies in the manner of detecting the synchronous speed. In IFO, the slip angle is computed and added to the rotor angle to find the synchronous speed. One must calculate, therefore, the slip-angle and estimate the rotor angle. In the current model employed in the IFO, dq -axes stator currents and precise rotor time-constants are needed to find the slip angle. However, in DFO, the rotor angle is computed from the ratio of dq -axes fluxes.

3.1. Flux Estimation

The logic underlying this flux observer is basically an advanced voltage model approach in which integration of the back-emf is calculated and compensated for the errors associated with pure integrator and stator resistance R_s measurement at low speeds. At high speeds, the voltage model provides an accurate stator flux estimate because the machine back emf dominates the measured terminal voltage. However, at low speeds, the stator IR drop becomes significant, causing the accuracy of the flux estimate to be sensitive to the estimated stator resistance. Due to this effect, at low excitation frequencies flux estimation based upon voltage model are generally not capable of achieving high dynamic performance at low speeds [15]. Consequences of these problems are compensated with the addition of a closed-loop in the flux observer. Basically, the fluxes obtained by current model are compared with those obtained by the voltage model with reference to the current model, or the

current model with reference to the voltage model according to the range in which one of these models is superior to other [22]. In this flux observer the voltage model is corrected by the current model through a basic PI block. In the end, the stator fluxes are used to obtain rotor fluxes and rotor flux angle. In the following parts, the superscript “v” and “i” corresponds to the values of voltage model and the values of current model respectively.

3.1.1. Estimation of the Flux Linkage Vector

Most of the sensorless control schemes rely directly or indirectly on the estimation of the stator flux linkage vector, ψ_s being defined as the time integral of the induced voltage,

$$\frac{d\psi^{s,v}}{dt} = u_s - R_s i_s + u_{off}, \quad (3-1)$$

$$\psi_s^v(0) = \psi_{s0}^v$$

where, ψ_{s0}^v is the initial value of flux linkage vector, u_{off} represents all disturbances such as offsets, unbalances and other errors present in the estimated induced emf. A major source of error in the emf is due to the changes in the model parameter R_s . The estimation of the flux vectors requires the integration of (3-1) in real-time. The integrator, however, will have an infinite gain at zero frequency, and the unavoidable offsets contained in the integrator input then make its output gradually drift away beyond limits.

3.1.1.1. Flux Estimation in Continuous Time

The rotor flux linkage dynamics in synchronously rotating reference frame ($w=w_e=w_{\psi r}$) being as;

$$\frac{d\psi_{dr}^{e,i}}{dt} = \frac{L_m}{\tau_r} i_{ds}^e - \frac{1}{\tau_r} \psi_{dr}^{e,i} + (\omega_e - \omega_r) \psi_{qr}^{e,i} \quad (3-2)$$

$$\frac{d\psi_{qr}^{e,i}}{dt} = \frac{L_m}{\tau_r} i_{qs}^e - \frac{1}{\tau_r} \psi_{qr}^{e,i} + (\omega_e - \omega_r) \psi_{dr}^{e,i} \quad (3-3)$$

where L_m is the magnetizing inductance (H), $\tau_r = L_r / R_r$ is the rotor time-constant (sec), and ω_r is the electrical angular velocity of the rotor (rad/sec). These equations are derived from the equations (2-64) and (2-68) of the previous chapter. In the current model, the total rotor flux-linkage is aligned with the d -axis component, and hence;

$$\psi_r^{e,i} = \psi_{dr}^{e,i}$$

$$\psi_{qr}^{e,i} = 0$$

Substitution of $\psi_{qr}^{e,i} = 0$ into (3-2) and (3-3) yields the oriented rotor flux dynamics as;

$$\frac{d\psi_{dr}^{e,i}}{dt} = \frac{L_m}{\tau_r} i_{ds}^e - \frac{1}{\tau_r} \psi_{dr}^{e,i} \quad (3-4)$$

$$\psi_{qr}^{e,i} = 0 \quad (3-5)$$

Note that (3-4) and (3-5) are the commonly recognized forms of the rotor flux vector equations. When, the rotor flux linkages in (3-4) and (3-5) undergoes the inverse park transformation in the stationary reference frame the result becomes.

$$\psi_{dr}^{s,i} = \psi_{dr}^{e,i} \cos(\theta_{\psi_r}) - \psi_{qr}^{e,i} \sin(\theta_{\psi_r}) = \psi_{dr}^{e,i} \cos(\theta_{\psi_r}) \quad (3-6)$$

$$\psi_{qr}^{s,i} = \psi_{qr}^{e,i} \cos(\theta_{\psi_r}) + \psi_{dr}^{e,i} \sin(\theta_{\psi_r}) = \psi_{dr}^{e,i} \sin(\theta_{\psi_r}) \quad (3-7)$$

where θ_{ψ_r} is the rotor flux angle (rad). The stator flux linkages in stationary reference frame are then computed using (3-6), (3-7) and (2-68) as;

$$\psi_{ds}^{s,i} = L_s i_{ds}^s + L_m i_{dr}^s = \left(\frac{L_s L_r - L_m^2}{L_r} \right) i_{ds}^s + \frac{L_m}{L_r} \psi_{dr}^{s,i} \quad (3-8)$$

$$\psi_{qs}^{s,i} = L_s i_{qs}^s + L_m i_{qr}^s = \left(\frac{L_s L_r - L_m^2}{L_r} \right) i_{qs}^s + \frac{L_m}{L_r} \psi_{qr}^{s,i} \quad (3-9)$$

The stator flux linkages in the voltage model, however, are computed by integrating the back emf's and compensated voltages taken into account.

$$\psi_{ds}^{s,v} = \int (u_{ds}^s - i_{ds}^s R_s - u_{comp,ds}) dt \quad (3-10)$$

$$\psi_{qs}^{s,v} = \int (u_{qs}^s - i_{qs}^s R_s - u_{comp,q_s}) dt \quad (3-11)$$

The compensated voltages, on the other hand, are computed by the PI control law as follows:

$$u_{comp,ds} = K_p (\psi_{ds}^{s,v} - \psi_{ds}^{s,i}) + \frac{K_p}{T_I} \int (\psi_{ds}^{s,v} - \psi_{ds}^{s,i}) dt \quad (3-12)$$

$$u_{comp,qs} = K_p (\psi_{qs}^{s,v} - \psi_{qs}^{s,i}) + \frac{K_p}{T_I} \int (\psi_{qs}^{s,v} - \psi_{qs}^{s,i}) dt \quad (3-13)$$

The proportional gain K_p and the reset time T_I are chosen such that the flux linkages computed by the current model becomes dominant at low speed. The reason for that is the back emfs computed by the voltage model result to be extremely low at this speed range (even zero for back emfs at zero speed). While the motor is running at high speed range, the flux linkages computed by voltage model becomes dominant over the flux linkage components computed through the current model.

Once the stator flux linkages in (3-10) and (3-11) are calculated, the rotor flux linkages based on the voltage model are computed once more through (3-14) and (3-15) which are only rearranged forms of (3-8) and (3-9), as

$$\psi_{dr}^{s,v} = -\left(\frac{L_s L_r - L_m^2}{L_m}\right) i_{ds}^s + \frac{L_r}{L_m} \psi_{ds}^{s,v} \quad (3-14)$$

$$\psi_{qr}^{s,v} = -\left(\frac{L_s L_r - L_m^2}{L_m}\right) i_{qs}^s + \frac{L_r}{L_m} \psi_{qs}^{s,v} \quad (3-15)$$

It is then a straight process to compute the rotor flux angle based on the voltage model as;

$$\theta_{\psi_r} = \tan^{-1}\left(\frac{\psi_{qr}^{s,v}}{\psi_{dr}^{s,v}}\right) \quad (3-16)$$

The overall flux estimator structure is as in Figure 3-1.

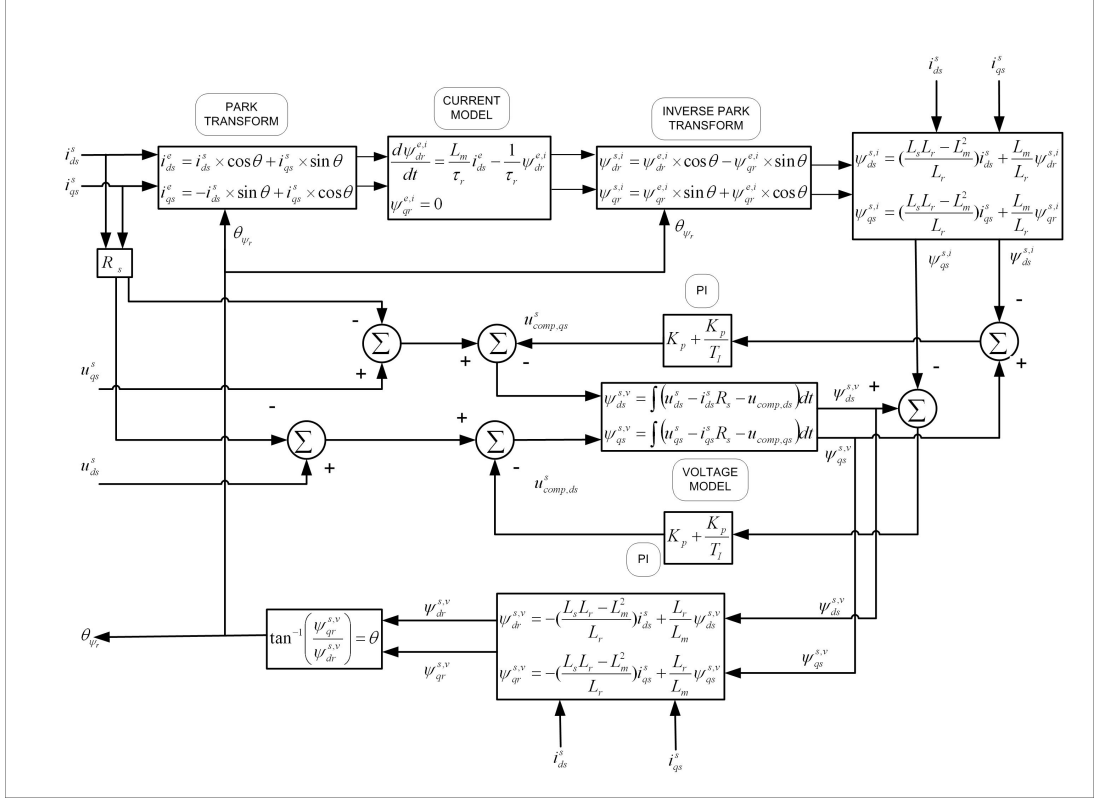


Figure 3-1 Flux estimation structure

3.1.1.2. Flux Estimation in Discrete Time

The oriented rotor flux dynamics in (3-4) is discretized by using backward approximation as:

$$\frac{\psi_{dr}^{e,i}(k) - \psi_{dr}^{e,i}(k-1)}{T} = \frac{L_m}{\tau_r} i_{ds}^e(k) - \frac{1}{\tau_r} \psi_{dr}^{e,i}(k) \quad (3-17)$$

where T being the sampling period (sec). When rearranged (3-17) gives

$$\psi_{dr}^{e,i}(k) = \frac{\tau_r}{\tau_r + T} \psi_{dr}^{e,i}(k-1) - \frac{L_m \times T}{\tau_r + T} i_{ds}^e(k) \quad (3-18)$$

The stator flux linkages in (3-10) and (3-11) are discretized by using trapezoidal approximation as;

$$\psi_{ds}^{s,v}(k) = \psi_{ds}^{s,v}(k-1) + \frac{T}{2} (e_{ds}^s(k) - e_{ds}^s(k-1)) \quad (3-19)$$

$$\psi_{qs}^{s,v}(k) = \psi_{qs}^{s,v}(k-1) + \frac{T}{2} (e_{qs}^s(k) - e_{qs}^s(k-1)) \quad (3-20)$$

where the back emf's are computed as;

$$e_{ds}^s(k) = u_{ds}^s(k) - i_{ds}^s(k)R_s - u_{comp,ds}^s(k) \quad (3-21)$$

$$e_{qs}^s(k) = u_{qs}^s(k) - i_{qs}^s(k)R_s - u_{comp,qs}^s(k) \quad (3-22)$$

Similarly, the PI control laws in (3-12) and (3-13) are also discretized by using trapezoidal approximation as

$$u_{comp,ds}(k) = K_p (\psi_{ds}^{s,v}(k) - \psi_{ds}^{s,i}(k)) + u_{comp,ds,i}(k-1) \quad (3-23)$$

$$u_{comp,qs}(k) = K_p (\psi_{qs}^{s,v}(k) - \psi_{qs}^{s,i}(k)) + u_{comp,qs,i}(k-1) \quad (3-24)$$

where the accumulating integral terms are;

$$\begin{aligned}
u_{comp,ds,i}(k) &= u_{comp,ds,i}(k-1) + \frac{K_p T}{T_I} (\psi_{ds}^{s,v}(k) - \psi_{ds}^{s,i}(k)) \\
&= u_{comp,ds,i}(k-1) + K_p K_I (\psi_{ds}^{s,v}(k) - \psi_{ds}^{s,i}(k))
\end{aligned} \tag{3-25}$$

$$\begin{aligned}
u_{comp,qs,i}(k) &= u_{comp,qs,i}(k-1) + \frac{K_p T}{T_I} (\psi_{qs}^{s,v}(k) - \psi_{qs}^{s,i}(k)) \\
&= u_{comp,qs,i}(k-1) + K_p K_I (\psi_{qs}^{s,v}(k) - \psi_{qs}^{s,i}(k))
\end{aligned} \tag{3-26}$$

3.1.1.3. Flux Estimation in Discrete Time and Per-Unit

All equations are needed to be normalized into per-unit by the specified base quantities. Firstly, the rotor flux linkage in current model (3-18) is normalized by dividing the base flux linkage ψ_b as

$$\psi_{dr,pu}^{e,i}(k) = \frac{\tau_r}{\tau_r + T} \psi_{dr,pu}^{e,i}(k-1) - \frac{T}{\tau_r + T} i_{ds,pu}^e(k) \tag{3-27}$$

where $\psi_B = L_m I_B$ is the base flux linkage and I_B is the base current. Next, the stator flux linkages in the current model (3-8) and (3-9) are similarly normalized by dividing the base flux linkage as

$$\psi_{ds,pu}^{s,i}(k) = \frac{L_s L_r - L_m^2}{L_s L_r} i_{ds,pu}^s(k) + \frac{L_m}{L_r} \psi_{dr,pu}^{s,i}(k) \tag{3-28}$$

$$\psi_{qs,pu}^{s,i}(k) = \frac{L_s L_r - L_m^2}{L_s L_r} i_{qs,pu}^s(k) + \frac{L_m}{L_r} \psi_{qr,pu}^{s,i}(k) \quad (3-29)$$

Then, the back emf's in (3-21) and (3-22) are normalized by dividing the base phase voltage V_B .

$$e_{ds,pu}^s(k) = u_{ds,pu}^s(k) - \frac{I_b R_s}{V_b} i_{ds,pu}^s(k) - u_{comp,ds,pu}^s(k) \quad (3-30)$$

$$e_{qs,pu}^s(k) = u_{qs,pu}^s(k) - \frac{I_b R_s}{V_b} i_{qs,pu}^s(k) - u_{comp,qs,pu}^s(k) \quad (3-31)$$

Next, the stator flux linkages in the voltage model (3-19) and (3-20) are divided by the base flux linkage.

$$\psi_{ds,pu}^{s,v}(k) = \psi_{ds,pu}^{s,v}(k-1) + \frac{V_b T}{L_m I_b} \left(\frac{e_{ds,pu}^s(k) + e_{ds,pu}^s(k-1)}{2} \right) \quad (3-32)$$

$$\psi_{qs,pu}^{s,v}(k) = \psi_{qs,pu}^{s,v}(k-1) + \frac{V_b T}{L_m I_b} \left(\frac{e_{qs,pu}^s(k) + e_{qs,pu}^s(k-1)}{2} \right) \quad (3-33)$$

Similar to (3-28) and (3-29) the normalized rotor flux linkages in the voltage model are:

$$\psi_{dr,pu}^{s,v}(k) = -\frac{L_s L_r - L_m^2}{L_m L_m} i_{ds,pu}^s(k) + \frac{L_r}{L_m} \psi_{ds,pu}^{s,v}(k) \quad (3-34)$$

$$\psi_{qr,pu}^{s,v}(k) = -\frac{L_s L_r - L_m^2}{L_m L_m} i_{qs,pu}^s(k) + \frac{L_r}{L_m} \psi_{qs,pu}^{s,v}(k) \quad (3-35)$$

In conclusion, the discrete-time, per-unit equations are rewritten in terms of constants.

The rotor flux linkages developed by the current model in synchronously rotating reference frame ($w=w_{\psi r}$) are:

$$\psi_{dr,pu}^{e,i}(k) = K_1 \psi_{dr,pu}^{e,i}(k-1) - K_2 i_{ds,pu}^e(k) \quad (3-36)$$

where

$$K_1 = \frac{\tau_r}{\tau_r + T} \quad (3-37)$$

$$K_2 = \frac{T}{\tau_r + T}$$

The rotor flux linkages developed by the current model in the stationary reference frame ($w=0$) are:

$$\psi_{ds,pu}^{s,i}(k) = K_4 i_{ds,pu}^s(k) + K_3 \psi_{dr,pu}^{s,i}(k) \quad (3-38)$$

$$\psi_{qs,pu}^{s,i}(k) = K_4 i_{qs,pu}^s(k) + K_3 \psi_{qr,pu}^{s,i}(k) \quad (3-39)$$

$$K_4 = \frac{L_s L_r - L_m^2}{L_s L_r} \quad (3-40)$$

$$K_3 = \frac{L_m}{L_r}$$

The back emf's developed by the voltage model in the stationary reference frame ($w=0$) is

$$e_{ds,pu}^s(k) = u_{ds,pu}^s(k) - K_5 i_{ds,pu}^s(k) - u_{comp,ds,pu}^s(k) \quad (3-41)$$

$$e_{qs,pu}^s(k) = u_{qs,pu}^s(k) - K_5 i_{qs,pu}^s(k) - u_{comp,qs,pu}^s(k) \quad (3-42)$$

$$K_5 = \frac{I_b R_s}{V_b} \quad (3-43)$$

The stator flux linkages developed by the voltage model in the stationary reference frame ($w=0$) are:

$$\psi_{ds,pu}^{s,v}(k) = \psi_{ds,pu}^{s,v}(k-1) + K_6 \left(\frac{e_{ds,pu}^s(k) + e_{ds,pu}^s(k-1)}{2} \right) \quad (3-44)$$

$$\psi_{qs,pu}^{s,v}(k) = \psi_{qs,pu}^{s,v}(k-1) + K_6 \left(\frac{e_{qs,pu}^s(k) + e_{qs,pu}^s(k-1)}{2} \right) \quad (3-45)$$

$$K_6 = \frac{V_b T}{L_m I_b} \quad (3-46)$$

The rotor flux linkages developed by the voltage model in the stationary reference frame ($w=0$) are:

$$\psi_{dr,pu}^{s,v}(k) = -K_8 i_{ds,pu}^s(k) + K_7 \psi_{ds,pu}^{s,v}(k) \quad (3-47)$$

$$K_8 = \frac{L_s L_r - L_m^2}{L_m L_m} \quad (3-48)$$

$$K_7 = \frac{L_r}{L_m}$$

The rotor flux angle developed by the voltage model

$$\theta_{\psi r,pu}(k) = \frac{1}{2\pi} \tan^{-1} \left[\frac{\psi_{qr,pu}^{s,v}(k)}{\psi_{dr,pu}^{s,v}(k)} \right] \quad (3-49)$$

The required parameters for this module are summarized as follows:

- The machine Parameters:
- Stator resistance (R_s)
- Rotor resistance (R_r)
- Stator leakage inductance (L_{ls})
- Rotor leakage inductance (L_{lr})
- Magnetizing inductance (L_m)
- The based quantities:
- Base current (I_b)
- Base phase voltage (V_b)
- The sampling period(T)

The stator self inductance is $L_s = L_{ls} + L_m$ and the rotor self inductance is $L_r = L_{lr} + L_m$.

CHAPTER 4

SPEED ESTIMATION FOR SENSORLESS DIRECT FIELD

ORIENTED CONTROL OF INDUCTION MACHINE

The rotor speed estimation is examined with three estimation schemes. The reactive power MRAS speed estimator, open-loop speed estimator, speed estimator using Kalman filter are implemented.

4.1. Reactive Power MRAS Scheme

Model Reference Adaptive System (MRAS) is one of the most popular adaptive control method used in motor control applications for tracking and observing system parameters and states [23-27, 30-31]. There exist a number of different model reference adaptive control techniques such as parallel model, series model, direct model and indirect model etc. MRAS used in this thesis is parallel model MRAS that compares both the outputs of a reference model and adaptive model and processes the error between these two according to the appropriate adaptive laws that do not deteriorate the stability requirements of the applied system.

In a MRAS system, some state variables x_d, x_q (e.g. back e.m.f components (e_{md}, e_{mq}) reactive power components (q_{md}, q_{mq}), rotor flux components (ψ_{rd}, ψ_{rq}) etc.) of the induction machine, which are obtained from sensed variables such as stator voltage and currents, are estimated in reference model and are then compared with state variables \hat{x}_d and \hat{x}_q estimated by using adaptive model. The difference between these state variables is then used in adaptation mechanism, which outputs the estimated value of the rotor speed (w_r) and adjusts the adaptive model until satisfactory performance is obtained. Such a scheme is shown in Figure 4-1

corresponds to implementation of MRAS for speed estimation using space vectors, and components of the space vector are shown.

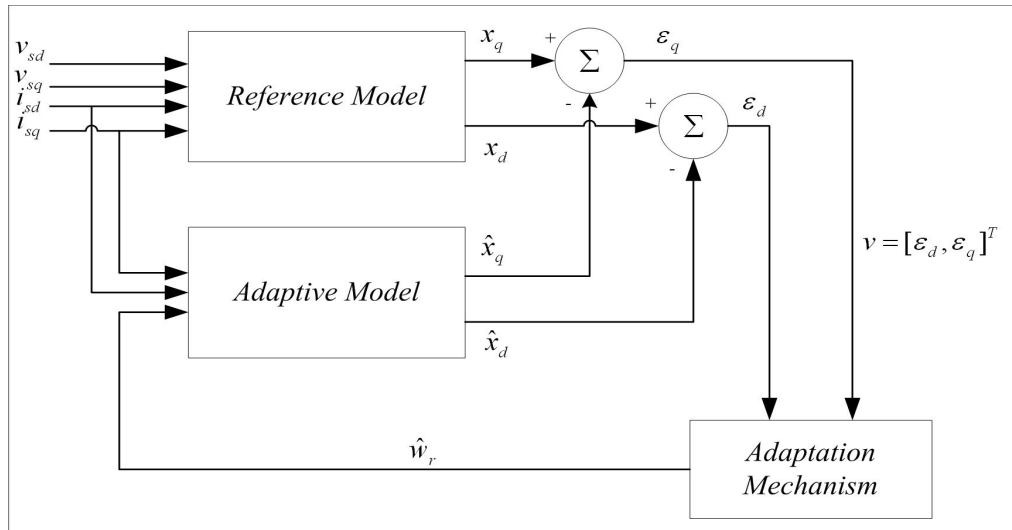


Figure 4-1 MRAS based speed estimator scheme using space vector

To improve the performance of the observers described in this section, various practical techniques are also discussed which avoid use of pure integrators. Pure integrators leads drift and initial condition problems in digital applications, so recent speed sensorless algorithms tend to avoid pure integrators. Most of the traditional vector control algorithms use low-pass filter instead of pure integrators that also causes serious problems at low speed range. Reactive power scheme described below is robust to stator resistance and rotor resistance variations and can even be applied at very low speeds [23].

Equations for an induction motor in the stationary frame can be expressed as:

$$V_S = R_S i_S + \sigma L_S \frac{di_S}{dt} + e_m \quad (4-1)$$

where $\sigma = 1 - \frac{L_m^2}{L_r L_s}$ (*leakage coefficient*).

$$\frac{di_m}{dt} = \bar{w}_r \times i_m - \frac{1}{\tau_r} i_m + \frac{1}{\tau_r} i_s \quad (4-2)$$

where \bar{w}_r is a vector whose magnitude w_r is rotor electrical angular velocity, and whose direction is determined according to right hand system of coordinates as shown in Figure 4-2 “ \times ” denotes the cross product of vectors respectively

From (4-1) and (4-2), e_m and structure of MRAS can be derived as follows:

$$e_m = V_s - \left(R_s i_s + \sigma L_s \frac{di_s}{dt} \right) \quad (4-3)$$

$$e_m = L'_m \frac{di_m}{dt} \quad (4-4)$$

$$= L'_m \left(w_r \times i_m - \frac{1}{\tau_r} i_m + \frac{1}{\tau_r} i_s \right) \quad (4-5)$$

where $L'_m = \frac{L_m^2}{L_r}$ and $\tau_r = \frac{L_r}{R_r}$

If we rewrite the equations above for the direct and quadrature-axis back-emf in the following forms:

$$\begin{aligned}
e_{md} &= L_m \frac{di_{md}}{dt} = \frac{L_m}{L_r} \frac{d\psi_{rd}}{dt} \\
&= V_{sd} - \left(R_s i_{ds} + \sigma L_s \frac{di_{sd}}{dt} \right)
\end{aligned} \tag{4-6}$$

$$\begin{aligned}
e_{mq} &= L_m \frac{di_{mq}}{dt} = \frac{L_m}{L_r} \frac{d\psi_{rq}}{dt} \\
&= V_{sq} - \left(R_s i_{sq} + \sigma L_s \frac{di_{sq}}{dt} \right)
\end{aligned} \tag{4-7}$$

Instantaneous reactive power is defined as q_m as the cross product of the counter emf vector e_m and the stator current vector. That is

$$q_m \overset{\Delta}{=} i_s \times e_m \tag{4-8}$$

q_m is a vector, whose direction is shown in Figure 4-2 and whose magnitude q_m represents the instantaneous reactive power maintaining the magnetizing current.

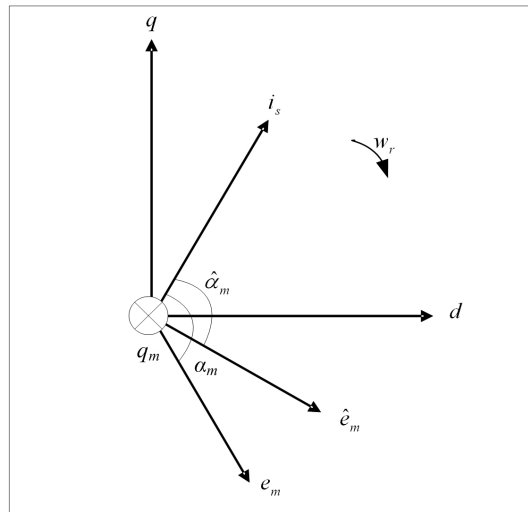


Figure 4-2 Coordinates in stationary reference frame

Substituting (4-6) and (4-7) for e_m in (4-8) noting that $i_s \times i_s = 0$, we have

$$q_m = i_s \times \left(v_s - \sigma L_s \frac{di_s}{dt} \right) \quad (4-9)$$

$$q_m = \frac{L_m^2}{L_r} \left((i_m \bullet i_s) \omega_r + \frac{1}{\tau_r} i_m \times i_s \right) \quad (4-10)$$

Using (4-9) and (4-10) as the reference model and the adaptive model, respectively and it is evident that the speed estimation system of Figure 4-3 is completely robust to the stator resistance, besides requiring no integral calculation.

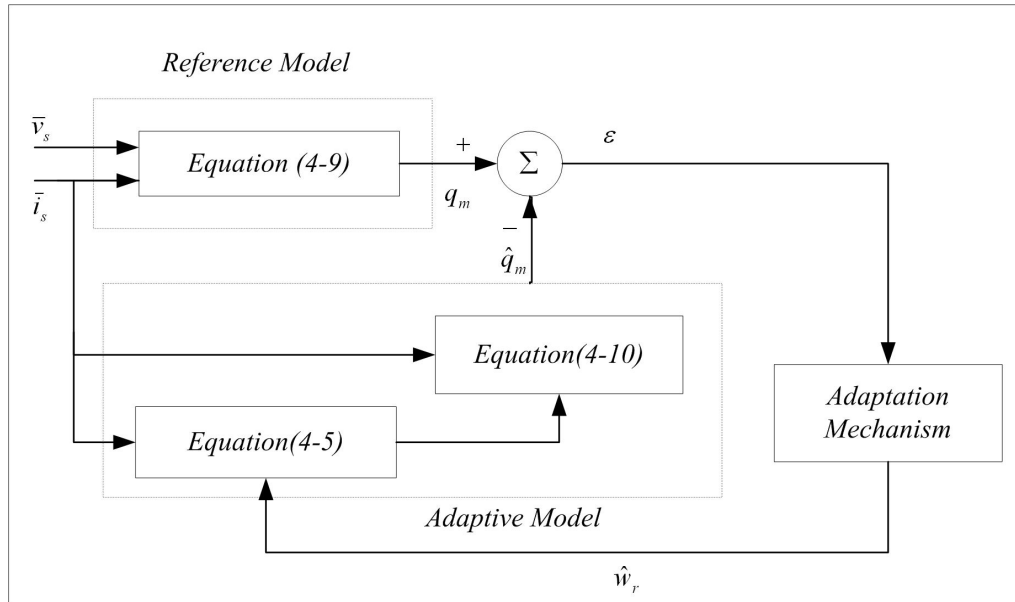


Figure 4-3 System structure of rotor speed observer using the tuning signal ε

The information required for this module is stator voltage and stator current components in the dq stationary reference frame. Two sets of equations are developed to compute reactive power of the induction motor in the reference and adaptive models. The reference model does not involve the rotor speed while the adaptive model needs the estimated rotor speed to adjust the computed reactive power to that computed from the reference model. Notice that the representation of complex number is defined for the stator voltages and currents in the stationary reference frame i.e., $v_s = v_{sd} + jv_{sq}$ and $\bar{i}_s = i_{sd} + ji_{sq}$.

4.1.1. Reference Model Continuous Time Representation

The back-emf of the induction motor can be expressed in the stationary frame as follows

$$\hat{e}_{md} = \frac{L_m}{L_r} \frac{d\psi_{rd}}{dt} = v_{sd} - R_s i_{sd} - \sigma L_s \frac{di_{sd}}{dt} \quad (4-11)$$

$$\hat{e}_{mq} = \frac{L_m}{L_r} \frac{d\psi_{rq}}{dt} = v_{sq} - R_s i_{sq} - \sigma L_s \frac{di_{sq}}{dt} \quad (4-12)$$

$$\bar{e}_m = e_{md} + je_{mq} \quad (4-13)$$

The reactive power of the induction motor can be computed from cross product of stator currents and back-emf vectors as follows:

$$q_m = \bar{i}_s \times \bar{e}_m = \bar{i}_s \times \left(v_s - R_s \bar{i}_s - \sigma L_s \frac{d\bar{i}_s}{dt} \right) = \bar{i}_s \times \bar{v}_s - \bar{i}_s \times \sigma L_s \frac{d\bar{i}_s}{dt} \quad (4-14)$$

where $\bar{i}_s \times \bar{i}_s = i_{sd}i_{sq} - i_{sq}i_{sd} = 0$. As a result the reactive power shown in (4-14) can further be derived as

$$q_m = i_{sd}v_{sq} - i_{sq}v_{sd} - \sigma L_s \left(i_{sd} \frac{di_{sq}}{dt} - i_{sq} \frac{di_{sd}}{dt} \right) \quad (4-15)$$

4.1.2. Adaptive Model Continuous Time Representation

The estimated back-emf computed in the adaptive model can be expressed as follows:

$$\hat{e}_{md} = \frac{L_m^2}{L_r} \frac{di_{md}}{dt} = \frac{L_m^2}{L_r} \left(-\tau_r \hat{\omega}_r i_{mq} - i_{md} + i_{sd} \right) \quad (4-16)$$

$$\hat{e}_{mq} = \frac{L_m^2}{L_r} \frac{di_{mq}}{dt} = \frac{L_m^2}{L_r} \left(-\tau_r \hat{\omega}_r i_{md} - i_{mq} + i_{sq} \right) \quad (4-17)$$

$$\hat{e}_m = \hat{e}_{md} + j\hat{e}_{mq} \quad (4-18)$$

where $\tau_r = \frac{L_r}{R_r}$ is the rotor time constant, i_{md} , i_{mq} are computed from the following equations:

$$\frac{di_{md}}{dt} = -\hat{\omega}_r i_{mq} - \frac{1}{\tau_r} i_{md} + \frac{1}{\tau_r} i_{sd} \quad (4-19)$$

$$\frac{di_{mq}}{dt} = -\hat{\omega}_r i_{md} - \frac{1}{\tau_r} i_{mq} + \frac{1}{\tau_r} i_{sq} \quad (4-20)$$

Once the estimated back-emf computed by (4-16)-(4-20), the estimated reactive power can be computed as follows:

$$\hat{q}_m = \bar{i}_s \times \hat{e}_m = i_{sd} \hat{e}_{mq} - i_{sq} \hat{e}_{md} \quad (4-21)$$

Then, the PI controller tunes the estimated rotor speed such that the reactive power generated by adaptive model matches that generated by reference model. The speed tuning signal is the error of reactive power that can be expressed as follows:

$$\varepsilon_{\Delta e} = \bar{i}_s \times (\bar{e}_m - \hat{e}_m) = q_m - \hat{q}_m \quad (4-22)$$

When this observer is used in a vector-controlled drive, it is possible to obtain satisfactory performance even at very low speeds. The observer can track the actual rotor speed with a bandwidth that is only limited by noise, so the PI controller gains should be as large as possible. The scheme is insensitive to stator resistance variations. The parameter τ_r has a negligible influence on the operation of both of the overall MRAS vector control systems. If the MRAS successfully maintains nearly zero error, and if the same value of τ_r is used in the MRAS adjustable models and in the function block for calculating w_{sl} , then we have the following relations:

$$w_e = \hat{w}_e \quad \text{and} \quad \tau_r w_{sl} = \hat{\tau}_r \hat{w}_{sl}$$

where variables without “^” are actual values, and ones with “^” represent the corresponding values used in the MRAS vector control systems. Thus, if $\tau_r \neq \hat{\tau}_r$, then $w_{sl} \neq \hat{w}_{sl}$, but $w_e = \hat{w}_e$, which is used for orienting the stator current vector. Therefore, complete field orientation can be achieved even if the value of τ_r is quite wrong. The error in the value of τ_r , however, produces an error in the speed feedback, thus affecting the accuracy of the speed control as follows:

$$\varepsilon_w = \hat{w}_r - w_r = \left(1 - \frac{\tau_r}{\hat{\tau}_r}\right) w_{sl} \quad (4-23)$$

This also holds for the previous MRAS scheme. However, the accuracy of the speed estimation system discussed depends on the transient stator inductance and also referred magnetizing inductance. The latter quantity is not too problematic, since it does not change with temperature. Furthermore, deviations of τ_r from its correct value produce a steady-state error in the estimated speed and this error become significant at low speeds.

4.1.3. Discrete Time Representation

For implementation on digital system, the differential equations need to be transformed to difference equations. Due to high sampling frequency compared to bandwidth of the system, the simple approximation of numerical integration, such as forward, backward, or trapezoidal rules, can be adopted [34]. Consequently, the reactive power equations in both the reference and the adaptive models are discretized as follows:

4.1.3.1. Reference Model

According to (4-15) reference model reactive power is given as:

$$q_m = i_{sd} v_{sq} - i_{sq} v_{sd} - \sigma L_s \left(i_{sd} \frac{di_{sq}}{dt} - i_{sq} \frac{di_{sd}}{dt} \right)$$

Using backward approximation:

$$q_m(k) = i_{sd}(k)v_{sq}(k) - i_{sq}(k)v_{sd}(k) - \sigma L_s \left(i_{sd}(k) \frac{i_{sq}(k) - i_{sq}(k-1)}{T} - i_{sq}(k) \frac{i_{sd}(k) - i_{sd}(k-1)}{T} \right) \quad (4-24)$$

and this equation can be further simplified as:

$$q_m(k) = i_{sd}(k)v_{sq}(k) - i_{sq}(k)v_{sd}(k) - \frac{\sigma L_s}{T} (i_{sd}(k-1)i_{sq}(k) - i_{sd}(k)i_{sq}(k-1)) \quad (4-25)$$

where T is the sampling time.

4.1.3.2. Adaptive Model

According to (4-21), reactive power in adaptive model is derived as

$$\hat{q}_m = \bar{i}_s \times \hat{e}_m = i_{sd} \hat{e}_{mq} - i_{sq} \hat{e}_{md}$$

whose discrete time representation is:

$$\hat{q}_m(k) = i_{sd}(k) \hat{e}_{mq}(k) - i_{sq}(k) \hat{e}_{md}(k) \quad (4-26)$$

where $\hat{e}_{md}(k)$ and $\hat{e}_{mq}(k)$ are computed as follows:

Continuous time representation:

$$\begin{aligned}\hat{e}_{md} &= \frac{L_m^2}{L_r} \frac{di_{md}}{dt} = \frac{L_m^2}{L_r} \left(-\tau_r \hat{\omega}_r i_{mq} - i_{md} + i_{sd} \right) \\ \hat{e}_{mq} &= \frac{L_m^2}{L_r} \frac{di_{mq}}{dt} = \frac{L_m^2}{L_r} \left(-\tau_r \hat{\omega}_r i_{md} - i_{mq} + i_{sq} \right)\end{aligned}\tag{4-27}$$

Discrete time representation:

$$\begin{aligned}\hat{e}_{md}(k) &= \frac{L_m^2}{L_r} \left(-\tau_r \hat{\omega}_r(k) i_{mq}(k) - i_{md}(k) + i_{sd}(k) \right) \\ \hat{e}_{mq}(k) &= \frac{L_m^2}{L_r} \left(-\tau_r \hat{\omega}_r(k) i_{md}(k) - i_{mq}(k) + i_{sq}(k) \right)\end{aligned}\tag{4-28}$$

and $i_{md}(k), i_{mq}(k)$ can be solved by using trapezoidal integration method, it yields

Continuous time representation:

$$\begin{aligned}\frac{di_{md}}{dt} &= -\hat{\omega}_r i_{mq} - \frac{1}{\tau_r} i_{md} + \frac{1}{\tau_r} i_{sd} \\ \frac{di_{mq}}{dt} &= -\hat{\omega}_r i_{md} - \frac{1}{\tau_r} i_{mq} + \frac{1}{\tau_r} i_{sq}\end{aligned}\tag{4-29}$$

Discrete time representation:

$$\begin{aligned}
 i_{md}(k) &= i_{md}(k-1) \left[-\frac{T^2}{2} \hat{w}_r^2(k) + 1 - \frac{T}{\tau_r} + \left(\frac{T}{\tau_r} \right)^2 \right] - \\
 & i_{mq}(k-1) \hat{w}_r(k) \left[T - \frac{T^2}{\tau_r} \right] + i_{sd}(k) \left[\frac{T}{T_r} - \frac{T^2}{2\tau_r^2} \right] - \\
 & i_{sq}(k) \hat{w}_r(k) \left[\frac{T^2}{2\tau_r} \right]
 \end{aligned} \tag{4-30}$$

$$\begin{aligned}
 i_{mq}(k) &= i_{mq}(k-1) \left[-\frac{T^2}{2} \hat{w}_r^2(k) + 1 - \frac{T}{\tau_r} + \left(\frac{T}{\tau_r} \right)^2 \right] - \\
 & i_{md}(k-1) \hat{w}_r(k) \left[T - \frac{T^2}{\tau_r} \right] + i_{sq}(k) \left[\frac{T}{T_r} - \frac{T^2}{2\tau_r^2} \right] - \\
 & i_{sd}(k) \hat{w}_r(k) \left[\frac{T^2}{2\tau_r} \right]
 \end{aligned} \tag{4-31}$$

4.2. Open Loop Speed Estimator

The open loop speed estimator based on the equations of the induction motor in the stationary reference frame [35]. Rotor flux linkage equations are as given below in (4-32) and (4-33).

$$\psi_{dr}^s = L_r i_{dr}^s + L_m i_{ds}^s \tag{4-32}$$

$$\psi^s_{qr} = L_r i^s_{qr} + L_m i^s_{qs} \quad (4-33)$$

The rotor currents can be expressed as in (4-34), (4-35).

$$i^s_{dr} = \frac{1}{L_r} (\psi^s_{dr} - L_m i^s_{ds}) \quad (4-34)$$

$$i^s_{qr} = \frac{1}{L_r} (\psi^s_{qr} - L_m i^s_{qs}) \quad (4-35)$$

The rotor voltage equations are used to find rotor flux dynamics as in (4-36), (4-37).

$$0 = R_r i^s_{dr} + \omega_r \psi^s_{qr} + \frac{d\psi^s_{dr}}{dt} \quad (4-36)$$

$$0 = R_r i^s_{qr} + \omega_r \psi^s_{dr} + \frac{d\psi^s_{qr}}{dt} \quad (4-37)$$

Substituting the current equations (4-34), (4-35) into (4-36), (4-37) rotor flux dynamics can be stated as in (4-38), (4-39).

$$\frac{d\psi^s_{dr}}{dt} = -\frac{1}{\tau_r} \psi^s_{dr} + \frac{L_m}{\tau_r} i^s_{ds} - \omega_r \psi^s_{qr} \quad (4-38)$$

$$\frac{d\psi_{qr}^s}{dt} = -\frac{1}{\tau_r}\psi_{qr}^s + \frac{L_m}{\tau_r}i_{qs}^s + \omega_r\psi_{dr}^s \quad (4-39)$$

where $\tau_r = \frac{L_r}{R_r}$ is the rotor time constant.

Then rotor flux linkage magnitude and the angle can be computed as:

$$\psi_r^s = \sqrt{\psi_{qr}^s{}^2 + \psi_{dr}^s{}^2} \quad (4-40)$$

$$\theta_{\psi_r} = \tan^{-1}\left(\frac{\psi_{qr}^s}{\psi_{dr}^s}\right) \quad (4-41)$$

This method is sensitive to parameter estimation. Nevertheless, the open-loop speed estimation is changed that uses computed flux angle; the flux angle from adaptive flux estimator is used instead which gives a better estimate for flux angle due to its adaptive mechanism. Then the electrically angular velocity is calculated taking the derivative of the flux angle in (4-41).

$$\omega_e = \frac{d\theta_{\psi_r}}{dt} = \frac{(\psi_{dr}^s)^2}{(\psi_r^s)^2} \left(\frac{\psi_{dr}^s \frac{d\psi_{qr}^s}{dt} - \psi_{qr}^s \frac{d\psi_{dr}^s}{dt}}{(\psi_{dr}^s)^2} \right) \quad (4-42)$$

Substituting equations (4-38), (4-39) into (4-42) and rearranging (4-43) is obtained.

$$w_e = \frac{d\theta_{\psi_r}}{dt} = w_r + \frac{1}{(\psi_r^s)^2} \frac{L_m}{\tau_r} (\psi_{dr}^s i_{qs}^s - \psi_{qr}^s i_{ds}^s) \quad (4-43)$$

The second term in the right hand side is the angular slip velocity term $w_{sl}=(I-S)w_e$ which is proportional to the electromagnetic torque while the rotor flux magnitude is maintained constant. Then the rotor speed can be found as:

$$w_r = w_e - \frac{1}{(\psi_r^s)^2} \frac{L_m}{\tau_r} (\psi_{dr}^s i_{qs}^s - \psi_{qr}^s i_{ds}^s) \quad (4-44)$$

The rotor speed output is filtered with a first order low pass filter to eliminate high frequency noise which comes from the differentiation.

4.3. Kalman Filter for Speed Estimation

4.3.1. Discrete Kalman Filter

In 1960, R.E. Kalman published recursive solution to the discrete data linear filtering problem Kalman60. Since that time, due in large part to advances in digital computing; the Kalman filter has been the subject of extensive research and application, particularly in the area of autonomous or assisted navigation. The Kalman filter addresses the general problem of trying to estimate the state $x \in \mathfrak{R}^n$ of a discrete-time controlled process that is governed by the linear stochastic difference equation [36]:

$$x_k = Ax_{k-1} + Bu_{k-1} + w_{k-1}, \quad (4-45)$$

with a measurement $z \in \mathfrak{R}^m$ that is

$$z_k = Hx_k + v_k . \quad (4-46)$$

The random variables w_k and v_k represent the process and measurement noise (respectively). They are assumed to be independent (of each other), white, and with normal probability distributions

$$p(w) \approx N(0, Q), \quad (4-47)$$

$$p(v) \approx N(0, R). \quad (4-48)$$

In practice, the process noise covariance Q and measurement noise covariance R matrices might change with each time step or measurement, however here it is assumed that they are constant. The $n \times n$ matrix A in the difference equation (4-45) relates the state at the previous time $k-1$ step to the state at the current step k , in the absence of either a driving function or process noise. In practice A might change with each time step, but here we assume it is constant. The matrix B relates the optional control input $u \in \mathfrak{R}^l$ to the state x . The $m \times n$ matrix H in the measurement equation (4-46) relates the state to the measurement z_k . In practice H might change with each time step or measurement, but here we assume it is constant.

4.3.2. Computational Origins of the Filter

Kalman Filter has two state estimates of the process a priori state estimate $\hat{x}_k^- \in \mathfrak{R}^n$ at step k given knowledge of the process prior to step k , and $\hat{x}_k \in \mathfrak{R}^n$ to be our a posteriori state estimate at step k given measurement z_k . Then, a priori and a posteriori estimate errors are defined.

$$e_k^- \equiv x_k - \hat{x}_k^-, \text{ and} \quad (4-49)$$

$$e_k \equiv x_k - \hat{x}_k. \quad (4-50)$$

The a priori estimate error covariance is then

$$P_k^- = E[e_k^- e_k^{-T}], \quad (4-51)$$

and the a posteriori estimate error covariance is

$$P_k = E[e_k e_k^T]. \quad (4-52)$$

An equation that computes an a posteriori state estimate as a linear combination of an a priori estimate and a weighted difference between an actual measurement and a measurement prediction is derived as shown below in (4-53).

$$\hat{x}_k = \hat{x}_k^- + K(z_k - H\hat{x}_k^-) \quad (4-53)$$

The difference $(z_k - H\hat{x}_k^-)$ in (4-53) is called the measurement *innovation*, or the *residual*. The residual reflects the discrepancy between the predicted measurement $H\hat{x}_k^-$ and the actual measurement z_k . A residual of zero means that the two are in complete agreement.

The matrix K in (4-53) is chosen to be the *gain* or *blending* factor that minimizes the a posteriori error covariance (4-52). This minimization can be accomplished by first substituting (4-53) into the above definition for e_k , substituting that into (4-52), performing the indicated expectations, taking the derivative of the trace of the result with respect to K , setting that result equal to zero, and then solving for K Maybeck79, Brown92, Jacobs93. One form of the resulting K that minimizes (4-52) is given by Brown92 [36].

$$K_k = P_k^- H^T (H P_k^- H^T + R)^{-1} \quad (4-54)$$

From this it can be seen that when the measurement error covariance matrix R reaches zero, the Kalman gain will weigh the residual more heavily:

$$\lim_{R_k \rightarrow 0} K_k = H^{-1}.$$

If this is the case, the actual measurement z_k is trusted more and more. At the same time, the predicted measurement $H\hat{x}_k^-$ is trusted less and less. If however the a priori estimate error covariance matrix P_k^- reaches zero, the Kalman gain will weigh the residual less heavily:

$$\lim_{P_k^- \rightarrow 0} K_k = 0 .$$

When this is the situation, as covariance matrix P_k^- approaches zero, the actual measurement is trusted less and less; on the other hand predicted measurement $H\hat{x}_k^-$ is trusted more and more.

4.3.3. The Discrete Kalman Filter Algorithm

The Kalman filter estimates a process by using a form of feedback control: the filter estimates the process state at some time and then obtains feedback in the form of (noisy) measurements. As such, the equations for the Kalman filter fall into two groups: time update equations and measurement update equations. The time update equations are responsible for projecting forward (in time) the current state and error covariance estimates to obtain the a priori estimates for the next time step. The measurement update equations are responsible for the feedback, i.e. for incorporating a new measurement into the a priori estimate to obtain an improved a posteriori estimate. The time update equations can also be thought of as predictor equations, while the measurement update equations can be thought of as corrector equations. Indeed the final estimation algorithm resembles that of a predictor-corrector algorithm for solving numerical problems.

Then the time update equations can be expressed as in (4-55), (4-56).

$$\hat{x}_k^- = A\hat{x}_{k-1} + Bu_{k-1} \tag{4-55}$$

$$P_k^- = AP_{k-1}A^T + Q \tag{4-56}$$

where these equations project the state and covariance estimates from $k-1$ to k .

The measurement update equations first calculate the Kalman gain K_k , (4-57). The next step is to actually measure the process to obtain z_k , then to produce an “a posteriori” state estimate (4-58) and the last step is to calculate an “a posteriori error covariance” estimate (4-59).

$$K_k = P_k^- H^T (H P_k^- H^T + R)^{-1} \quad (4-57)$$

$$\hat{x}_k = \hat{x}_k^- + K_k (z_k - H \hat{x}_k^-) \quad (4-58)$$

$$P_k = (I - K_k H) P_k^- \quad (4-59)$$

Then, the overall system diagram is as shown below in Figure 4-4.

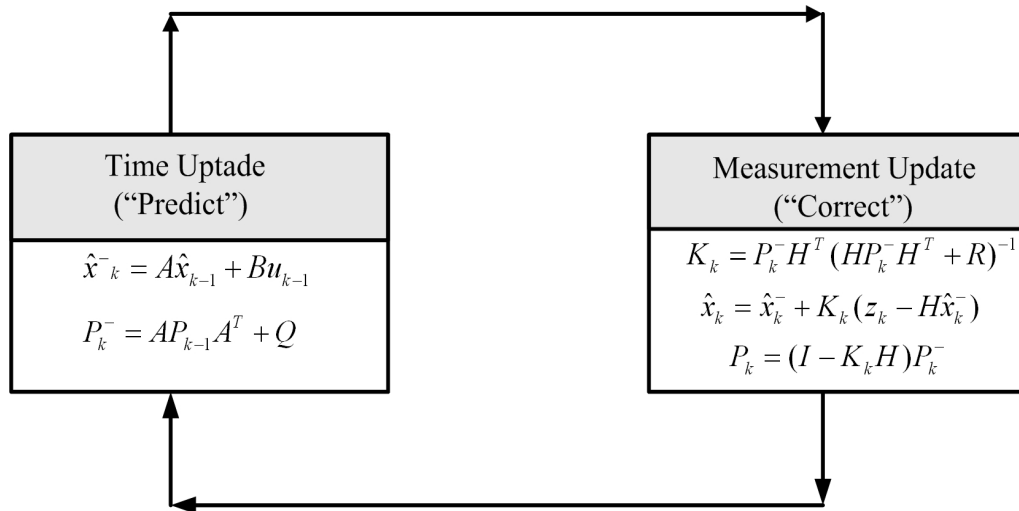


Figure 4-4 Kalman filter cycle

Filter recursively conditions the current estimate on all of the past measurements. After each “time” and “measurement update” pair, the process is repeated with the previous “a posteriori” estimates, used to project or predict the new “a priori estimates”.

Regarding to the speed estimator, the measurement used for this system is rotor

flux angle for z_k ; the A matrix is $\begin{bmatrix} 1 & T & T^2/2 \\ 0 & 1 & T \\ 0 & 0 & 1 \end{bmatrix}$, and the H matrix is $[1 \ 0 \ 0]$. Also,

the P_{k-1} for $k=0$ chosen to be $\begin{bmatrix} 1 & 1 & 1 \\ 1 & 1 & 1 \\ 1 & 1 & 1 \end{bmatrix}$ as initial condition for convergence. The first

row in A corresponds to position, second and third rows for velocity and acceleration respectively.

Finally, the overall sensorless, closed loop direct field oriented system structure is presented as in Figure 4-5.

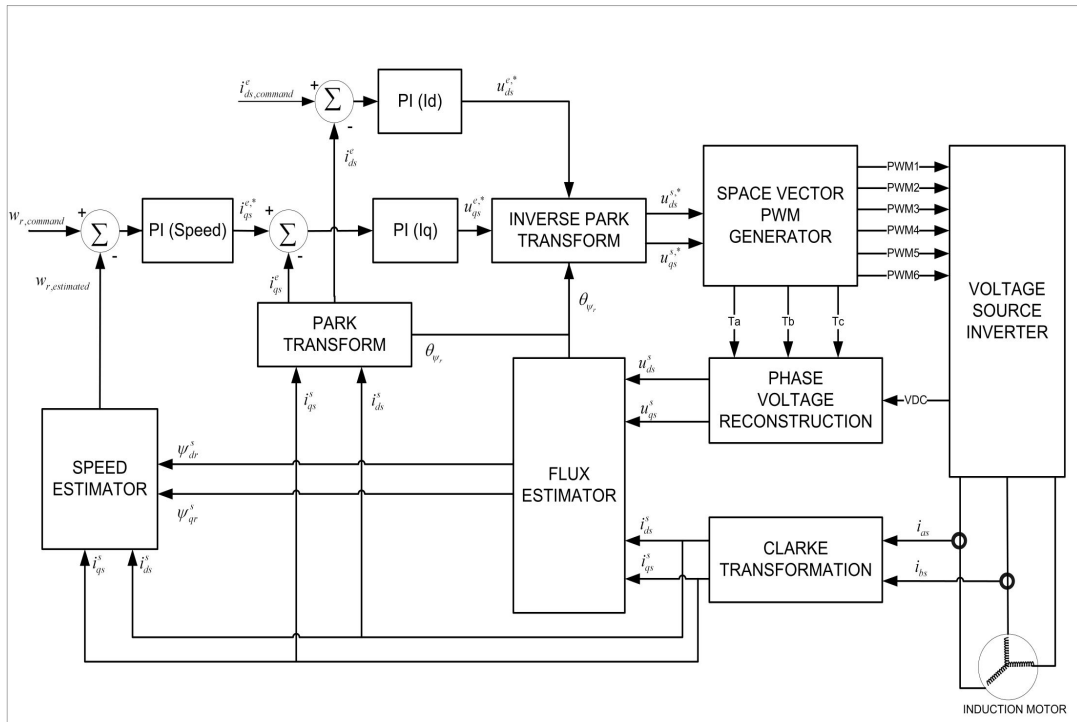


Figure 4-5 The overall sensorless DFOC scheme

CHAPTER 5

SIMULATIONS AND EXPERIMENTAL WORK

5.1. Simulations

Simulations were done to investigate effectiveness of the derived algorithms for the MRAS flux observer, open loop speed estimator and Kalman filter speed estimator. MATLAB Simulink is used as simulation tool. Voltage inputs and current outputs of the induction machine are used as the inputs of speed and flux estimators. The simulation parameters are same as real motor used in the experiments. These parameters are kept constant during simulations. They are given in Table 5-1. All simulations are carried out in discrete-time. Sampling time of simulations is the same with the one used in discrete time estimators of experiments.

Table 5-1 Simulation Parameters

Rotor resistance per phase (referred)	2.19 Ω
Stator resistance per phase	1.80 Ω
Stator self inductance per phase	0.192 H
Rotor self inductance per phase	0.192 H
Magnetizing inductance	0.184 H
Base line current	7.5 A
Base per phase voltage	220 V
Base torque	12.375 Nm
Base linkage flux	1.38 Vsec/rad
Base electrical angular velocity	314 rad/sec
Number of motor poles	4
Sampling frequency	0.0002 sec

5.1.1. Comparison of MRAS Speed Estimator, Open Loop Speed Estimator and Kalman Filter Speed Estimators

For comparison, the speed estimation of MRAS speed observer, open loop speed estimator and Kalman filter speed estimators are used. The simulations are realized using phase voltages and current data obtained from drive system by closed-loop speed control with Kalman filter speed estimator. The field is being established from zero initial conditions in due course of motor acceleration. The phase currents and voltages from motor drive system are applied to the flux estimator and to the MRAS speed estimator. The speed estimations of the Kalman Filter estimator and open loop speed estimator are obtained using electrical flux angle from the flux estimator. Moreover, angular slip velocity speed estimation is taken into account for exact speed estimation. The simulations were done for reference speed commands: *250rpm*, *500rpm*, *1000rpm* and *1500rpm* of the real drive system. In Figures 5-1 to 5-4 the electrical flux angle estimated in simulation, MRAS speed observer estimate, open loop speed observer estimate, Kalman Filter Speed estimate, estimated angular slip velocity are given at steady state of speed commands.

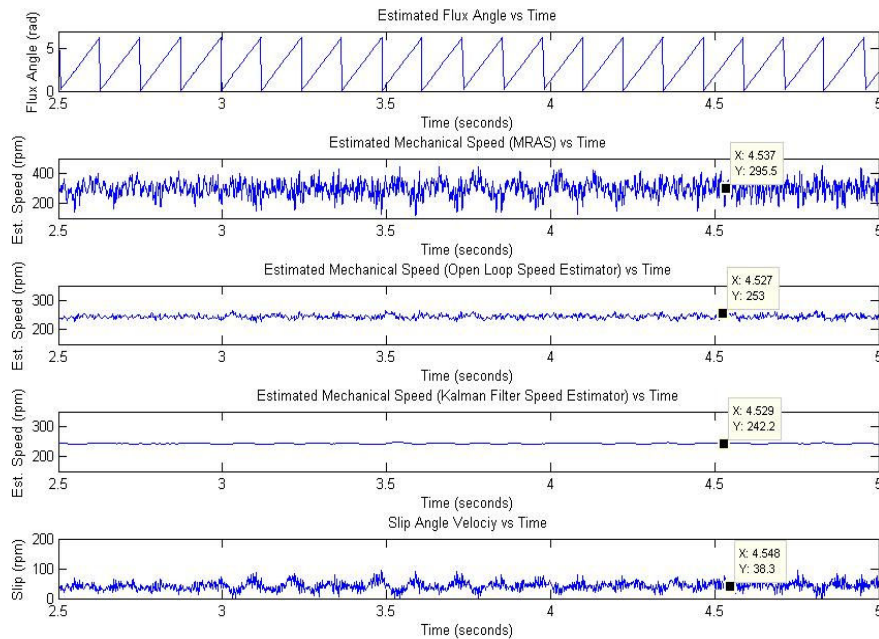


Figure 5-1 Comparison of performances of speed estimators for 250 rpm

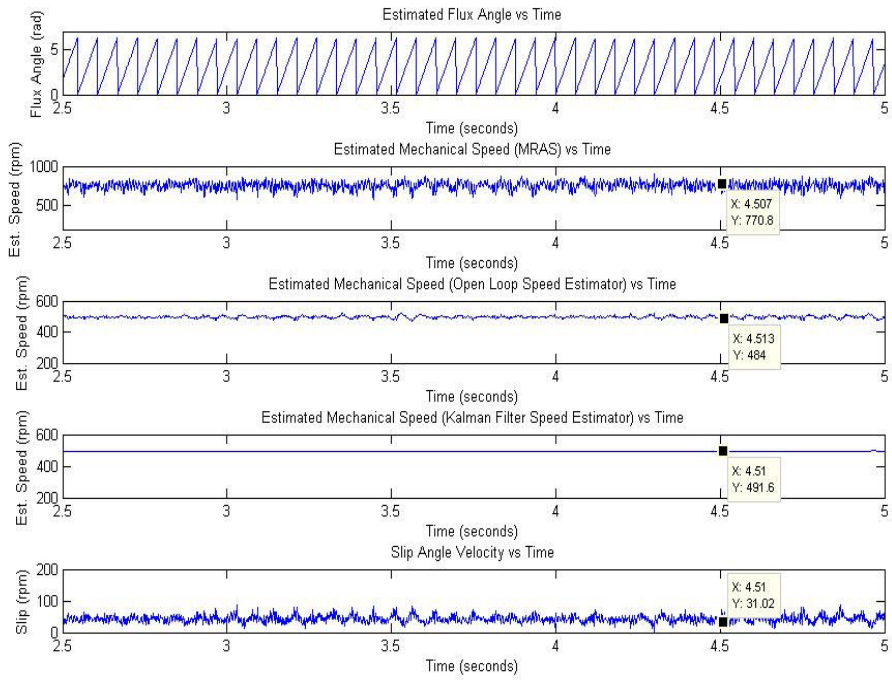


Figure 5-2 Comparison of performances of speed estimators for 500 rpm

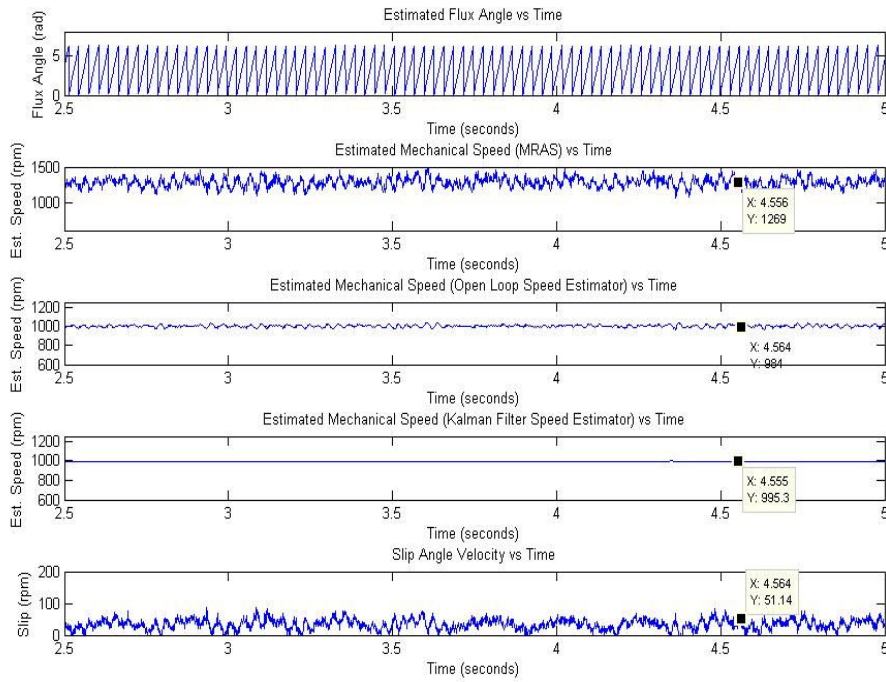


Figure 5-3 Comparison of performances of speed estimators for 1000 rpm

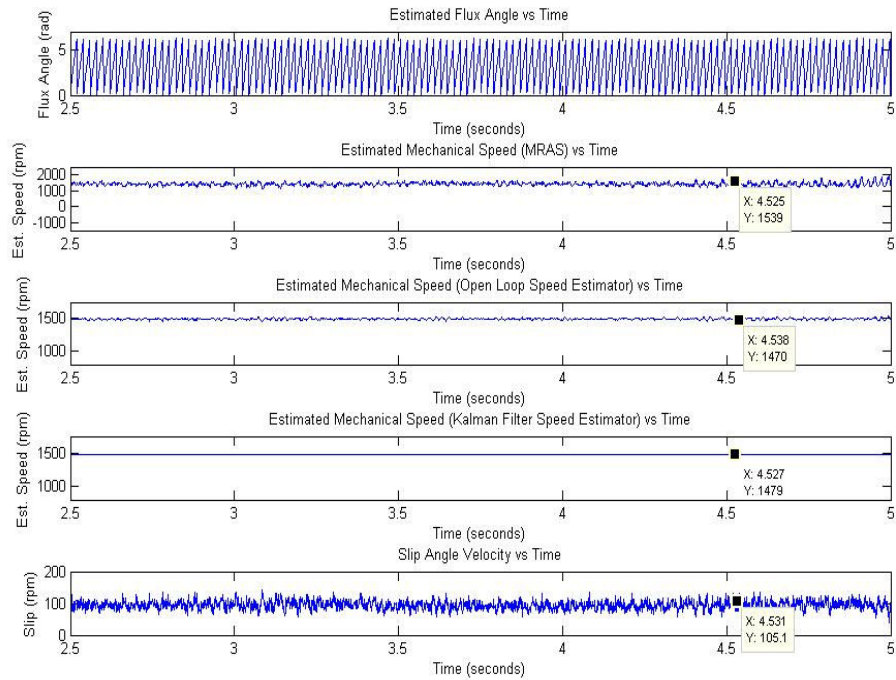


Figure 5-4 Comparison of performances of speed estimators for 1500 rpm

In these simulations required speed MRAS observer performance could not be obtained. This defectiveness probably comes from the PI regulator which is to minimize the reference and adaptive reactive power difference $\hat{q}_m - \hat{q}_m$ to give an estimate of the speed estimate $\hat{\omega}_m$. Moreover, in the drive system experiments MRAS observer constitutes a processor overloading problem due to high computational load. The Open loop speed estimator estimates speed with ripples which will be reflected to the closed-loop performance. In experiments, although it requires least computational load on the controller among the other concerned observers, it is not used because of its noisy output. On the other hand, the Kalman Filter speed observer has best performance in terms of estimation accuracy and low processing complexity. Therefore, the closed-loop experiments are focused on the models with Kalman filter speed estimator and detailed analysis is realized. The speed range chosen to be start 250rpm since flux estimator performance at the low speed it is not sufficient as estimation accuracy. In the rest of the simulations and succeeding

experiments same speed range used starting from 250rpm to the rated motor speed 1500rpm.

5.1.2. Speed Estimator Performance Verification

In this simulation, the speed estimator performance is investigated by applying angle values which are in the same form of the flux angle in the real system. The angle is generated from a counter in the simulation and directly applied to the Kalman filter speed estimator. By doing this, the speed estimator performance is studied distinctly from drive system. The simulations were done for 5rpm, 50rpm, 500rpm, 1000 rpm and 1500rpm. By estimating these speeds, the performance of the estimator is observed for different speeds. In Figures 5-5 to 5-9, the electrical angle applied to produce constant speed and the estimated speed by the speed estimator are given.

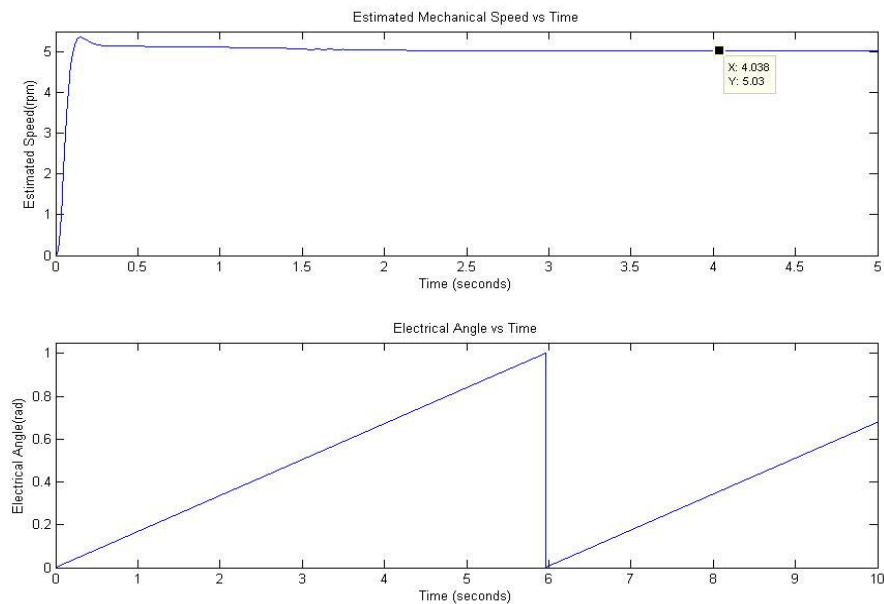


Figure 5-5 5rpm reference, Kalman filter performance verification

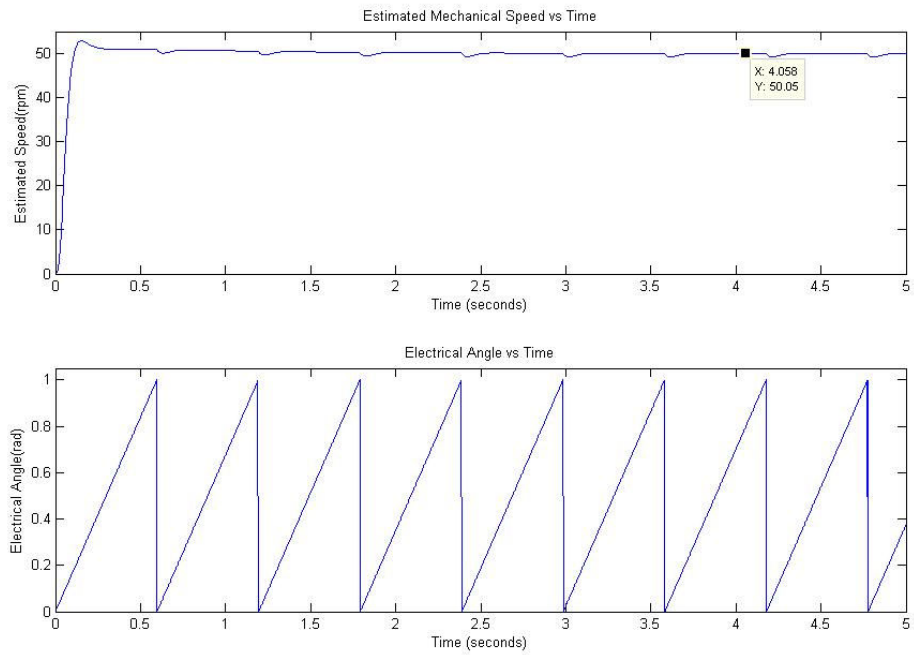


Figure 5-6 50rpm reference, Kalman filter performance verification

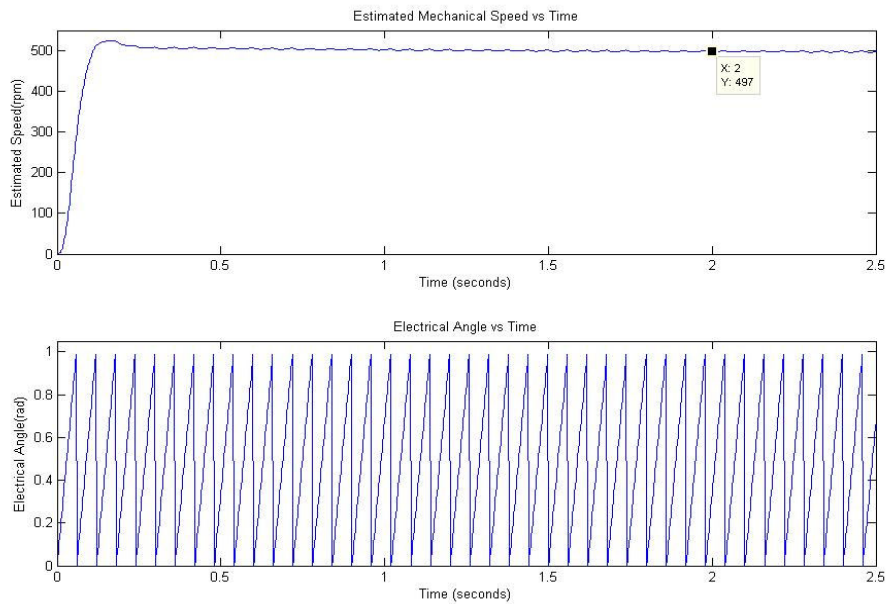


Figure 5-7 500rpm reference, Kalman filter performance verification

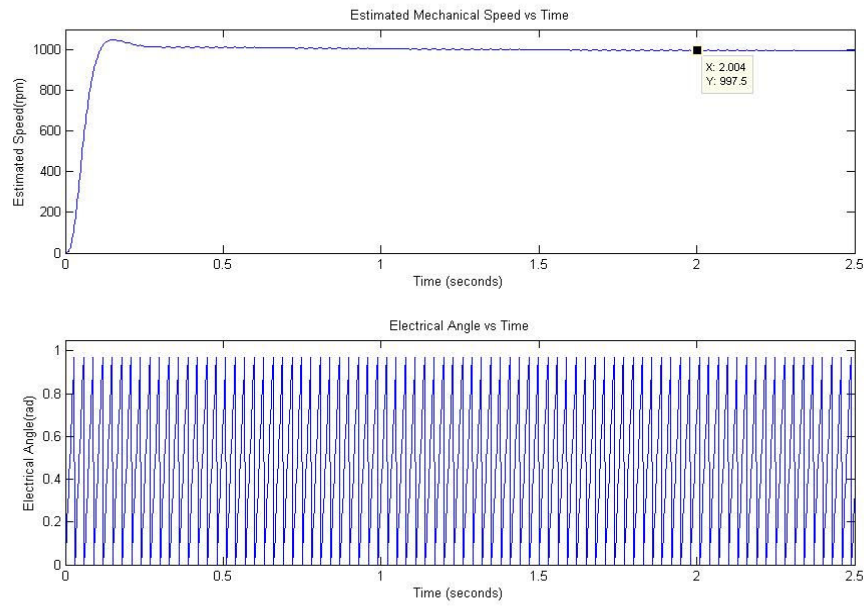


Figure 5-8 1000rpm reference, Kalman filter performance verification

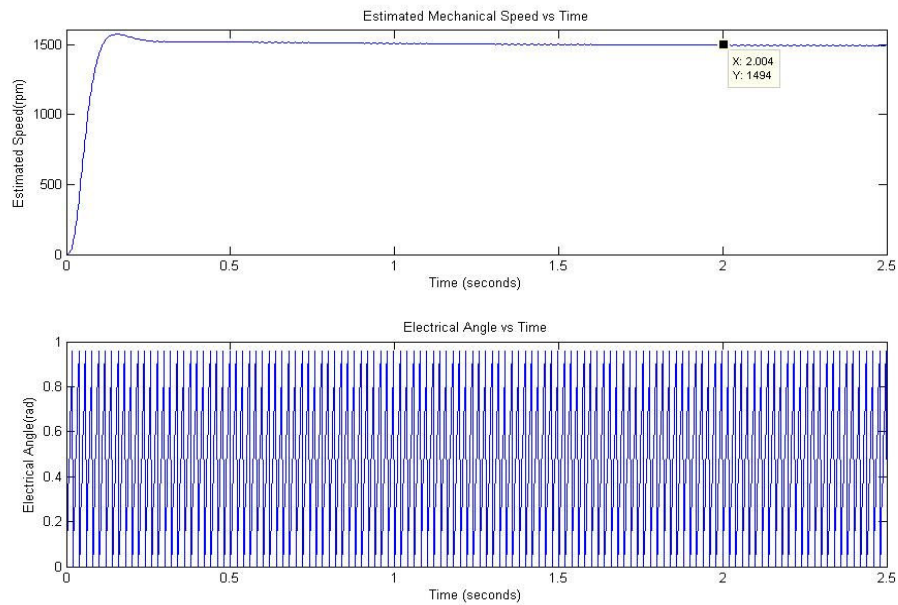


Figure 5-9 1500rpm reference, Kalman filter performance verification

In these simulations, motor speed estimation is quickly fits to desired speed with a small overshoot and a steady state speed error less than 1%. The rise time of the speed estimation of the estimator is also seen from graphs. These rise times also

affect the closed system performances since they are added as delay term to the speed loop response.

5.2. Experimental Work

The Speed estimator designed with Kalman Filter using electrical flux angle estimated by MRAS scheme have been tested experimentally for satisfactory operation at different speeds of motor. The observer was tuned for the whole speed range and for no-load and with load cases. During the tests, some processor overloading problems are occurred. The reasons of this overloading were handling flux and speed estimators' calculations and data logging altogether and ineffective code generation of software tools. Because of this drawback the torque loop could not be closed with *10 KHz* sampling rate. Thus, the sampling rate is slowed down to *5 KHz* for torque loop and to *1 KHz* for outer loops.

In the tests first, both I_d and I_q current control loops tuned using PI controllers which can be expressed as in (5-1) for continuous time.

$$PI_{I_{out}}(t) = K_p \cdot I_{error}(t) + K_I \int (I_{error}(t))dt \quad (5-1)$$

The continuous time PI controller equation discretized by using trapezoidal approximation as;

$$PI_{I_{out}}(z) = K_p \cdot I_{error}(z) + K_I \cdot I_{error}(z) \cdot T_s \frac{(z+1)}{2 \cdot (z-1)} \quad (5-2)$$

where T_s represents sample time.

For superior performance of speed loop, the proportional gain K_p and integral gain K_i parameters of these current loops must be fitted well to minimize the current errors. During the tuning of the PI regulator also some commonly used methods are tried; one of them is Ziegler-Nichols tuning criterion which is described as follows.

Step1: Set $K_i = 0$ and $K_d = 0$. Increase K_p in steps until the closed-loop response reaches a state of sustained oscillations. Mark this so-called ultimate gain denoted as K_{pu} . Measure the corresponding period of oscillation at the output, call it T_u .

Step2: Now set the parameters of the controller as $K_p = 0.45 * K_{pu}$, $K_i = 0.54 * K_{pu} / T_u$, $K_d = 0$.

With tuning of the current loops, closed loop torque control is achieved.

Then, the speed estimator is tuned by setting entries of the measurement noise covariance R matrix and the process noise covariance Q matrix to obtain fast and dynamic response and estimation accuracy. For the performance analysis of the estimator the machine is controlled in the speed loop with the Kalman filter speed estimator and closed loop speed control is achieved for induction motor. In order to, fulfill this operation again a PI controller is used which has same equations described in (5-1) and (5-2). The closed loop experiments first handled with an encoder coupled to the shaft of the induction motor to verify the estimation performance. Secondly, in no load case with the estimator to obtain the motor current and voltage data. Then, a permanent magnet motor is coupled with resolver to the induction motor to load the drive system and closed-loop speed control is verified under loading.

During the experiments, two of the three phase currents were measured. The phase voltages were calculated internally using measured DC-Link voltage. The current measurements and the DC-Link measurement were done with isolated transducers and 16-bit A/D conversion.

5.2.1. Experiments to Compare Speed Estimate with Actual Speed of Motor

In these no-load experiments, motor is run in the closed-speed loop mode and the quadrature encoder coupled to the shaft of the motor is used. The encoder index, A and B pulses are read with the event manager of the processor. Log of the mechanical rotor angle, the estimated speed, and the actual speed are taken for *250rpm*, *500rpm*, *1000rpm* and *1500rpm* constant speed requests and also, varying speeds of sinusoidal *250rpm*, *500rpm*, *1000rpm* and *1500rpm* amplitude with *0.1Hz* frequency are applied to examine whole speed range performance and zero speed crossing behavior of the drive system. In these experiments, since the encoder measures rotor angle rather than speed, the reference speed measure is obtained after Kalman filtering of actual motor rotor angle. However, Kalman filtered actual rotor position gives reliable speed estimate for comparison of drive system performance since filter performance is verified by simulations to have %1 steady state error in simulations.

In Figures 5-10 to 5-13; as expressed before, mechanical angle, estimated speed, and actual speeds taken for *250rpm*, *500rpm*, *1000rpm* and *1500rpm* are presented. The speed estimate from actual rotor position is given as dotted line.

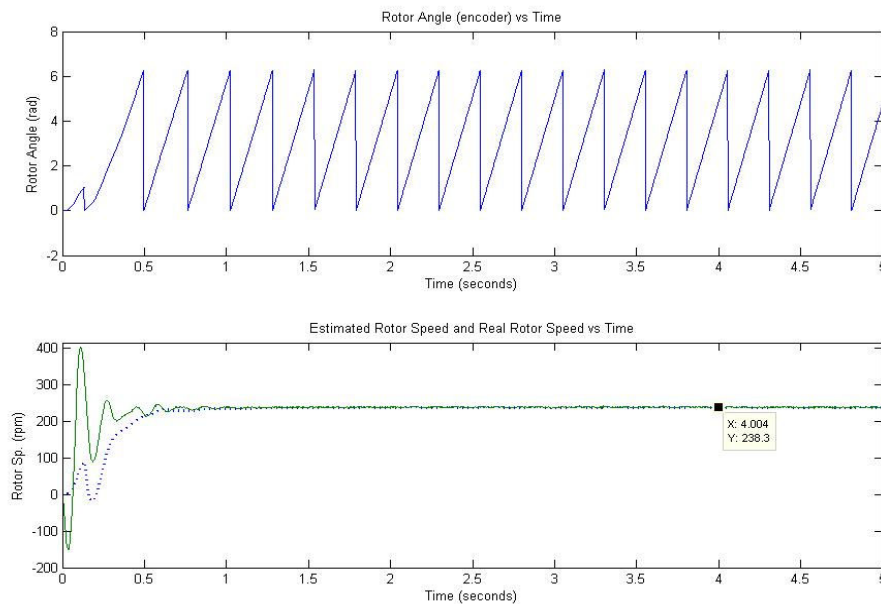


Figure 5-10 250rpm speed reference actual and estimated motor speeds

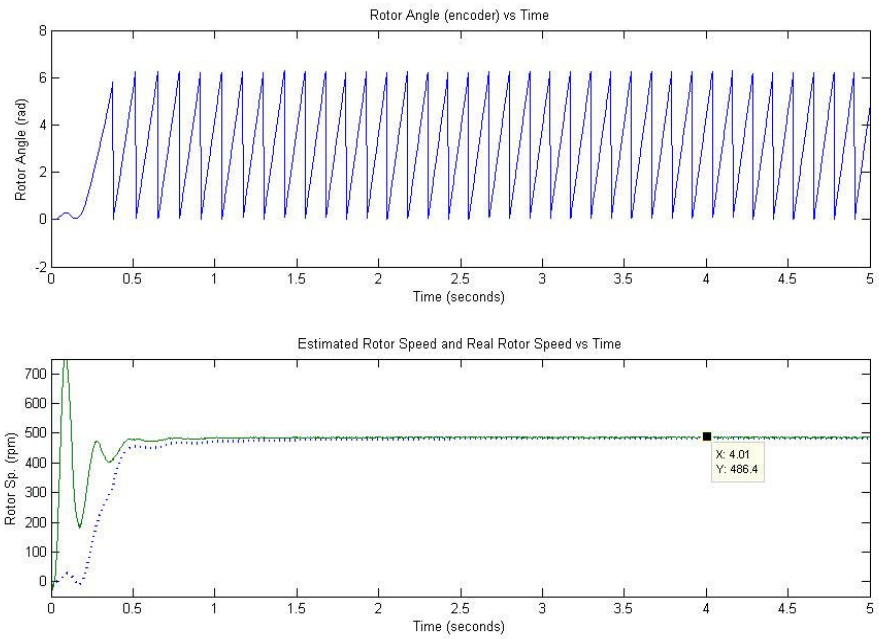


Figure 5-11 500rpm speed reference actual and estimated motor speeds

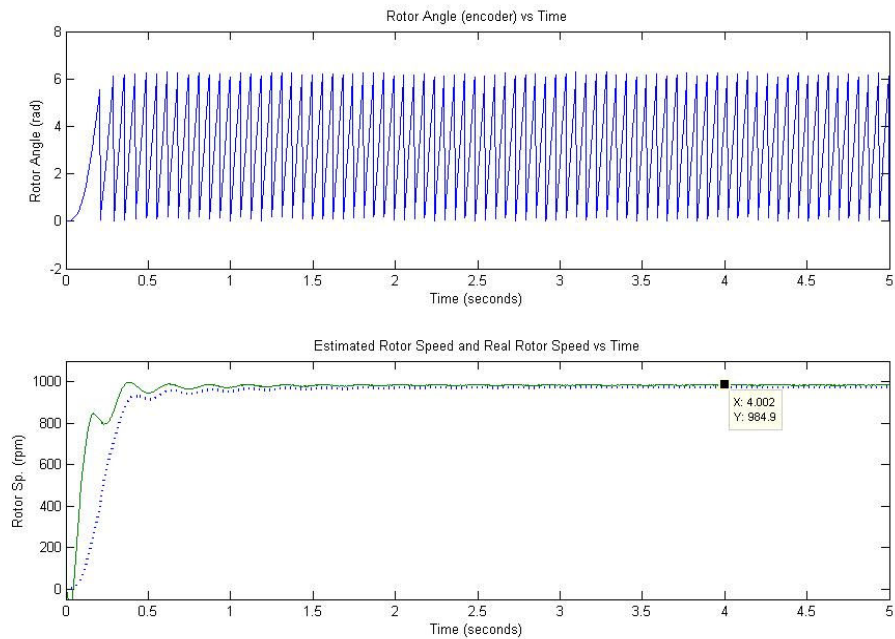


Figure 5-12 1000rpm speed reference actual and estimated motor speeds

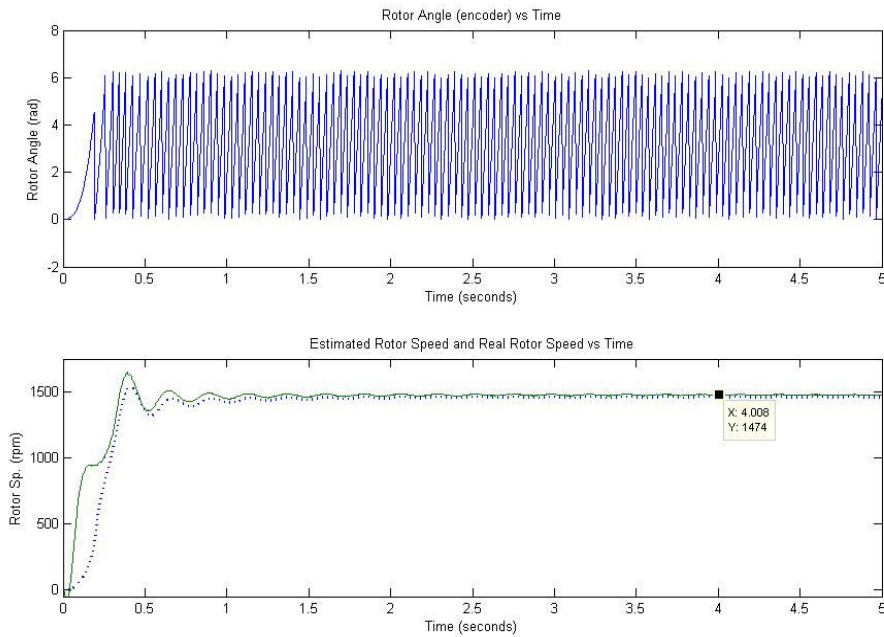


Figure 5-13 1500rpm speed reference actual and estimated motor speeds

The constant speed tests (in Figures 5-10 to 5-13) showed the differences between the estimated and the actual speeds from standstill to the set values. Until the settling time, the estimated speed settled to the steady state value faster but, deviates from actual speed values considerably. On the other hand, after the speed settles down, the responses fit to each other and the deviations are less than %5 from the reference values. These deviations are due to the inaccuracies made in estimations and the errors in the speed and the current PI controllers existing in their respective control loops.

The varying speed experiments are conducted to observe performance of drive system for acceleration, deceleration of the motor in both directions of rotation and to observe the behavior of the drive system around zero speed crossing. Sinusoidal speeds of amplitude *250rpm*, *500rpm*, *1000rpm* and *1500rpm* with *0.1 Hz* frequency applied as reference values and the results are presented in Figures 5-14 to 5-17. The speed estimate from actual rotor position is given as dotted line in the figures.

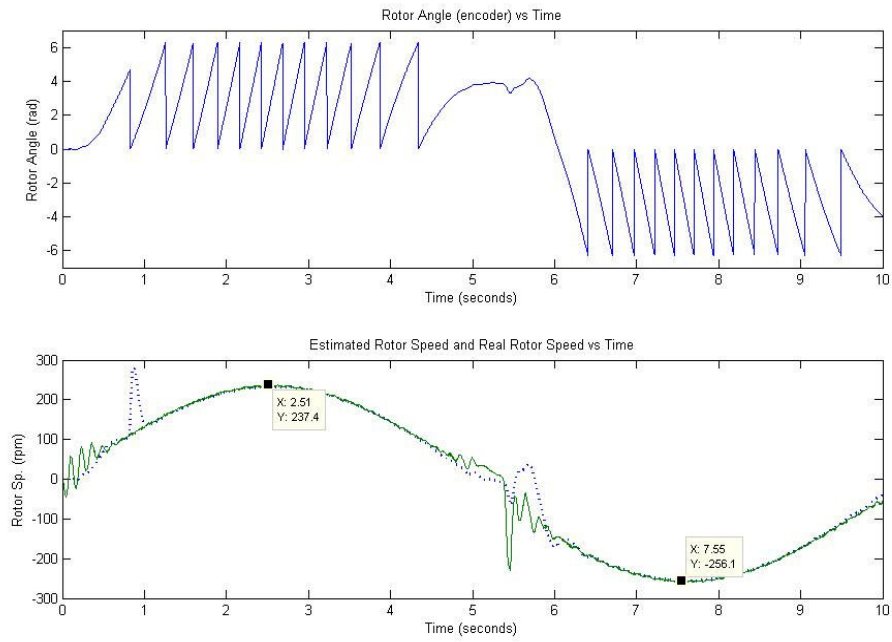


Figure 5-14 250rpm 0.1 Hz sinusoidal speed reference actual and estimated motor speeds

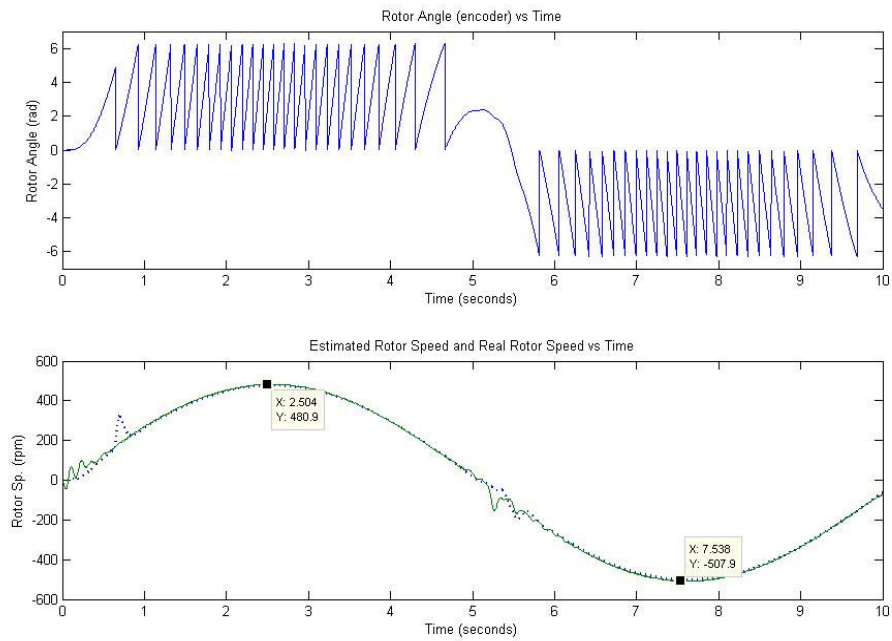


Figure 5-15 500rpm 0.1 Hz sinusoidal speed reference actual and estimated motor speeds

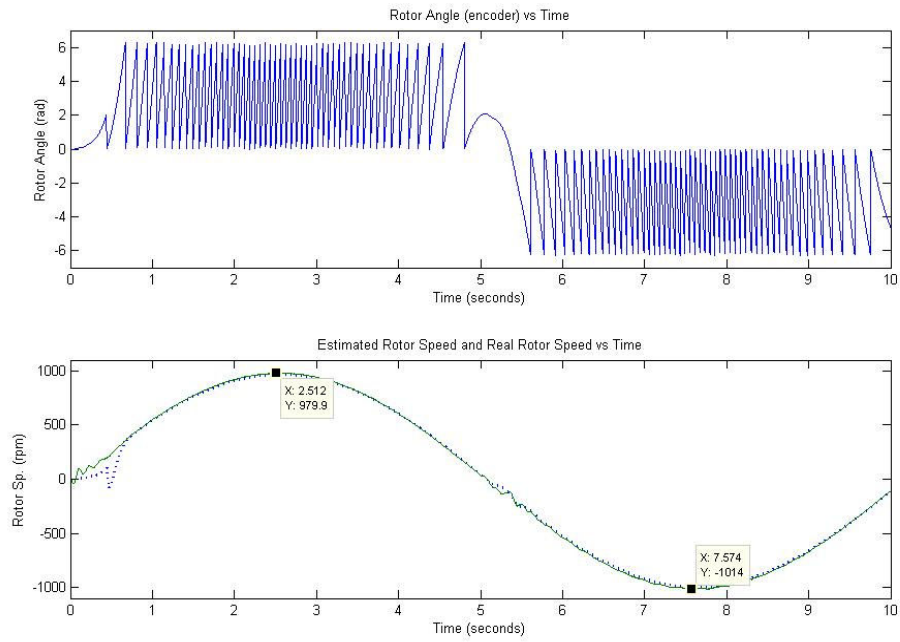


Figure 5-16 1000rpm 0.1 Hz sinusoidal speed reference actual and estimated motor speeds

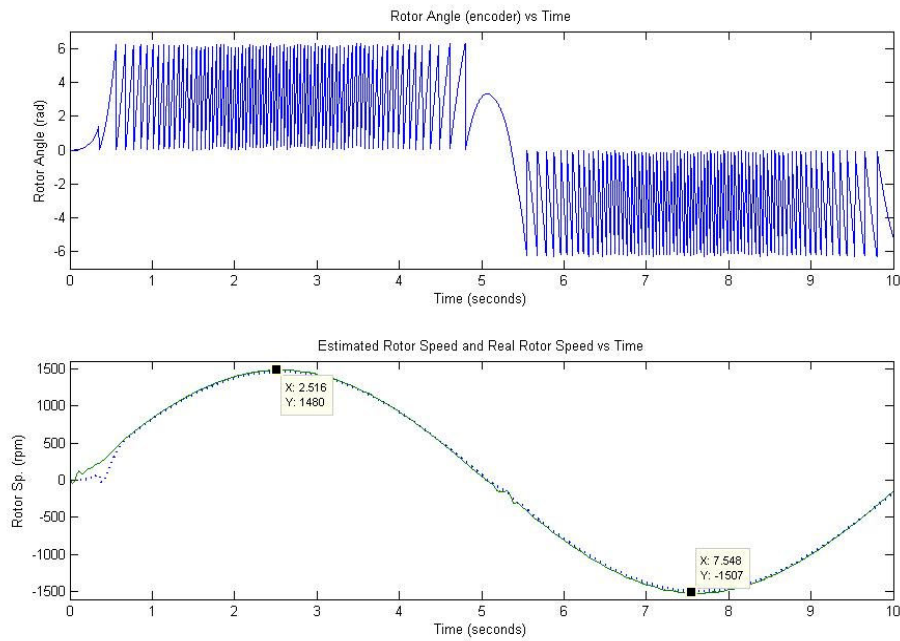


Figure 5-17 1500rpm 0.1 Hz sinusoidal speed reference actual and estimated motor speeds

The varying speed experiments showed that the estimated speed and the actual speeds are consistent and drive system follows the varying speed reference smoothly. However, in low speeds at the start and at the zero speed crossing system performance decreases due to the flux estimator characteristic.

5.2.2. Experiments of the Speed Estimator in No-Load

The subsection focuses on the time variations of the motor current and voltages in the closed loop operation under no-load conditions in comply with the tests made in section (5.2.1.). First, the responses are obtained for speed references applied in step form, from standstill conditions. Secondly, again speed varies sinusoidally at 0. 1Hz and voltage and current variations are obtained.

Concerning the constant speed reference experiments motor speed is set to *250rpm*, *500rpm*, *1000rpm* and *1500rpm* respectively.

In Figures 5-18 to 5-20 phase currents, voltages and speed data are given for *250rpm* case.

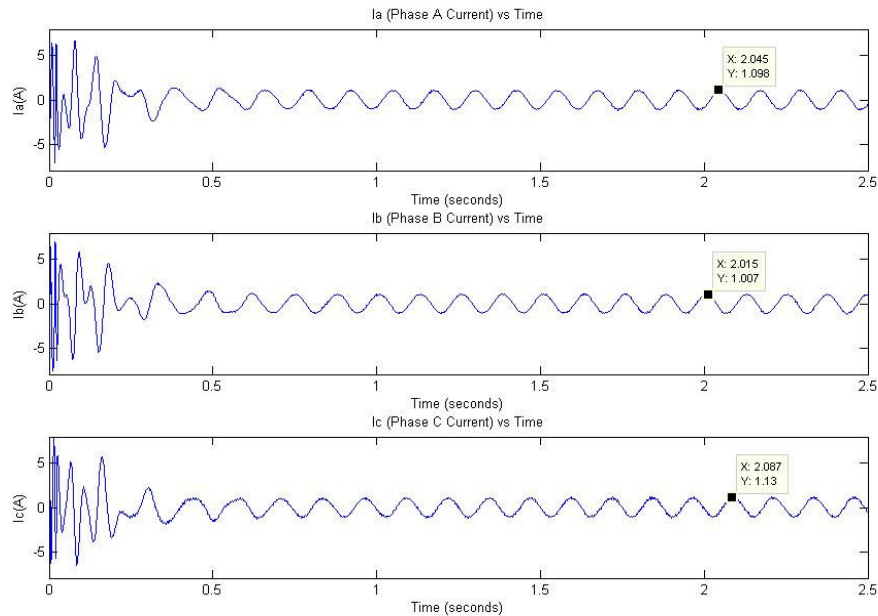


Figure 5-18 250rpm speed reference, motor phase currents

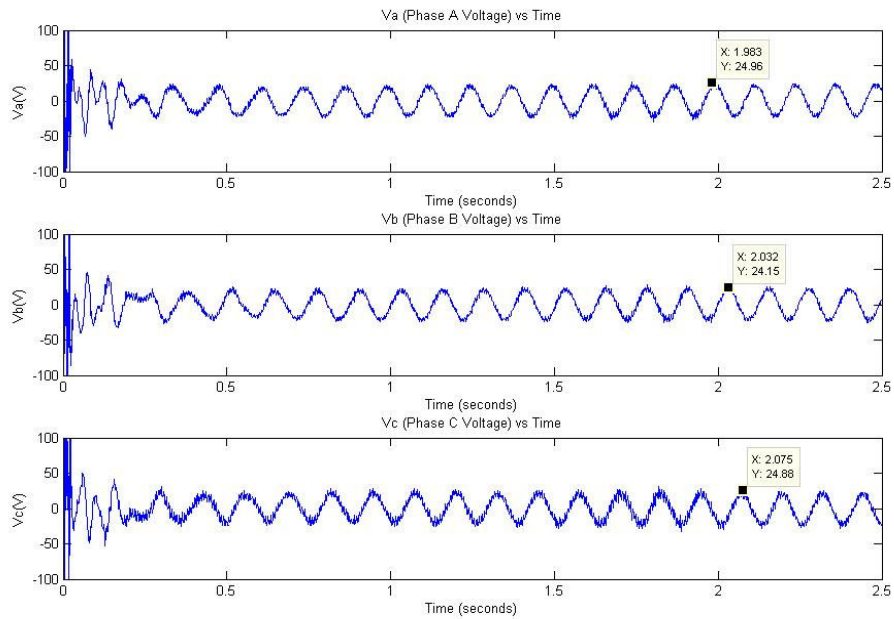


Figure 5-19 250rpm speed reference, motor phase voltages

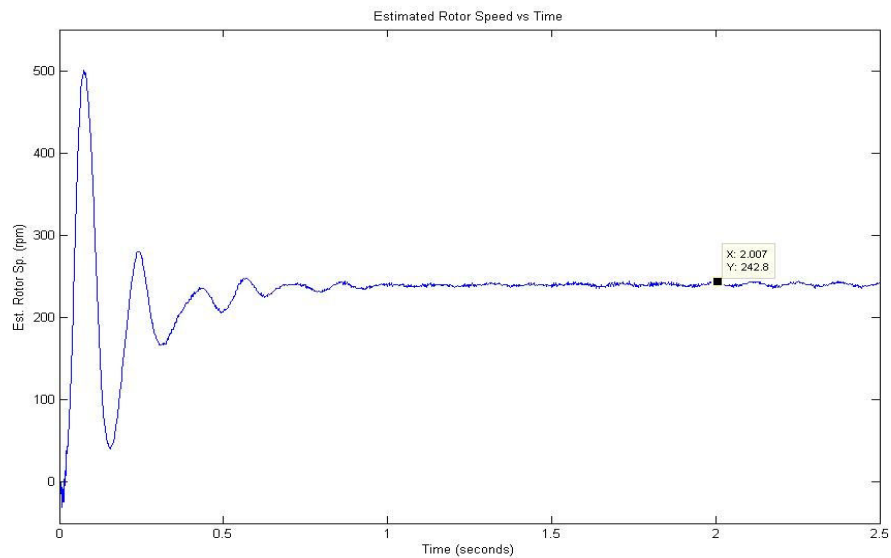


Figure 5-20 250rpm speed reference, motor speed estimate

In Figures 5-21 to 5-23 phase currents, voltages and speed data are given for 500rpm case.

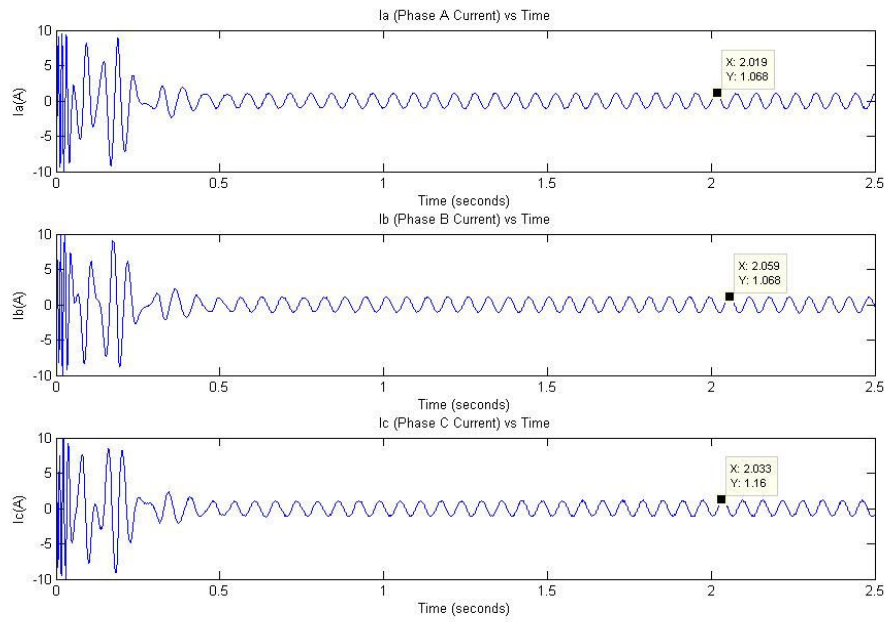


Figure 5-21 500rpm speed reference, motor phase currents

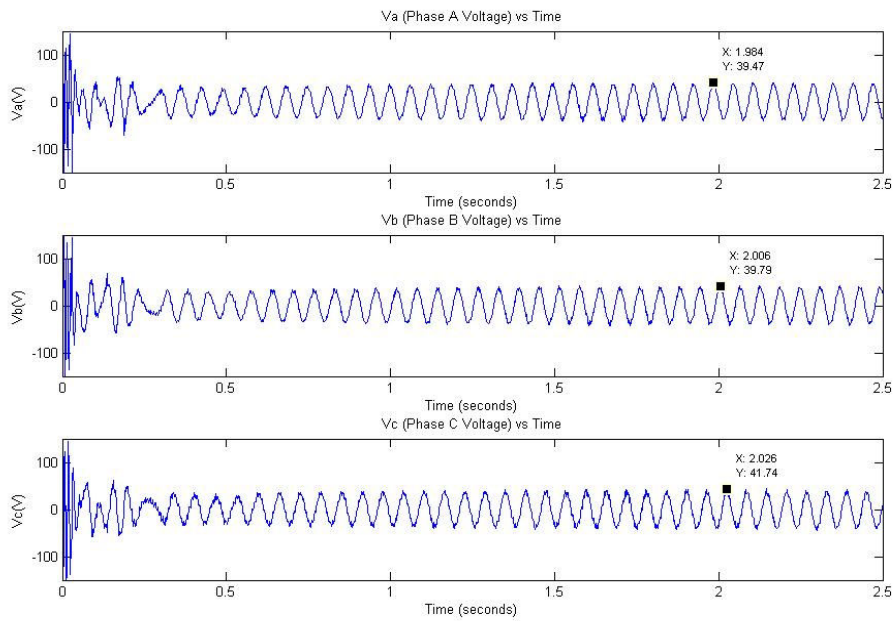


Figure 5-22 500rpm speed reference, motor phase voltages

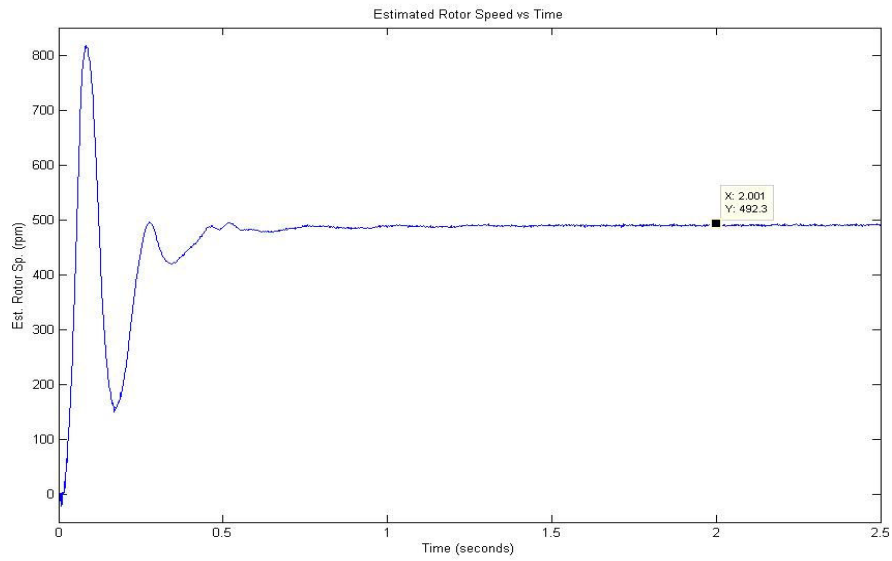


Figure 5-23 500rpm speed reference, motor speed estimate

In Figures 5-24 to 5-26 phase currents, voltages and speed data are given for 1000rpm case.

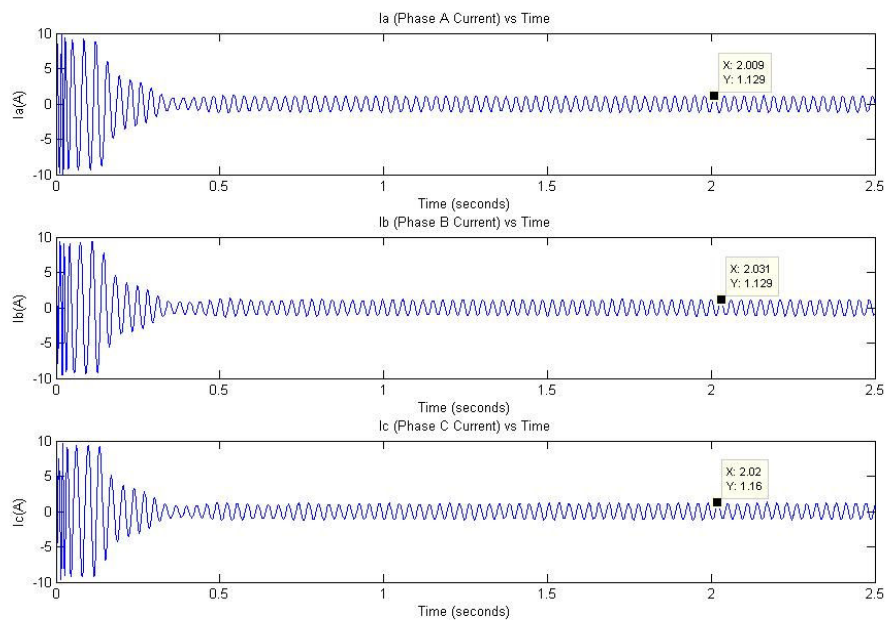


Figure 5-24 1000rpm speed reference, motor phase currents

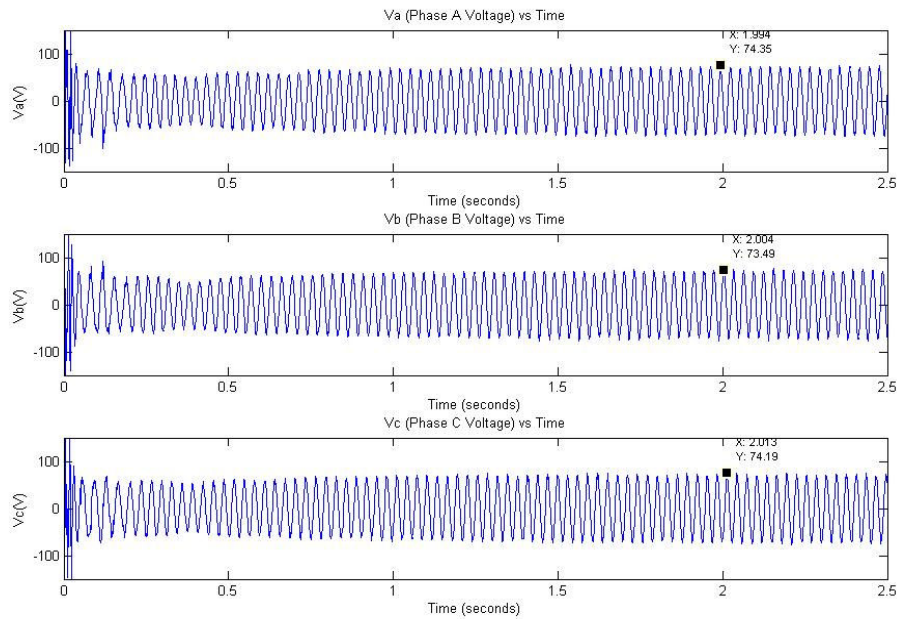


Figure 5-25 1000rpm speed reference, motor phase voltages

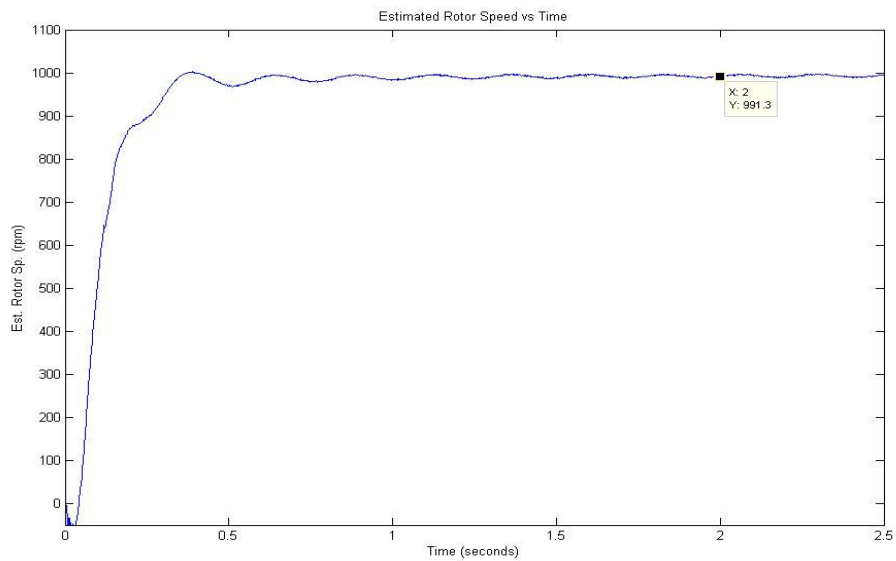


Figure 5-26 1000rpm speed reference, motor speed estimate

In Figures 5-27 to 5-29 phase currents, voltages and speed data are given for 1500rpm case.

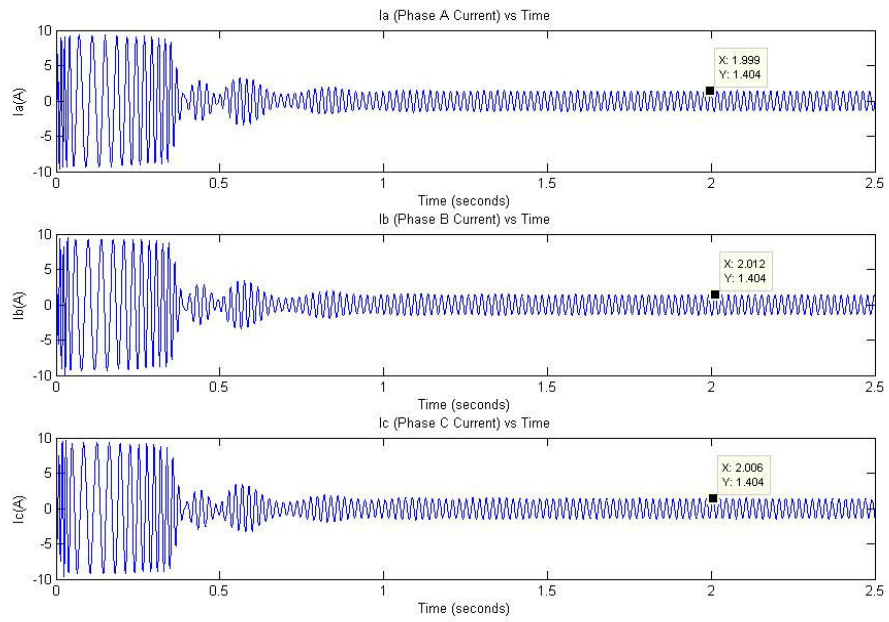


Figure 5-27 1500rpm speed reference, motor phase currents

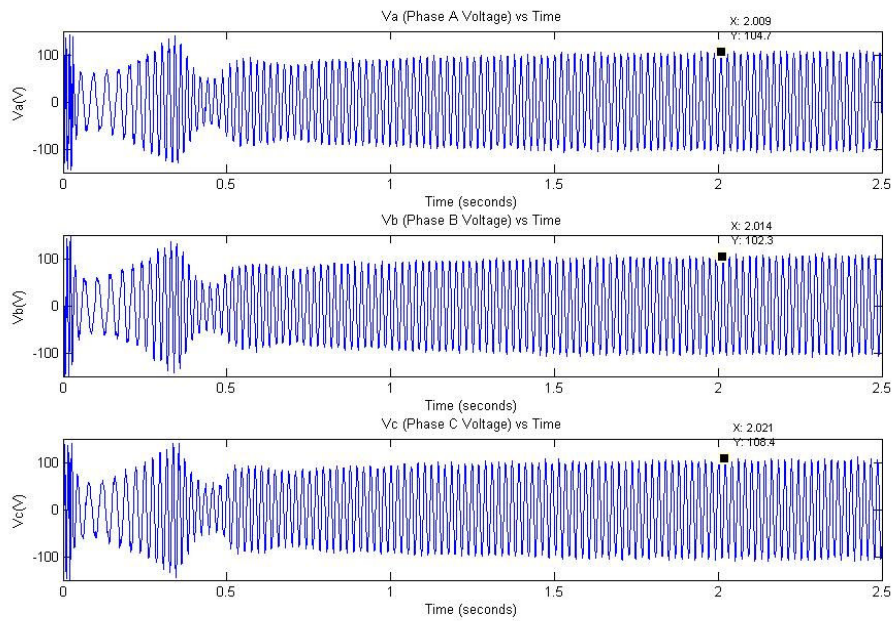


Figure 5-28 1500rpm speed reference, motor phase voltages

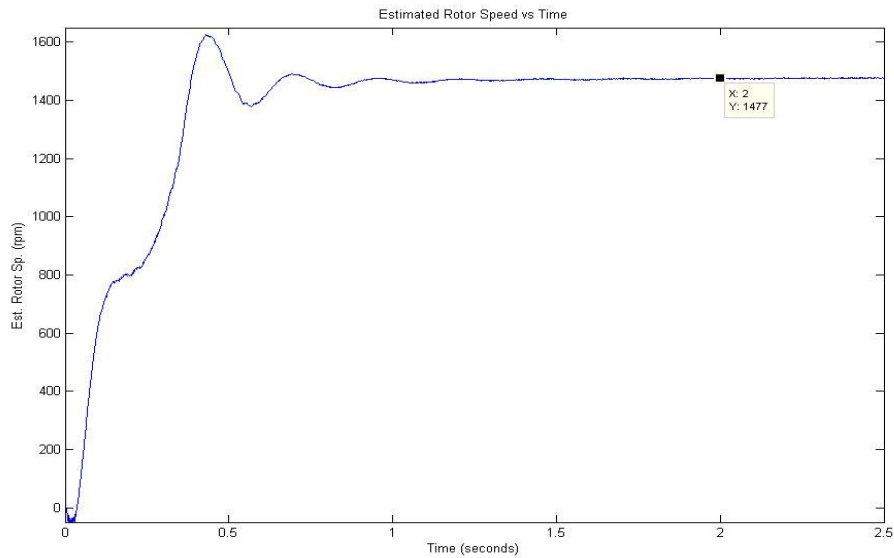


Figure 5-29 1500rpm speed reference, motor phase speed estimate

In these experiments, induction motor's phase voltages and phase currents behavior is seen from the figures. They reached to steady-state values in first second after the start of motor. This time increases with the increase in speed reference. Because to reach to referenced speed requires more time. The current values are almost same for all cases and very low since there is no loading. The voltage values increase with the speed reference proportionally as expected.

Varying speed experiments are realized for sinusoidal speed requests of 250rpm, 500rpm, 1000rpm and 1500rpm amplitude with 0.1Hz frequency.

In Figures 5-30 to 5-32 phase currents, voltages and speed data are presented for 250rpm amplitude 0.1Hz frequency.

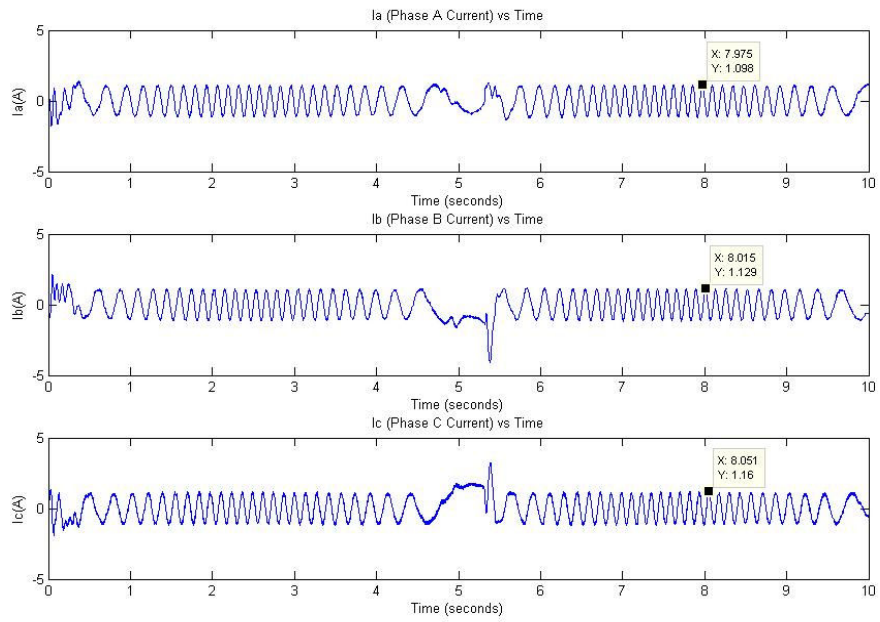


Figure 5-30 250rpm 0.1 Hz speed reference, motor phase currents

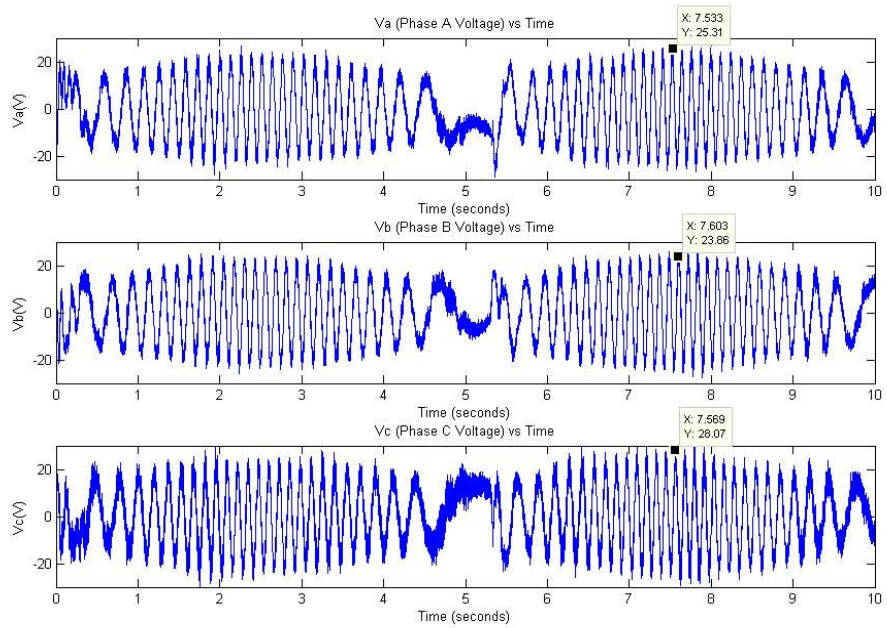


Figure 5-31 250rpm 0.1 Hz speed reference, motor phase voltages

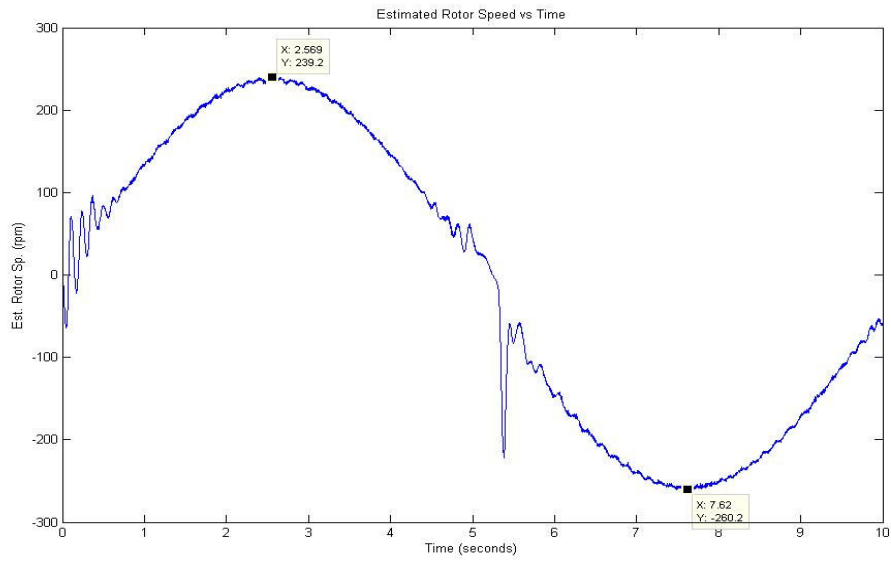


Figure 5-32 250rpm 0.1 Hz speed reference, motor speed estimate

In Figures 5-33 to 5-35 phase currents, voltages and speed data are presented for 500rpm amplitude 0.1Hz frequency.

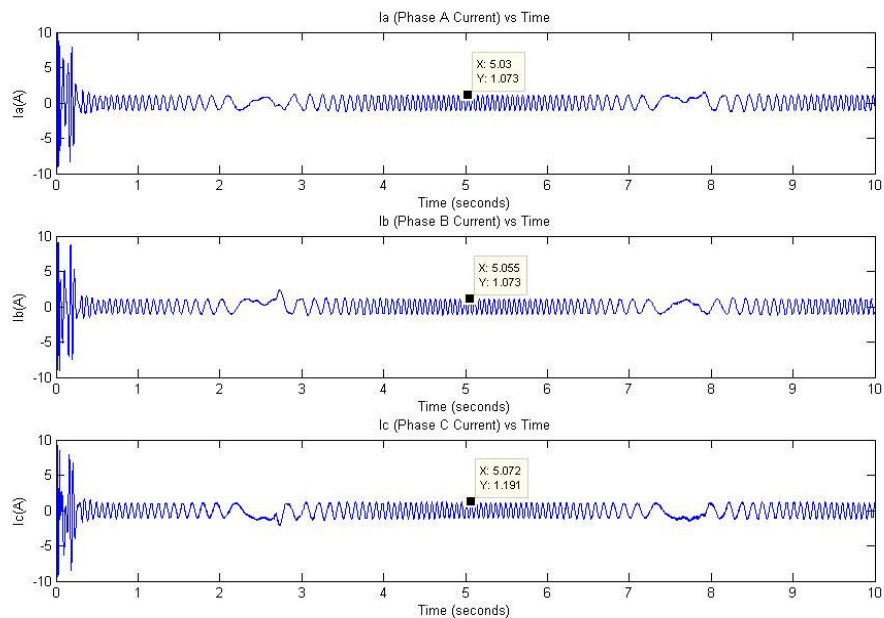


Figure 5-33 500rpm 0.1 Hz speed reference, motor phase current

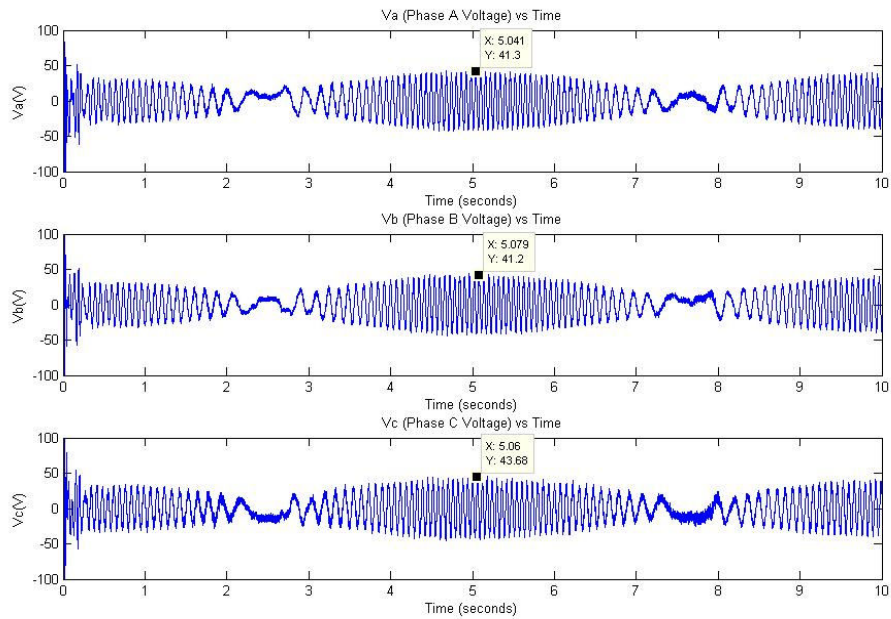


Figure 5-34 500rpm 0.1 Hz speed reference, motor phase voltages

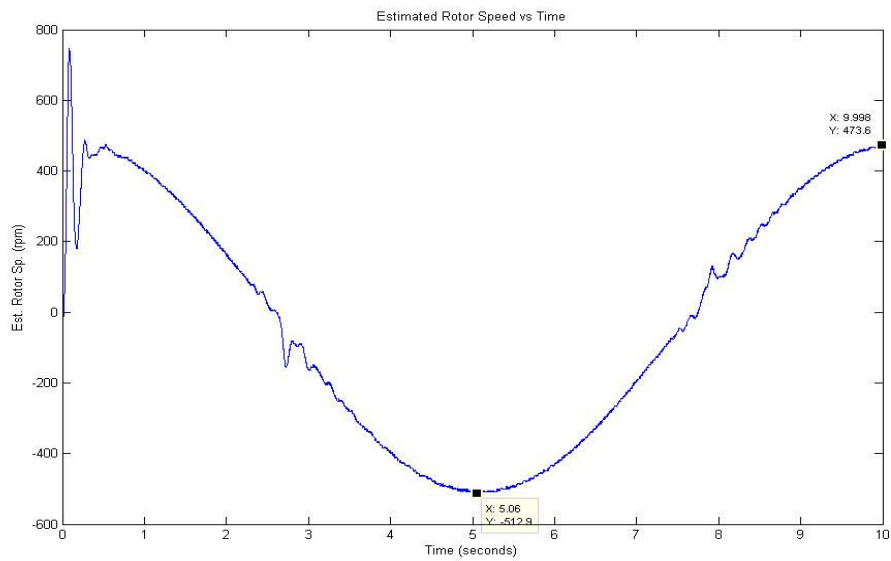


Figure 5-35 500rpm 0.1 Hz speed reference, motor speed estimate

In Figures 5-36 to 5-38 phase currents, voltages and speed data are presented for 1000rpm amplitude 0.1Hz frequency.

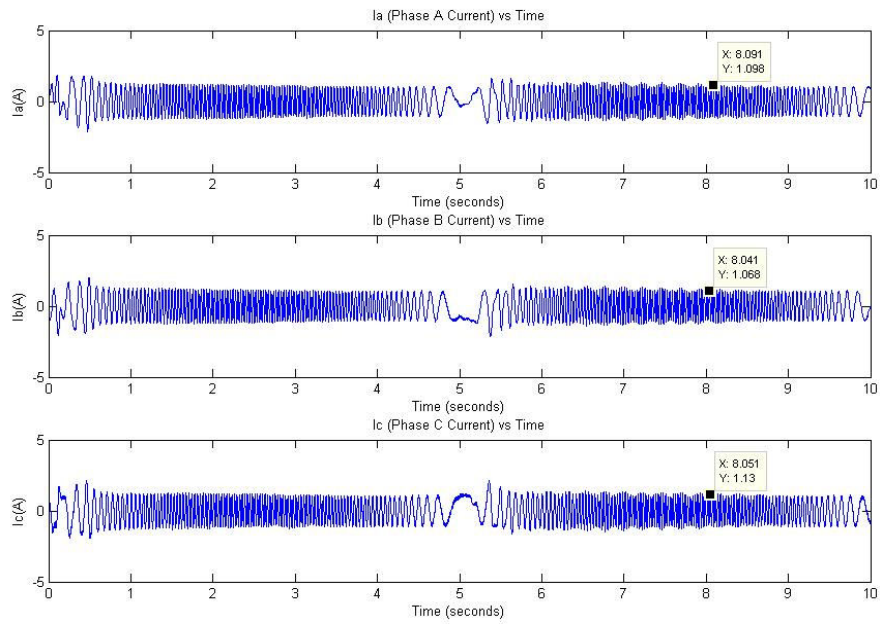


Figure 5-36 1000rpm 0.1 Hz speed reference, motor phase current

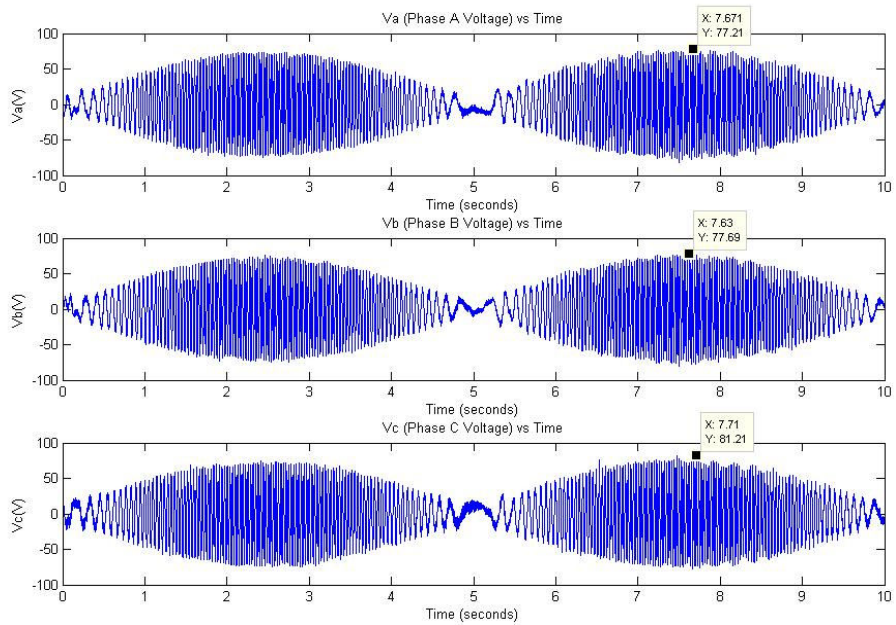


Figure 5-37 1000rpm 0.1 Hz speed reference, motor phase voltages

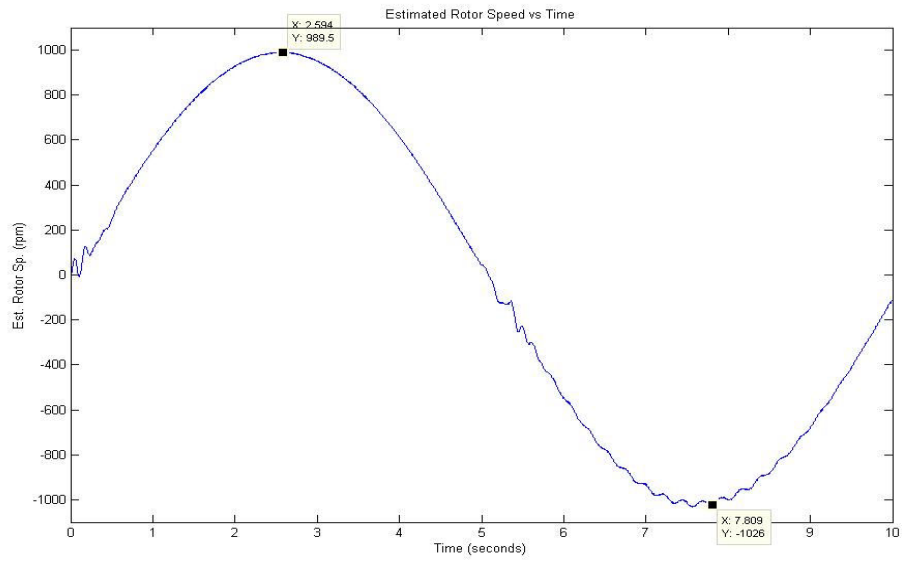


Figure 5-38 1000rpm 0.1 Hz speed reference, motor speed estimate

In Figures 5-39 to 5-41 phase currents, voltages and speed data are presented for 1500rpm amplitude 0.1Hz frequency.

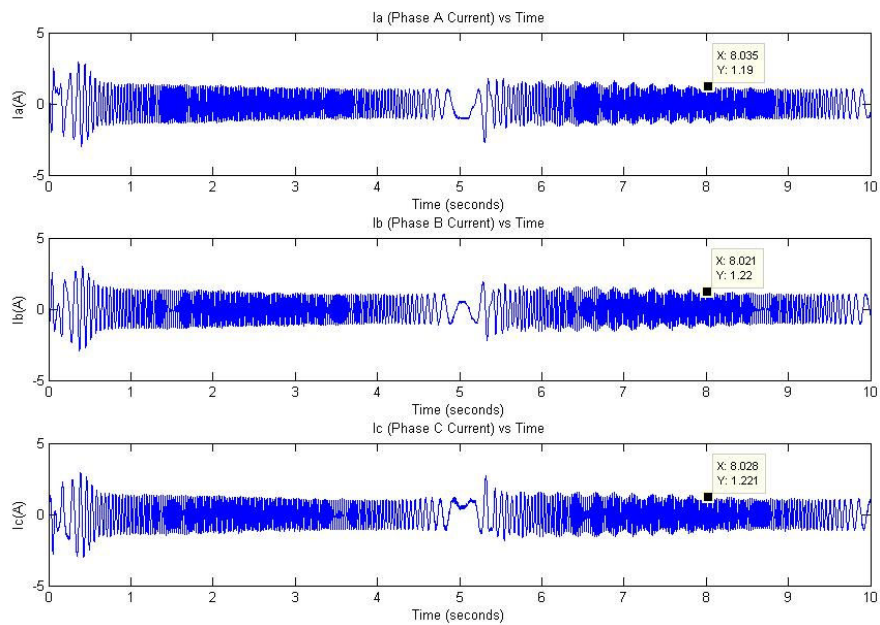


Figure 5-39 1500rpm 0.1 Hz speed reference, motor phase current

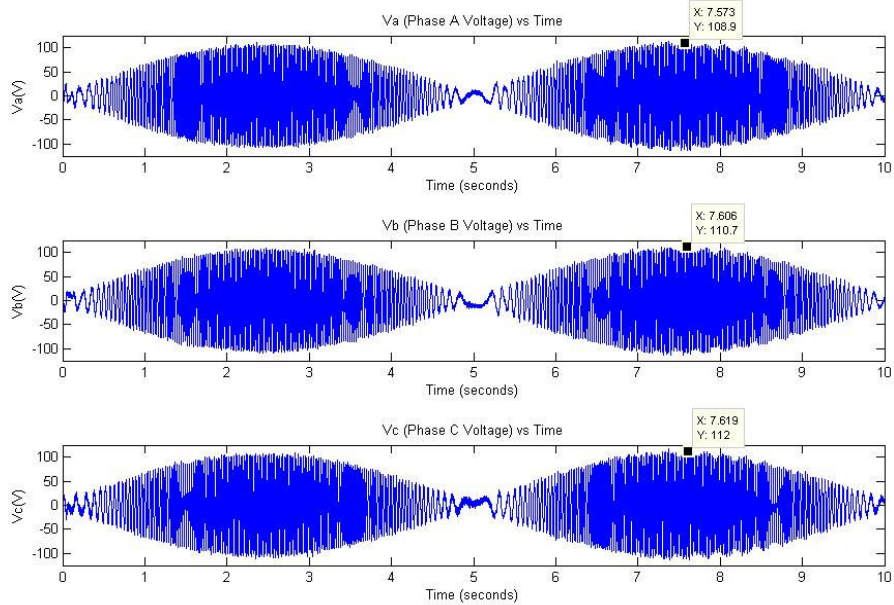


Figure 5-40 1500rpm 0.1 Hz speed reference, motor phase voltages

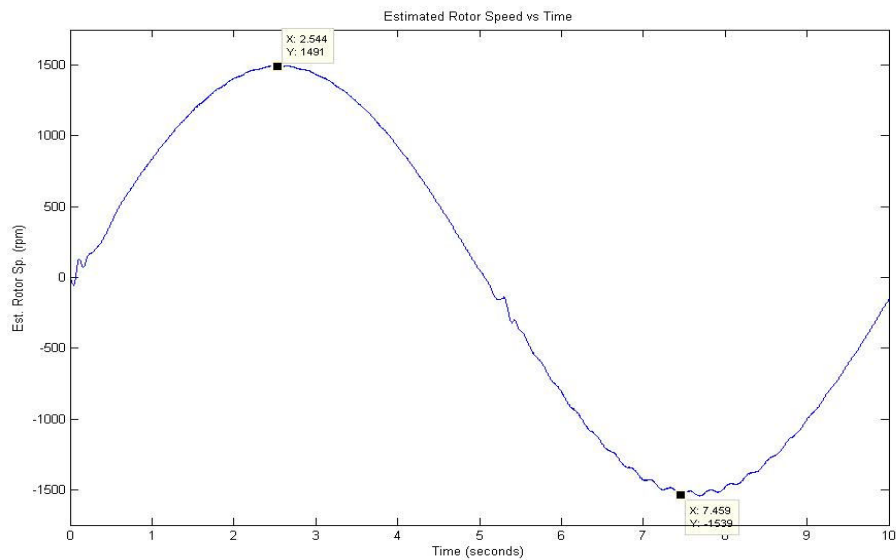


Figure 5-41 1500rpm 0.1 Hz speed reference, motor speed estimate

In sinusoidal speed reference experiments behavior and success of flux and speed estimator is observed for zero speed crossing. At the zero speed crossing, small speed

estimate error is seen in the figures. The performance improves with increasing speed reference.

5.2.3. The Speed Estimator Performance under Loading

In this section, the performance of the drive system is investigated under loading. The loading is obtained by using a three phase synchronous generator coupled to the shaft of the induction motor. The output of the synchronous generator is rectified with a full bridge rectifier and a capacitor bank which is connected to the output of the rectifier for voltage smoothing. The electrical load to the rectifier is a resistor. The Figure 5-42 shows the electrical block diagram of the load system. The synchronous generator has its own resolver coupled to its shaft. Thus, the actual speed of the overall rotating system can be measured by the resolver for comparison with the estimated speed. The resolver signals are read by a resolver to digital converter integrated circuit which can also compute the actual speed of the rotor.

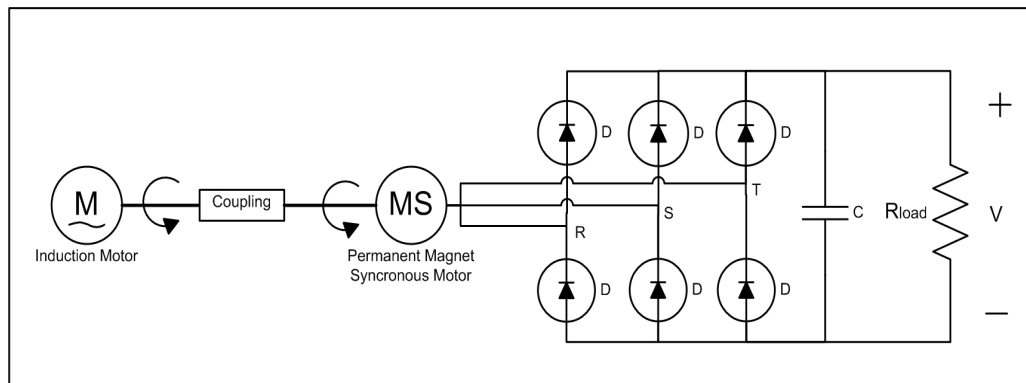


Figure 5-42 Load system electrical block diagram

The load motor has following properties: $V_n = 186V_{rms}$, $T_n = 10Nm$, $I_n = 8.4A_{rms}$, $P = 2.51kW$, $J_m = 0.9 Kg m^2$ and the load resistor is $16.5 Ohm$, $2kW$.

The first load experiments are at $250rpm$, $500rpm$, $750rpm$, $1000rpm$, $1250rpm$, and $1500rpm$ constant speed references. The Table 5-2 shows the references and

corresponding measurements. The second load experiments done with the same conditions, however, the load is switched on and off after the system started to rotate.

Table 5-2 Loading measurements

Speed Reference n (rpm)	Measured Speed n (rpm)	Output Power P_{out} (W)
250rpm	215rpm	12.74W
500rpm	450rpm	60.136W
750rpm	683rpm	105.89W
1000rpm	930rpm	252.135W
1250rpm	1140rpm	368.72W
1500rpm	1385rpm	535.51W

Before the loading tests, the setting for the I_d current was $0.1pu$ ($10A$ base) to overcome just friction and the DC-Bus voltage was $275VDC$. However, loading requires more flux to be produced to obtain required torque and this reference setting for I_d was insufficient. The Y-connection rating of the machine is $380V_{rm,max}$ which corresponds to $537.4VDC_{max}$ after rectification, whereas, $275VDC$ is too low for loading at rated speed. Therefore, the I_d reference setting increased to $0.25 pu$ and the bus voltage to $400VDC$. The reason for this change is the induction motor can not produce the speed with increased field at that phase voltage. Then, the drive system's PI controllers are tuned again with these parameter changes. Also, Kalman filter speed estimator is tuned to give faster speed estimation response and loading performance improved. To illustrate, the Kalman filter performance improvement is given in Figure 5-43 for $1500rpm$ speed command which had slowest settling time. The dashed line shows the previous case.

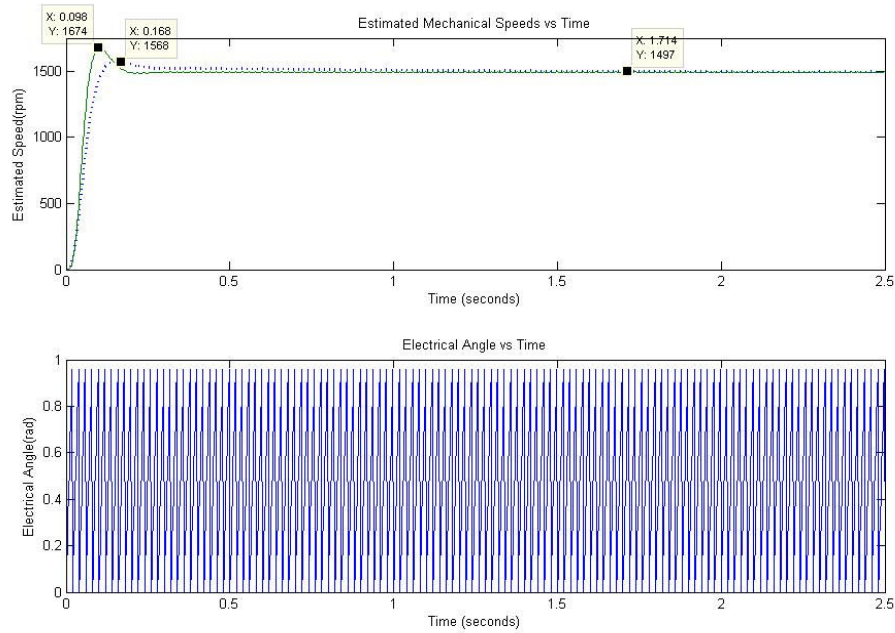


Figure 5-43 Kalman filter response improvement for better dynamic response

During the experiments the output power maximum of $536.51W$ at $1500rpm$ is reached. The load motor has rated speed of $3000rpm$ and at low speeds it can not produce required torque, hence, output voltage is small. At $1500rpm$ it could generate $94V$ and $535.51W$ could be drawn. The constant speed request is decreased the performance of speed loop to at most $\%15.6$ speed errors ($250rpm$ case). The measurements of induction motor are given in with phase currents, voltages and estimated speed for $250rpm$, $500rpm$, $1000rpm$, and $1500rpm$.

The Figures 5-44 to 5-46 present the phase currents, voltages and the estimated speed of the mechanical speed for $250rpm$ reference with loading.

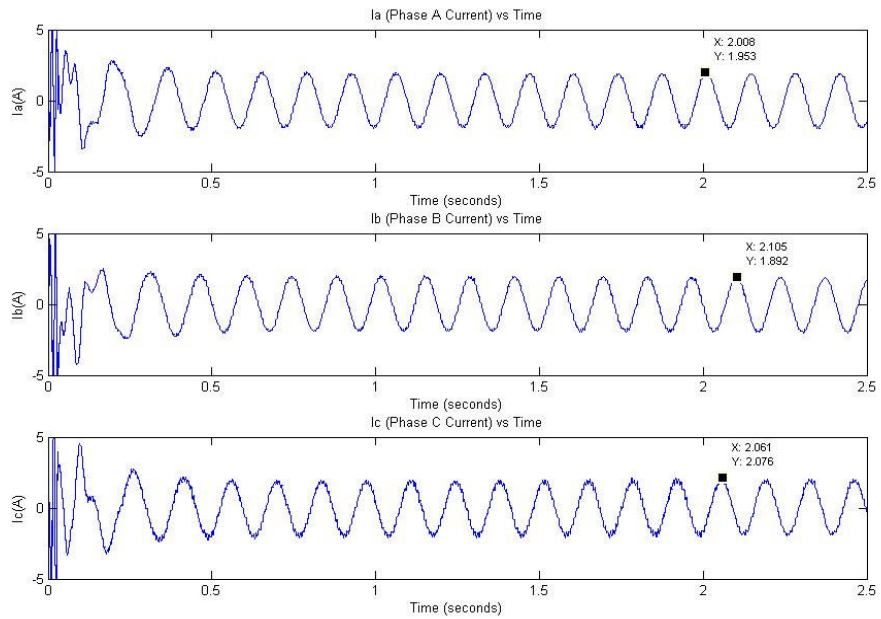


Figure 5-44 250rpm speed reference, motor phase currents constant under loading

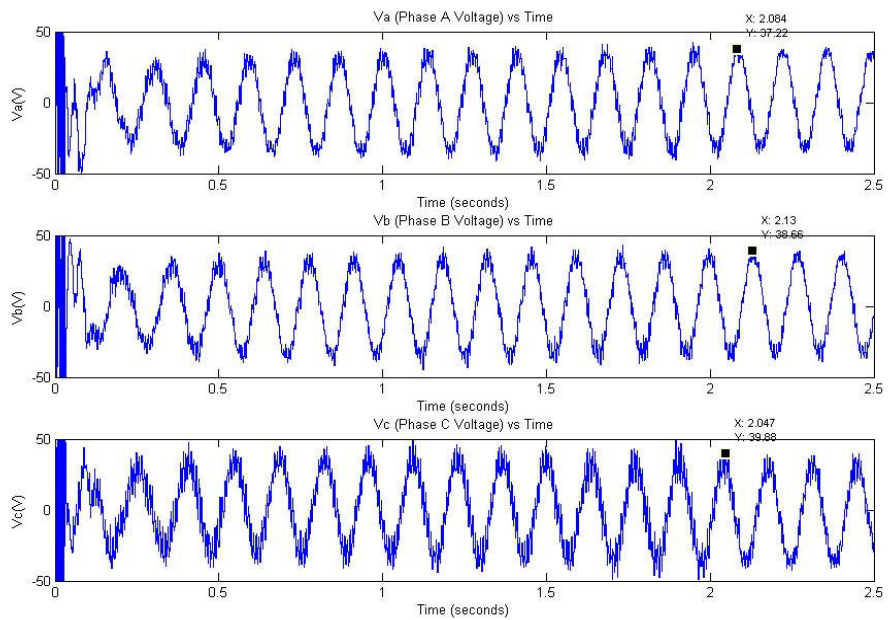


Figure 5-45 250rpm speed reference, motor phase voltages constant under loading

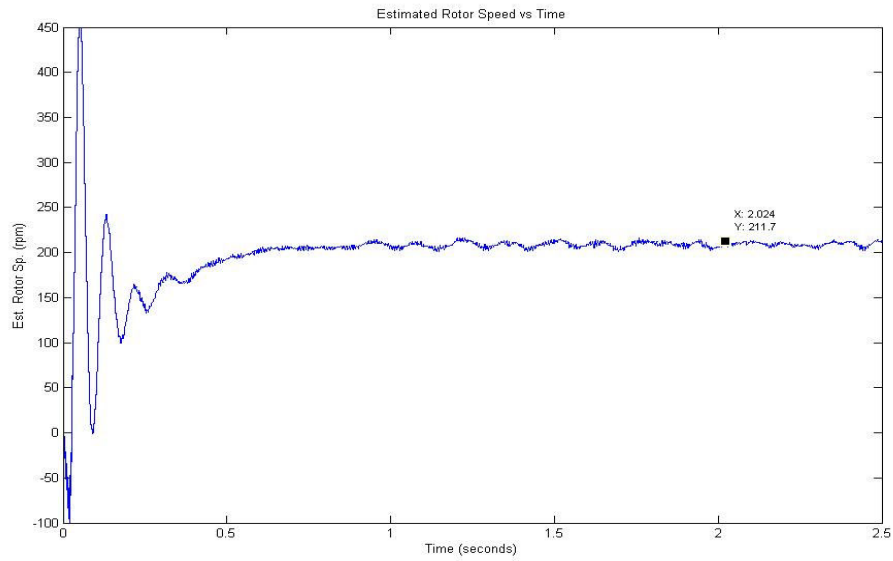


Figure 5-46 250rpm speed reference, motor speed estimate constant under loading

The Figures 5-47 to 5-49 present the phase currents, voltages and the estimated speed of the mechanical speed for 500rpm reference with loading.

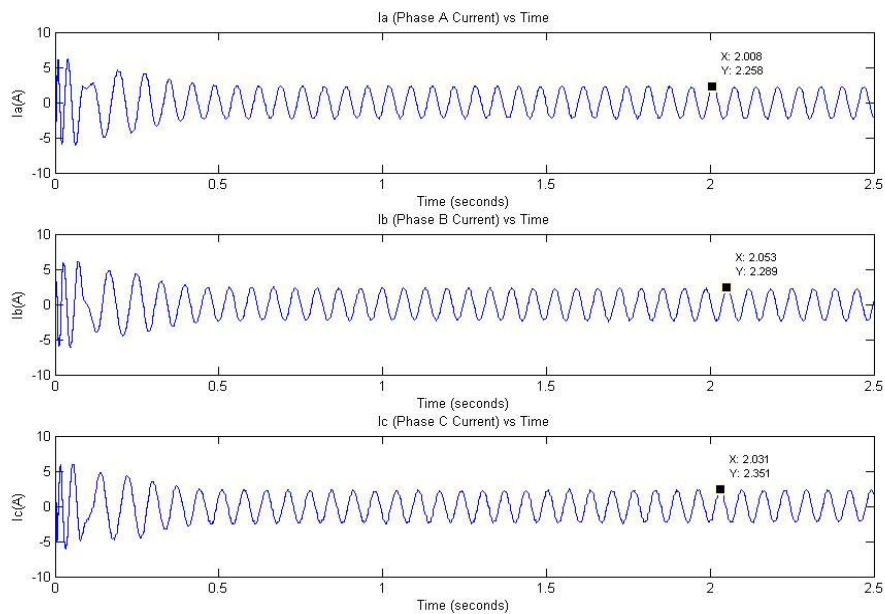


Figure 5-47 500rpm speed reference, motor phase currents constant under loading

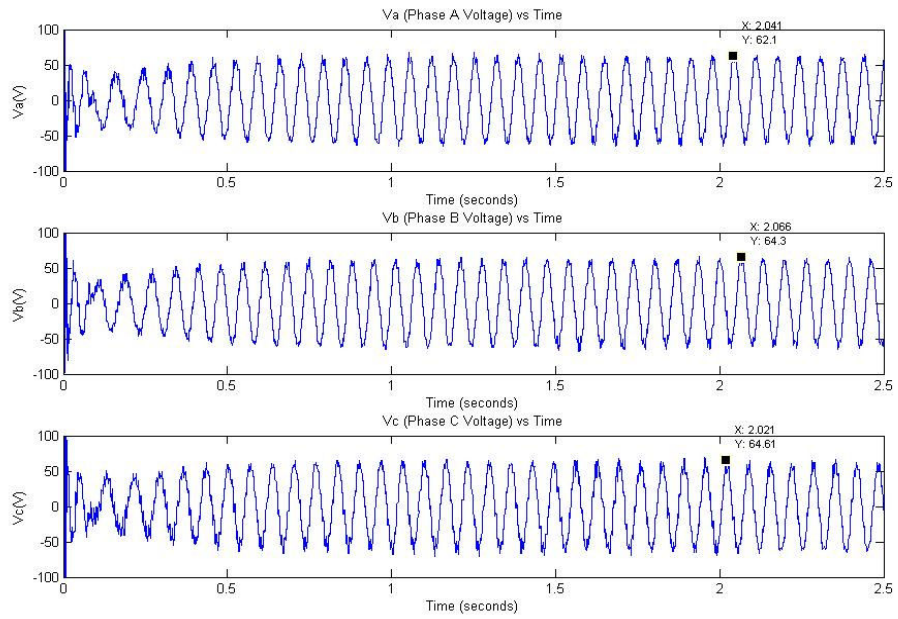


Figure 5-48 500rpm speed reference, motor phase voltages constant under loading

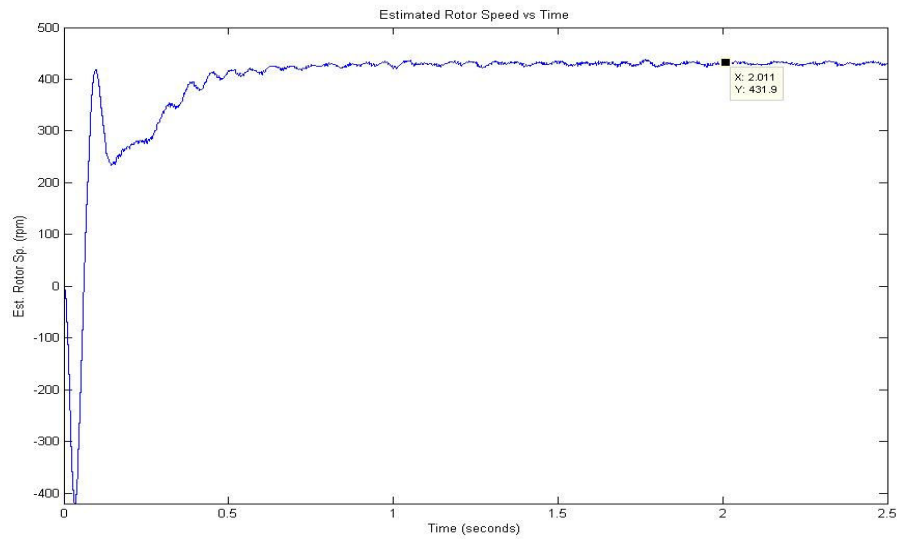


Figure 5-49 500rpm speed reference, motor speed estimate constant under loading

The Figures 5-50 to 5-52 present the phase currents, voltages and the estimated speed of the mechanical speed for 1000rpm reference with loading.

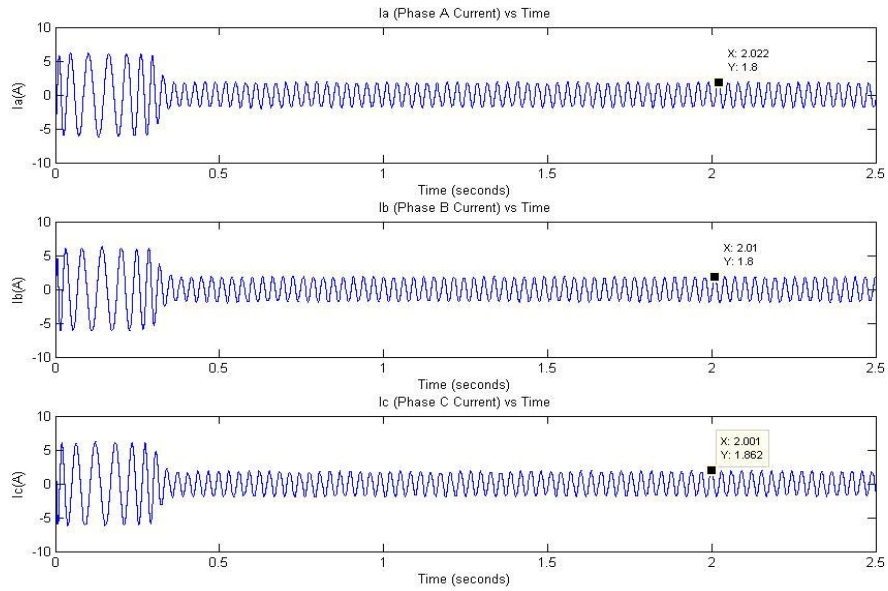


Figure 5-50 1000rpm speed reference, motor phase currents constant under loading

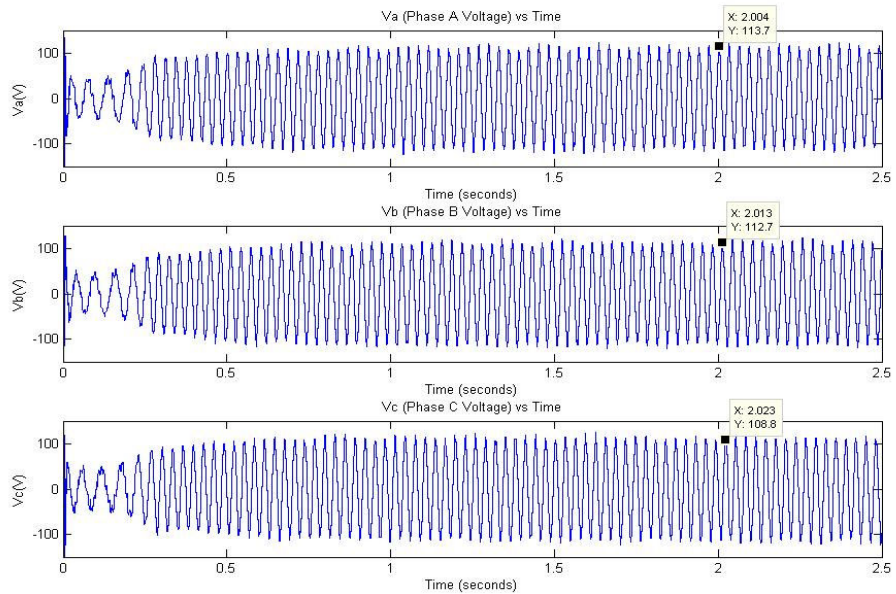


Figure 5-51 1000rpm speed reference, motor phase voltages under constant loading

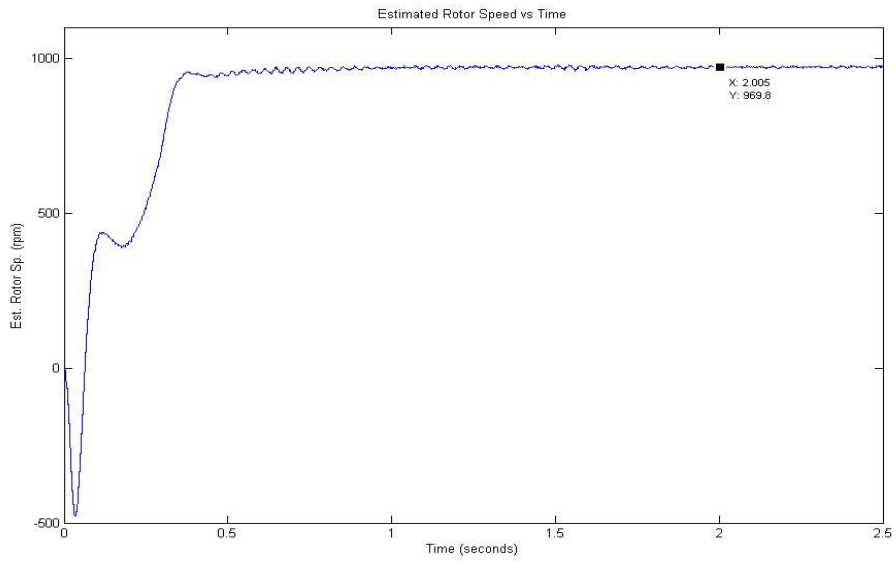


Figure 5-52 1000rpm speed reference, motor speed estimate under constant loading

The Figures 5-53 to 5-54 present the phase currents, voltages and the estimated speed of the mechanical speed for 1500rpm reference with loading.

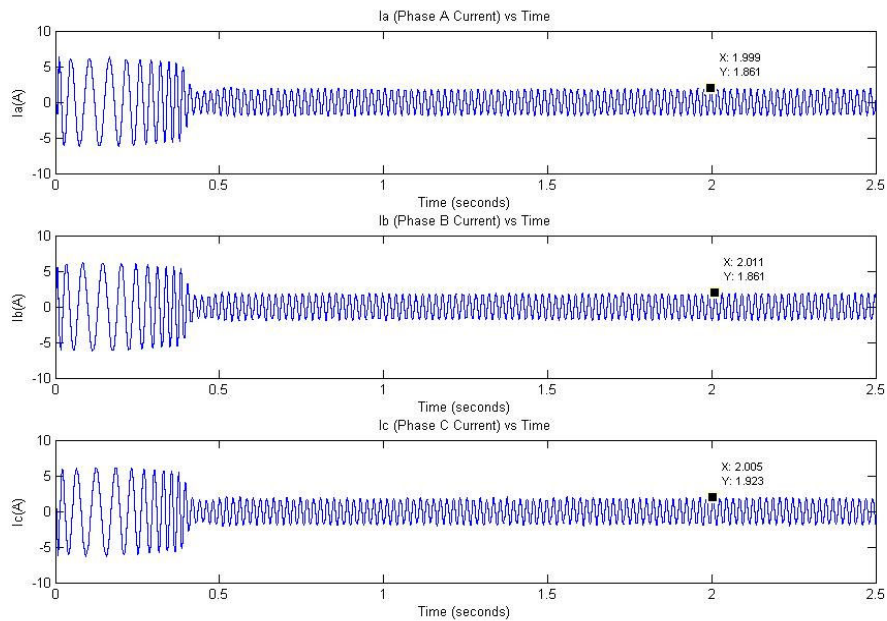


Figure 5-53 1500rpm speed reference, motor phase currents under constant loading

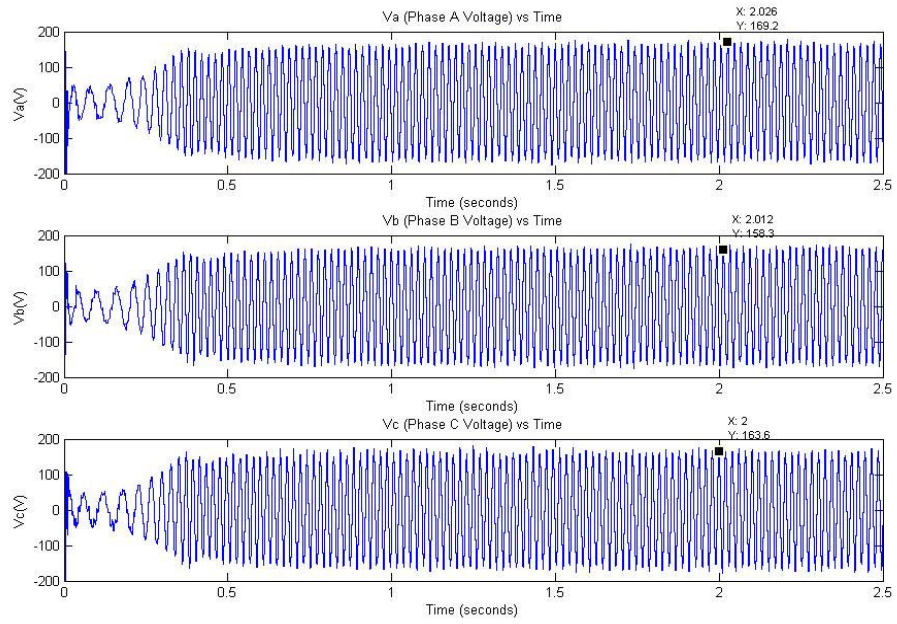


Figure 5-54 1500rpm speed reference, motor phase voltages under constant loading

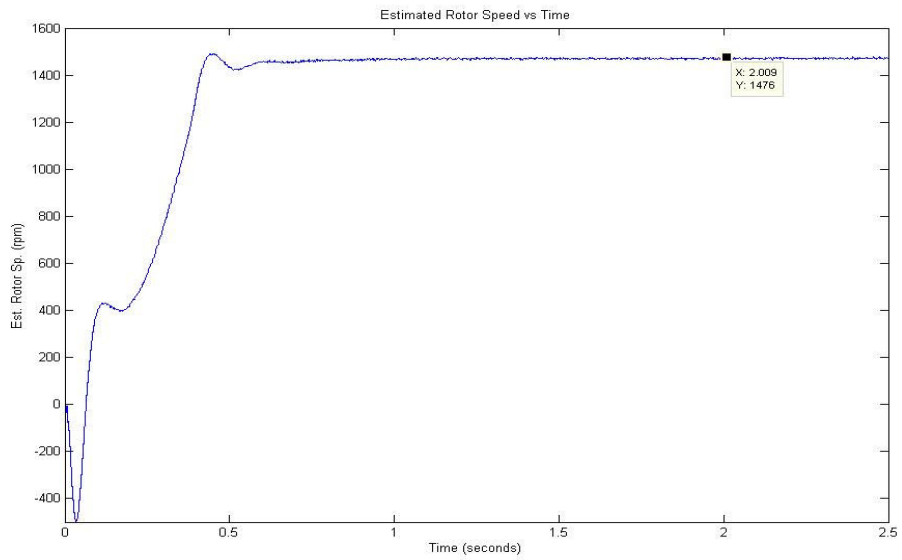


Figure 5-55 1500rpm speed reference, motor speed estimate under constant loading

The switched load experiments are done for $250rpm$, $500rpm$, $1000rpm$ and $1500rpm$ speed references. The load resistor is switched with a high current switch while motor currents, voltages and rotor speed are logged. In the experiments the speed variation due to switched loading is quite small and the drive system quickly reaches the steady state. The load switching times can be seen from speed graphs for time as speed decrease.

The Figures 5-56 to 5-58 present the phase currents, voltages and the estimated speed of the mechanical speed for $250rpm$ reference with switched load.

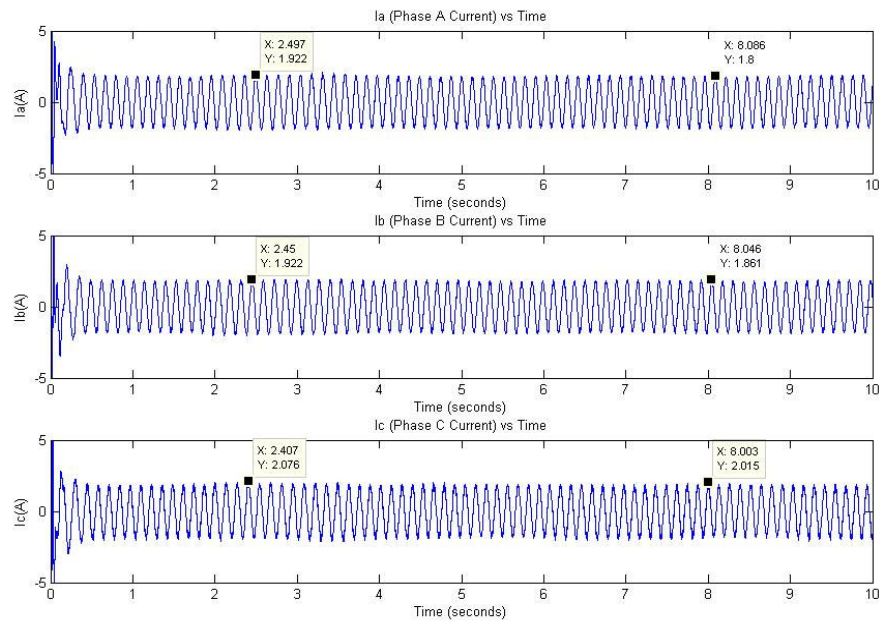


Figure 5-56 $250rpm$ speed reference, motor phase currents under switched loading

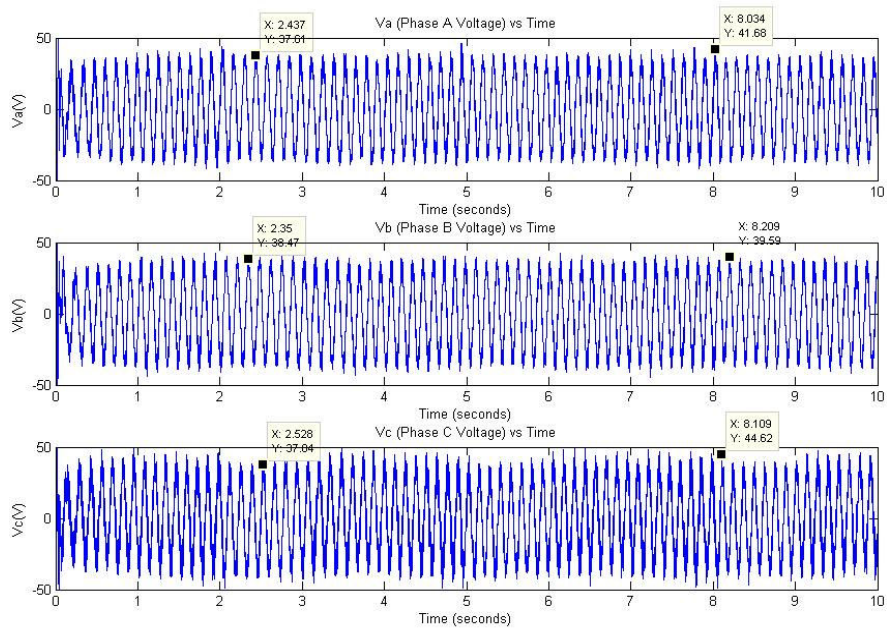


Figure 5-57 250rpm speed reference, motor phase voltages under switched loading

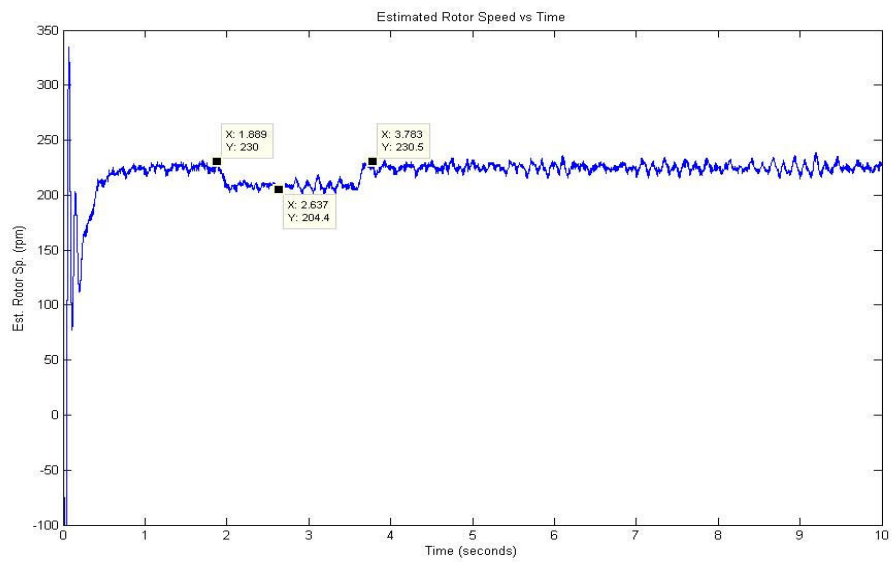


Figure 5-58 250rpm speed reference, motor speed estimate under switched loading

The Figures 5-59 to 5-61 present the phase currents, voltages and the estimated speed of the mechanical speed for 500rpm reference with switched load.

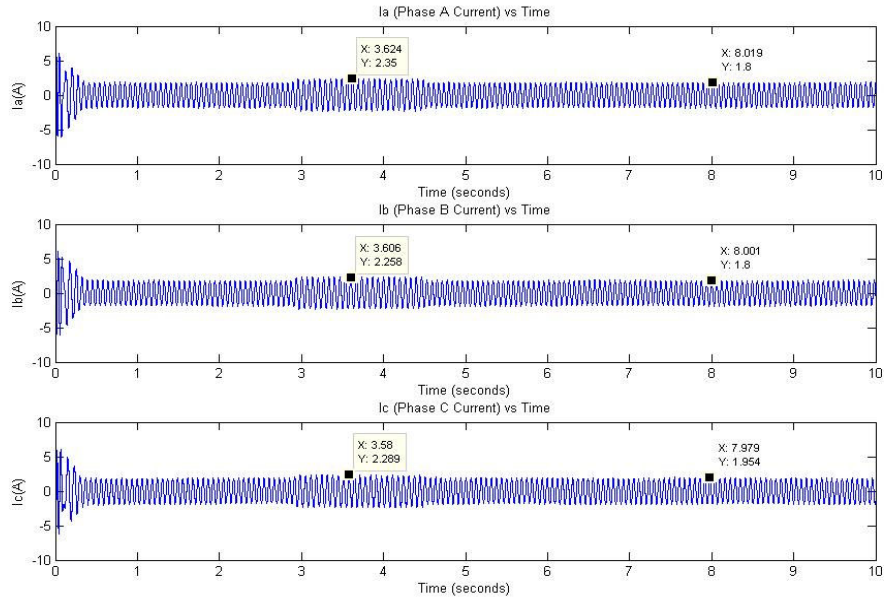


Figure 5-59 500rpm speed reference, motor phase currents under switched loading

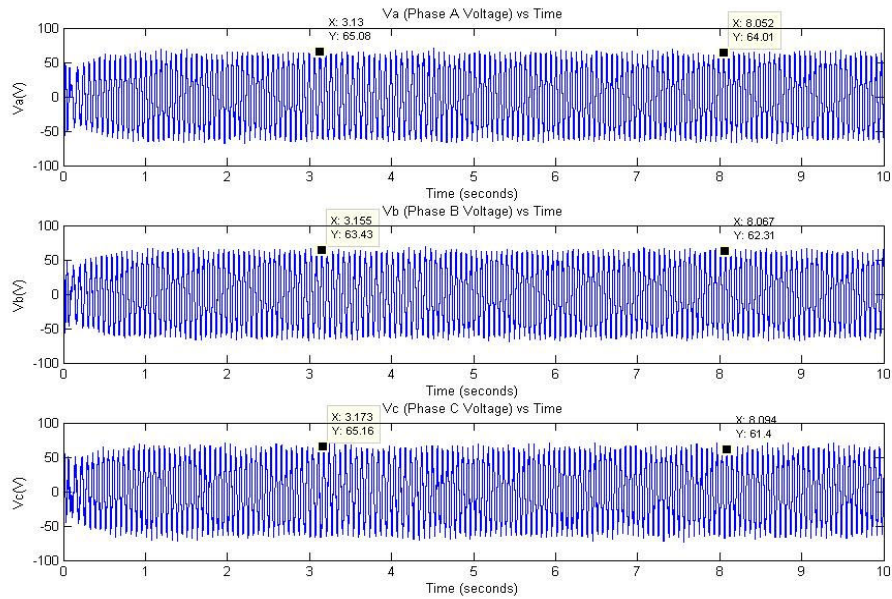


Figure 5-60 500rpm speed reference, motor phase voltages under switched loading

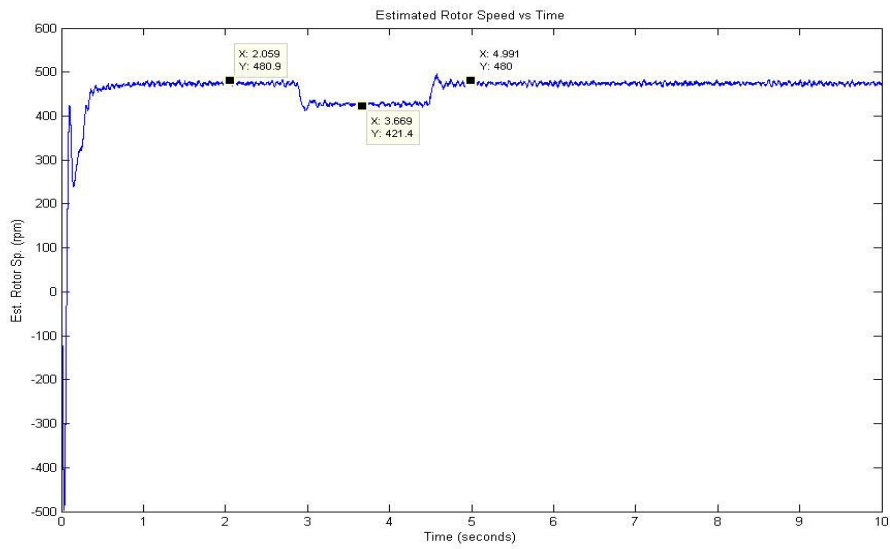


Figure 5-61 500rpm speed reference, motor speed estimate under switched loading

The Figures 5-62 to 5-64 present the phase currents, voltages and the estimated speed of the mechanical speed for 1000rpm reference with switched load.

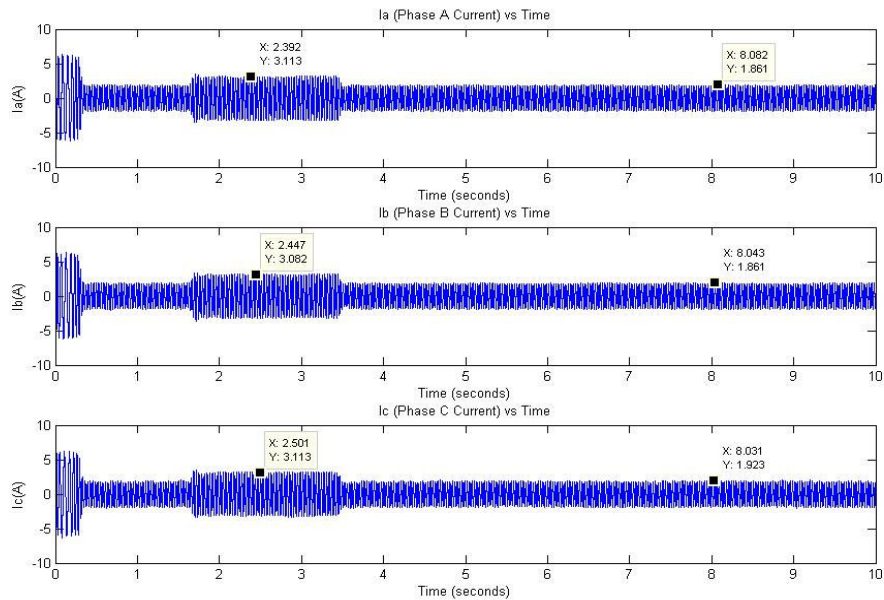


Figure 5-62 1000rpm speed reference, motor phase currents under switched loading

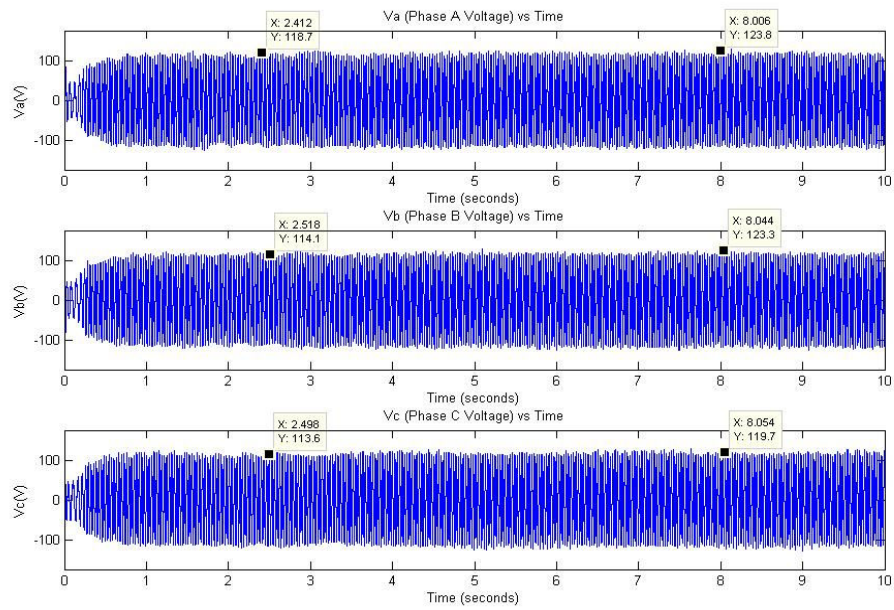


Figure 5-63 1000rpm speed reference, motor phase voltages under switched loading

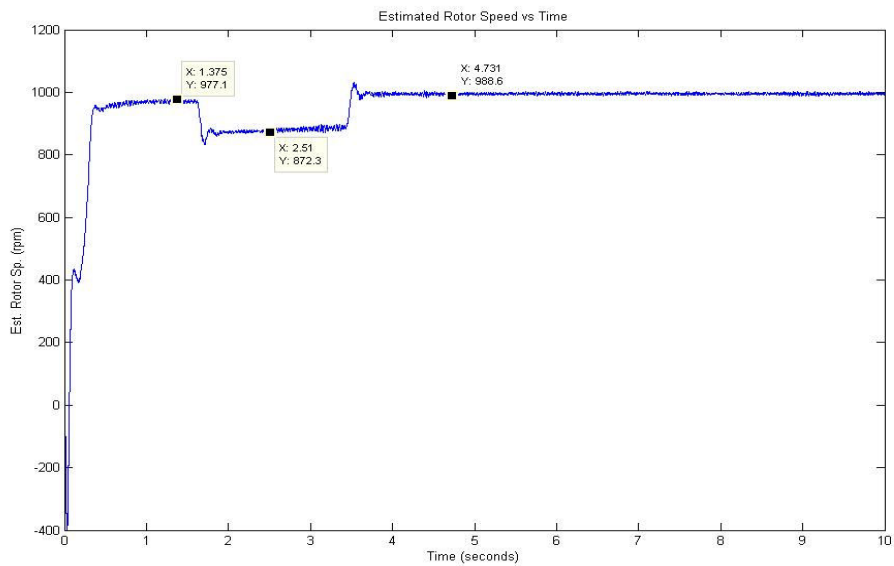


Figure 5-64 1000rpm speed reference, motor speed estimate under switched loading

The Figures 5-65 to 5-67 present the phase currents, voltages and the estimated speed of the mechanical speed for 1500rpm reference with switched load.

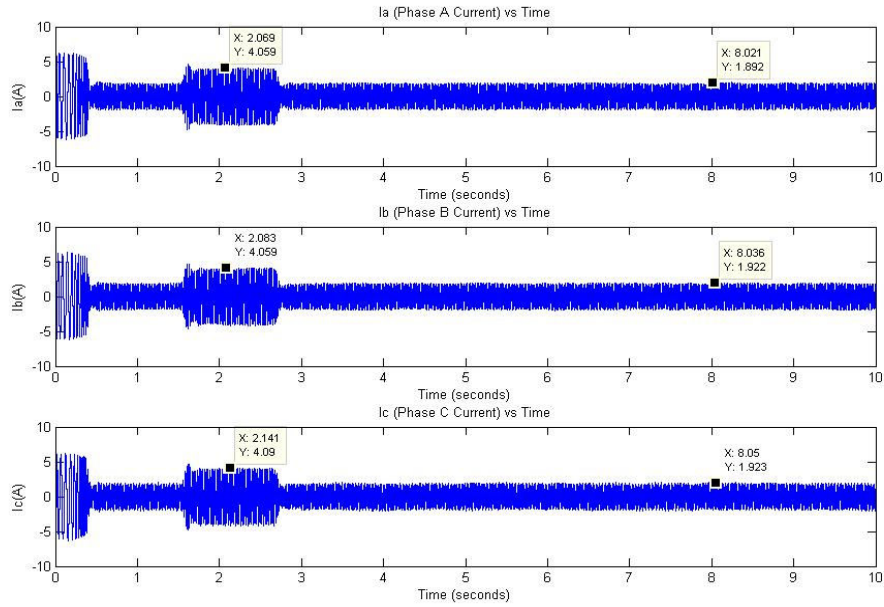


Figure 5-65 1500rpm speed reference, motor phase currents under switched loading

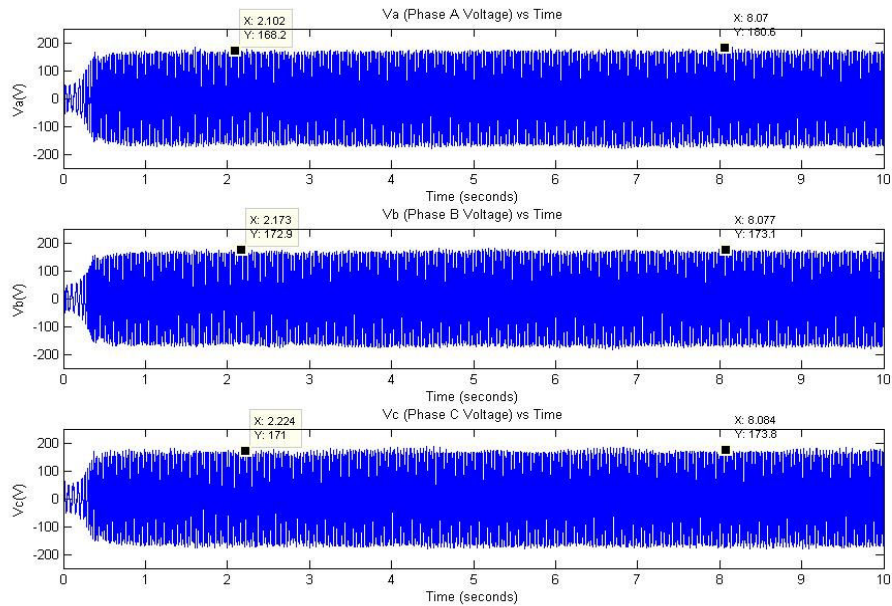


Figure 5-66 1500rpm speed reference, motor phase voltages under switched loading

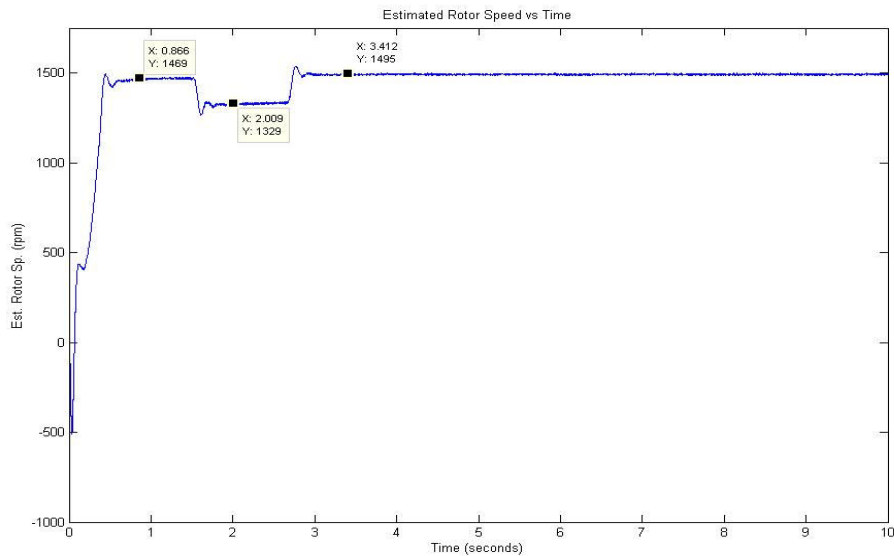


Figure 5-67 1500rpm speed reference, motor speed estimate under switched loading

As the set speed is increased, the phase current values increases since the loading of generator motor is increased. Meanwhile, peaks of the phase voltages do not change with loading as expected. Only frequency of phase voltage waveforms are affected resulting in speed deviations from set values. During the switched load tests the effect of load switching to the estimated speed is *18.4%* for *250rpm*, *15.8%* for *500rpm*, *12.8%* for *1000rpm*, *11.4%* for *1500rpm* as the percentage speed deviations, respectively. These large deviations come from the estimator estimation accuracy, current and speed regulation performance and current measurement accuracy. This again shows that the performance of the drive system improves with increasing speed. Although the speed reached deviates from the referenced values, the dynamic response of the system to the loading is quite satisfactory as seen from the graphs, however, this speed deviation shows that vector control performance should be increased.

The experiments showed that, speed estimator based on Kalman Filter and closed-loop rotor flux observer has very high tracking capability for whole speed range and for no-load and with load cases. However, the loop performance, the flux and the speed estimation accuracies should be improved for whole loading range and for low speeds.

CHAPTER 6

CONCLUSION

The focus of this work has been design and implementation of a speed estimator for sensorless closed-loop speed control of induction machine using direct field orientation technique. A Kalman filter has been considered for the estimator in the study. The application requires the use of another estimator for the estimation of the flux components and the rotor flux angle. This has been selected as a MRAS flux estimator scheme which uses integrals of back emfs. The flux observer relies on both current and voltage models of the machine to improve the dynamic performance of the estimator. The induction machine has been modeled both stationary and synchronously rotating dq axes system. The control system uses space vector PWM and field orientation concepts. They are introduced in the thesis in detailed form. MRAS speed estimator using reactive power and open-loop speed estimator using the estimated flux angle are also implemented for comparison of the speed estimation techniques. The performances of these speed estimators compared by simulations.

The Kalman filter technique is chosen as speed estimation scheme because of its estimation accuracy and low processing complexity. The closed-loop experiments are focused on detailed analysis of the model with Kalman filter speed estimator. Both simulations and experiments have been conducted to optimize and tune the controller parameters of the estimators, current and speed loops for both no-load and with load cases covering the entire speed range.

The simulations and experiments show that the sensorless speed control of the induction machine with described system is applicable; however, the performance of the system needs to be improved particularly for low speed range and for full loading of the machine. Also, the system stability against changes in loading should be improved to achieve better vector control performance.

For future work, the estimation accuracy and the dynamic response of the estimators may be improved by further efforts of re-tuning them; also the online parameter estimation techniques can be inserted into the algorithms to observe the effects of the change of motor parameters during operation. The estimators can be designed by other techniques, such as, extended Kalman filter (EKF) technique, neural networks based estimators, sliding mode estimators. Furthermore, more advanced control structures can be investigated for better control of both motor current loop and speed loop.

REFERENCES

- [1] H. Kubota and K. Matsuse “Flux observer of induction motor with parameter adaptation for wide speed range motor drives,” in Proc. IPEC’90, Tokyo, Japan, 1990, pp. 1213-1218.

- [2] R. Nilsen and M. Kazmierkowski, “New reduced-order observer with parameter adaptation for flux estimation in induction motors,” in Proc. PESC’92, 1992, pp. 245-252.

- [3] R. Lorenz and D. Lawson, “A simplified approach to continuous, on-line tuning of field-oriented induction machine drives,” IEEE Trans. Ind. Applicat., vol. 26, pp.420-425, May/Jun 1990.

- [4] K. T. Hung and R. D. Lorenz, “A rotor flux error-based adaptive tuning approach for feedforward field-oriented machine drives,” in Proc. 1990 IEEE-IAS, Annu. Meeting, pp. 589-594.

- [5] L. Garces, “Parameter adaptation for the speed-controlled static AC drive with a squirrel cage induction motor,” IEEE Trans. Ind. Applicat., vol. 16, pp. 173-178, Mar./Apr. 1980.

- [6] T. M. Rowan, R. J. Kerkman, and D. Leggate, “A simple on-line adaptation for indirect field-orientation of an induction machine,” in Proc. 1989 IEEE-IAS Annu. Meeting, pp.579-587.

- [7] J. Moreira, K. Hung and T. Lipo, “A simple and robust adaptive controller for the tuning correction in field-oriented induction machines,” IEEE Trans. Ind. Applicat., vol. 28, pp. 1359-1366, Nov./Dec. 1992.

- [8] P.L.Jansen and R.D.Lorenz “Transducerless position and velocity estimation in induction and salient ac machines”, IEEE Tran. IA, vol. 31, no.2, pp.240-247, Mar/April, 1995
- [9] R.Gabriel, W.L Leonhard and C.Nordby “ Field oriented control of standard AC motor using microprocessor”, IEEE Tran. IA, vol.16, no.2, pp.186.192, 1980
- [10] B.Robyens, B.Frederique, “A methodology to determine gains of induction motor flux observers based on a theoretical parameter sensitivity analysis”, IEEE Trans. PE, vol. 15, no.6, pp.983-995, 2000
- [11] Takahashi and T. Noguchi, “A new quick-response and high-efficiency control strategy of an induction motor,” IEEE Trans. Ind. Applicat., vol. 22, pp.820-827, Sep./Oct. 1986.
- [12] P. L. Jansen and R. D. Lorenz, “A physically insightful approach to the design and accuracy assessment of flux observers for field-oriented induction machine drives,” in Proc. IEEE-IAS Annu. Meeting, Oct.1992, pp. 570-577.
- [13] P. L. Jansen, C. O. Thompson, and R. D. Lorenz, “Observer based direct field orientation for both zero and very high speed operation,” in Proc. PCC, Yokohama, Japan, Apr. 1993, pp.432-437.
- [14] P. L. Jansen and R. D. Lorenz, “Accuracy limitations of velocity and flux estimation in direct field-oriented induction machines,” in Proc. EPE Conf., Brighton, England, Sep. 1993
- [15] P.L.Jansen and R.D.Lorenz “Observer based direct field orientation: Analysis and comparison of alternative methods”, IEEE Tran. IA, vol. 30, no.4, pp.945-953, Jul/Aug, 1994

- [16] K Minami, M. Vélez-Reyes, D. Elten, G. C. Verghese and D. Filbert, "Multi-stage speed and parameter estimation for induction machines," IEEE Power Electronics Specialist's Conference, Boston MA, Jun. 1991.
- [17] M. Vélez-Reyes and G. C. Verghese, "Decomposed algorithms for speed and parameter estimation in induction machines," IFAC Symposium on Non-linear Control System Design, Bordeaux, France, 1992.
- [18] M. Vélez-Reyes, K Minami, G. C. Verghese, "Recursive speed and parameter estimation for induction machines," IEEE Ind. Applicat. Society Meeting, San Diego, 1989
- [19] M. Bodson and J. Chiasson, "A comparison of sensorless speed estimation methods for induction motor control," Proc ACC, Anchorage, AK May.2002, pp. 3076-3081
- [20] I. J. Ha and S. H. Lee, "An on-line identification method for both stator and rotor resistances of induction motors without rotational transducers," ISIE'96, Warsaw, Poland, Jun. 1996.
- [21] H. S. Yoo and I. J. Ha, "A polar coordinate-oriented method of identifying rotor flux and speed of induction motors without rotational transducers," IEEE Trans. on Control Systems Technology, vol. 4, no. 3, pp. 230-243, May. 1996.
- [22] C.Lascu, I.Boldea, F.Blaabjerg "A Modified Direct Torque Control for Induction Motor Sensorless Drive" IEEE Tran. IA vol. 36, no. 1, pp. 122-130, Jan 2000
- [23] F.Z.Peng, T.Fukao "Robust Speed Identification for Speed Sensorless Vector Control of Induction Motors" IEEE Tran. IA vol. 30, no. 5, pp.1234-1239, Oct.1994

- [24] C.Schauder “Adaptive Speed Identification for Vector Control of Induction Motor without Rotational Transducers” IEEE Tran. IA vol. 28, no. 5, pp. 1054-1061, Oct.1992
- [25] G.Yang and T.Chin “Adaptive-Speed identification scheme for a vector controlled speed sensorless inverter induction motor drive” ,IEEE Tran. IA, vol. 29, no.4, pp.820-825, 1993
- [26] M.Elbuluk, N.Langovsky and D.Kankam “Design and Implementation of a Closed Loop Observer and Adaptive Controller for Induction Motor Drives” IEEE Tran. IA vol. 34 no. 3 pp. 435-443, May/June 1998
- [27] H.Tajima, Y.Hori “Speed Sensorless Field Orientation Control of the Induction Machine” IEEE Tran. IA vol. 29, no. 1, pp. 175-180, Feb.1993
- [28] D.W.Novotny and T.A.Lipo, “Vector Control and Dynamics of AC Drives”, Oxford University Press Inc., Oxford, New York, 1997.
- [29] H.Butler "Model Reference Adaptive Systems" London: Printice Hall,(1992)
- [30] L.Zhen and L. Xu “Sensorless Field Orientation Control of Induction Machines Based on Mutual MRAS Scheme” IEEE Tran. IE vol. 45 no. 5, pp. 824-831, October 1998
- [31] C.Attainese, Alfonso Damiano “Induction Motor Drive Parameters Identification” IEEE Tran. PE vol. 13, no. 6, pp. 1112-1123, Nov. 1998
- [32] H.Sugimoto and S.Tamai “Secondary Resistance Identification of an Induction Motor Applied Model Reference Adaptive System and its Characteristics” IEEE Tran. IA vol. 23, no. 2 pp. 296-303 March/April 1987

- [33] R.Krishnan, F.C.Doran “Study of parameter sensitivity in high performance inverter-fed induction motor drive systems” IEEE Tran. IA, vol. 23, pp.623-635, 1987
- [34] Texas Instruments, “Digital Motor Control Software Library” Literature number: SPRU 485 August 2001
- [35] A.M. Trzynadlowski, “The Field Orientation Principle in Control of Induction Motors, Kluwer Academic Publishers, pp. 176-180, 1994
- [36] G. Welch and G. Bishop, “An Introduction to the Kalman Filter”, April 5 2004
- [37] J. Holtz, “ Sensorless Control of Induction Motor Drives”, Proc. IEEE, vol. 90, No. 8, pp. 1359-1394, August 2002
- [38] G. Şimşek, “Sensorless Direct Field Oriented Control of Induction Machine by Flux and Speed Estimators Using Model Reference Adaptive System” M.S Thesis EE Dept. Metu, April 2004
- [39] E. Özçelik, “Speed Sensorless Vector Control of Induction Motor Drive” M.S Thesis EE Dept. Metu, April 2005
- [40] Gi-Won Chang, G. Espinosa-Pérez, E. Mendes, and R. Ortega, ”Tuning Rules for the PI Gains of Field-Oriented Controllers of Induction Motors”, IEEE Tran. on Industrial. Electronics, Vol. 47, No. 3, June 2000
- [41] Ong, Chee-Mun., “Dynamic Simulation of Electric Machinery”, Prentice Hall, 1998
- [42] Ned Mohan, “ Advanced Electric Drives” MNPERE, Minneapolis, 2001

APPENDIX

The Experimental Set-Up

The rectifier used in this drive is Semikron bridge rectifier (SKD-28) which is 1300V, 28A that consists of six uncontrolled diodes. The three-phase voltage is supplied over an autotransformer to the rectifier. The rectified voltage is filtered by two dc-link capacitors each being 1000 μ F and connected in series. 30K Ω , 1W resistors are connected across each capacitor for proper voltage sharing. The voltage at the beginning applied with a soft start resistor to limit the inrush current at starting. Then, when the capacitors are charged to predefined level, a relay disconnects the resistor and rectified voltage is applied directly. The inverter used in the drive system is Semikron IGBT module (SKM 40 GDL 123 D) with rated values 1200V and 40 A. IGBTs in this module are driven by a gate drive card, Semikron IGBT driver (SKHI 60 H4). The gate drive card provides short-circuit protection for all six IGBTs in the full bridge by real-time tracking of the collector-emitter voltage of the switches.

In order to run the real-time control algorithm and create PWM signals, Texas Instruments' TMS320 processor is used in this work. F2812 eZdsp board is used as DSP card. The F2812 is a member of the "C2000 DSP" platform, and is optimized specifically for motor control applications. It uses a 16-bit word length along with 32-bit registers. The F2812 has application-optimized peripheral units, coupled with the high-performance DSP core, enables the use of advanced control techniques for high-precision and high-efficiency full variable-speed control of motors. The event managers of F2812 include special pulse-width modulation (PWM) generation functions, such as a programmable dead-band function and a space-vector PWM state machine for 3-phase motors that provides quite a high efficiency in the switching of power transistors also, quadrature encoder pulse circuit module to read encoder signals. F2812 also contains 16 channels, 12-bit A/Ds, enhanced controller area network (eCAN), serial communication interface (SCI) and general purpose digital I/Os (GPIO) as peripherals.

The dc-link voltage is sensed with a voltage sensor (LV25-P) on the interface card. The magnitude of the dc-link voltage is sensed to re-build the phase voltages in the control software with the information of duty-cycles of the IGBTs. Another aim of the voltage sensor is to sense the overcharge on the dc-link capacitors. If the voltage level exceeds the predefined limit that is determined by the user, a comparator gives an error signal to set all the IGBTs to off-state. Also for used in the relay operation at the first power up. Moreover, the PWM signals generated by DSP are amplified to make them compatible with the gate drive card inputs. For this purpose, six PWM signals are adjusted to 15V peak without any other change. Finally, all the errors, (gate drive card errors, over-voltage error, over-current error, and an external error) are *OR* gated to set off IGBTs.

The other sensed variables are stator currents using current-sensors on the current measurement interface card. For this purpose (LA 25-NP) current transducers are used. These sensors are capable of sensing AC, DC and mixed current waveforms. The sensor has multi-range current sensing options depending on the pin connections. The sensors use hall-effect phenomena to sense the current. The output of these sensors is between $\pm 15V$ and unipolar. Since the ADCs on the DSP board cannot sense the negative voltage and requires signal between 0-3.3V, our current sensors are used with current interface card.

In case of noisy phase currents, optional low-pass filters are placed on the interface card with 1kHz cut-off frequency. The outputs of the current transducers are also used to provide over-current protection. The overall set-up is as in Figure A-1. Moreover, the block diagram of the set-up is given in Figure A-2 and the software block diagram from Matlab Simulink is as in Figure A-3.

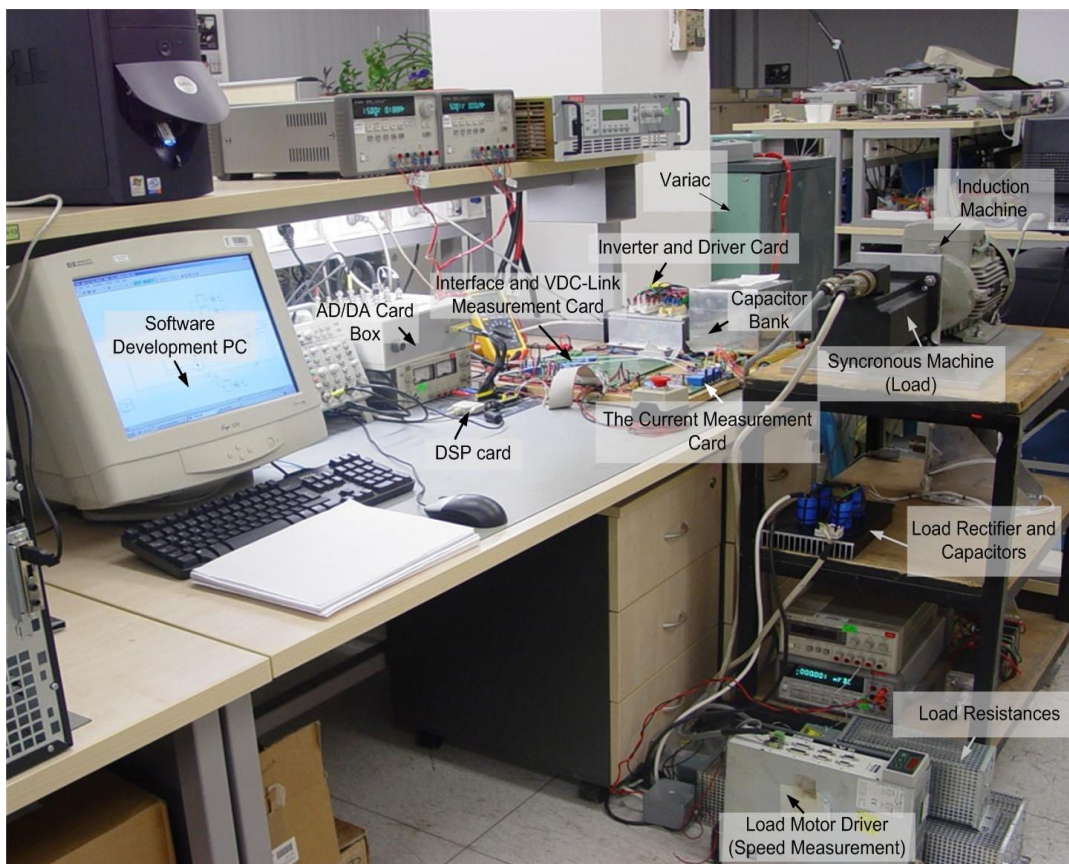


Figure A-1 The Experimental Set Up

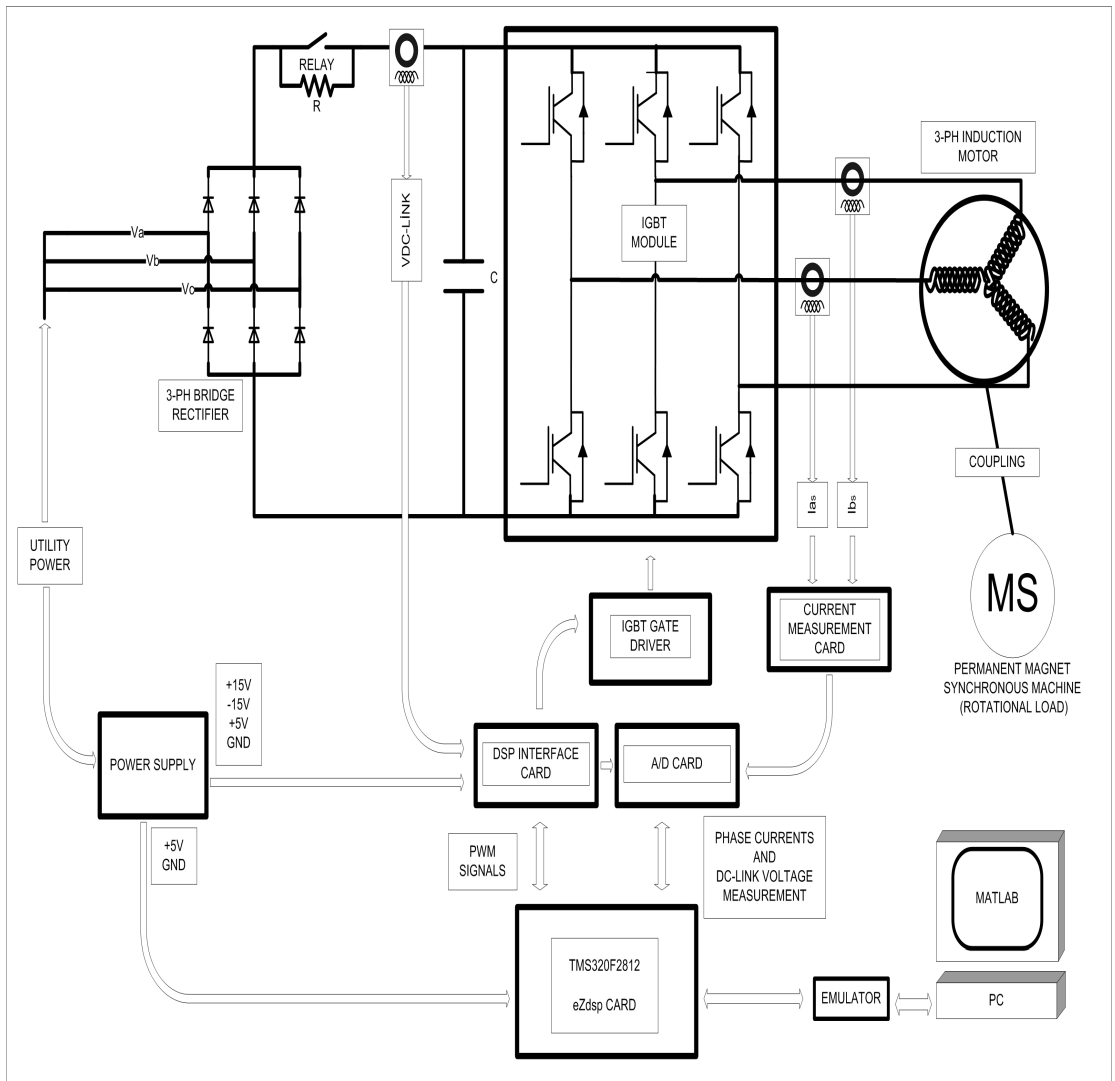


Figure A-2 The Experimental Set Up Block Diagram

